

Revisiting the Spectral-Energy Correlations of GRBs with *Fermi* Data I: Model-wise Properties

LIANG LI^{1,2,3}

¹*ICRANet, Piazza della Repubblica 10, I-65122 Pescara, Italy*

²*INAF – Osservatorio Astronomico d’Abruzzo, Via M. Maggini snc, I-64100, Teramo, Italy*

³*Dip. di Fisica and ICRA, Sapienza Università di Roma, Piazzale Aldo Moro 5, I-00185 Rome, Italy*

(Received ddmmyyyy; Revised March 15, 2023; Accepted ddmmyyyy; Published ddmmyyyy)

ABSTRACT

Gamma-ray bursts (GRBs) exhibit a diversity of spectra. Several spectral models (e.g., Band, cutoff power-law, and blackbody) and their hybrid versions (e.g., Band+blackbody) have been widely used to fit the observed GRB spectra. Here, we attempt to collect all the bursts detected by *Fermi*-GBM with known redshifts from July 2008 to May 2022, motivated to (i) provide a parameter catalog independent from the official *Fermi*/GBM team and (ii) achieve a “clean” model-based GRB spectral-energy correlation analysis. A nearly complete GRB sample was created, containing 153 such bursts (136 long gamma-ray bursts and 17 short gamma-ray bursts). Using the sample and by performing detailed spectral analysis and model comparisons, we investigate two GRB spectral-energy correlations: the cosmological rest-frame peak energy ($E_{p,z}$) of the νF_ν prompt emission spectrum correlated with (i) the isotropic-bolometric-equivalent emission energy $E_{\gamma,iso}$ (the Amati relation), and (ii) the isotropic-bolometric-equivalent peak luminosity $L_{p,iso}$ (the Yonetoku relation). From a linear regression analysis, a tight correlation between $E_{p,z}$ and $E_{\gamma,iso}$ (and $L_{p,iso}$) is found for both the Band-like and CPL-like bursts. More interestingly, the CPL-like bursts do not fall on the Band-like burst Amati and Yonetoku correlations, suggesting distinct radiation processes, and pointing towards the fact that these spectral-energy correlations are tightly reliant on the model-wise properties.

Keywords: Gamma-ray bursts (629); Astronomy data analysis (1858)

1. INTRODUCTION

Gamma-ray bursts (GRBs) are one of the most explosive events in the Universe. Two classes of GRBs have been identified in the CGRO/BATSE samples (Kouveliotou et al. 1993) based on their duration¹ t_{90} with a separation line $t_{90} \approx 2$ s, long bursts (LGRBs) with a $t_{90} \gtrsim 2$ s and short bursts (sGRBs) with a $t_{90} \lesssim 2$ s. The two GRB populations invoke distinct physical progenitors: LGRBs formed by the massive-star collapse and sGRBs generated by the binary neutron star or neutron star-black hole merger. Different progenitors of the two GRB populations may lead to different observational properties (e.g., duration, total energy, spectral properties, and parameter correlations).

Correlation analysis plays an important role in the understanding of GRB physics as it provides a crucial clue to revealing their nature (e.g., Amati et al. 2002; Yonetoku et al. 2004; Liang & Zhang 2005; Amati 2006; Dainotti et al. 2008; Yonetoku et al. 2010; Dainotti et al. 2008, 2010; Xu & Huang 2012; Zhang et al. 2012; Heussaff et al. 2013; Dainotti et al. 2013, 2015; Wang et al. 2015; Dainotti et al. 2016, 2017; Dainotti & Del Vecchio 2017; Dainotti & Amati 2018; Xu et al. 2021, and references therein). The two most widely discussed empirical correlations related to prompt emission mechanisms are the Amati (Amati et al. 2002) and Yonetoku (Yonetoku et al. 2004) relations, and both invoke the rest-frame peak energy $E_{p,z}=(1+z)E_p$ of the νF_ν prompt emission spectrum. The $E_{p,z}$ strongly correlates with the GRB isotropic-bolometric-equivalent emission energy $E_{\gamma,iso}$ at the cosmological rest frames, the

Corresponding author: Liang Li
liang.li@icranet.org

¹ The time is taken to accumulate 90% of the burst fluence starting at the 5% fluence level.

so-called Amati relation ($E_{p,z} \propto E_{\gamma,\text{iso}}^{0.5}$), which was first discovered in Amati et al. (2002) using a very small burst sample (twelve GRBs with redshift estimates) detected by BeppoSAX, and subsequently confirmed by larger samples detected by other satellites (e.g., HETE II, Konus/WIND, INTEGRAL, *Swift*, and *Fermi*). These correlations were first established for LGRBs (Amati et al. 2002), and further research (e.g., Ghirlanda et al. 2009; Amati 2010) has shown that sGRBs have comparable $E_p - E_{\gamma,\text{iso}}$ correlation features to long GRBs, but do not share the same $E_p - E_{\gamma,\text{iso}}$ correlation (e.g., Zhang et al. 2012, 2018). This is because the spectra-energy properties between LGRBs and sGRBs are usually distinctly different (Kouveliotou et al. 1993), sGRBs are typically hard with a relatively high E_p (e.g., Ghirlanda et al. 2004) while LGRBs are typically soft with a relatively low E_p (e.g., Ghirlanda et al. 2009). This may also be attributed to their short duration, as given the same $E_{p,z}$, short bursts are typically less energetic (Zhang 2018).

The Amati correlation has been widely used as a powerful tool in understanding the nature and differences of GRBs for the following aspects: (i) studying the physics of jet structure and GRB unification scenarios (Amati 2006); (ii) investigating the existence of different sub-classes of GRBs, such as distinguishing between the properties of long and short bursts (e.g., Amati et al. 2002; Amati 2006), or diagnosing the classification properties of different pulses within a burst (Li et al. 2023, in prep.); (iii) as a cosmological tool applied to GRBs (e.g., Wang et al. 2015, for a review), for discussion on selection biases of the use of this and other prompt correlations see Dainotti & Amati (2018); (iv) it can be used to diagnose the radiation mechanism of GRBs, e.g., the synchrotron shock models (Rees & Meszaros 1994) or the photospheric emission models (Rees & Mészáros 2005; Pe’er et al. 2006), since these observational correlations can be reproduced by the photospheric emission models, however, they may be difficult to reproduce within the framework of the synchrotron shock models. Another related correlation, i.e., the correlation between the peak energy $E_{p,z}$ and peak luminosity $L_{p,\text{iso}}$, known as the Yonetoku relation, was discovered in Yonetoku et al. (2004), and was used as the standard candle to estimate the redshift of the 689 GRBs with no known distances in the BATSE catalog. Unlike the Amati correlation, several previous studies (e.g., Zhang et al. 2009; Ghirlanda et al. 2009; Guiriec et al. 2013) revealed that short and long GRBs are no longer well distinguished in the $E_{p,z} - L_{\gamma,p,\text{iso}}$ plane, suggesting similar radiation processes.

Before *Fermi*, the observations covered a relatively narrower window into the energy (e.g., *Swift*-BAT; 15-350 keV, Barthelmy et al. 2005). Usually, determining E_p from the spectral analysis is a difficult task. For instance, the BAT is a narrow-band (15-150 keV) instrument, so constraining E_p straight from the Band-function spectral fit is frequently challenging due to the fact that in some cases E_p typically beyond the passband of the instrument. It is therefore likely that E_p cannot be measured accurately, at least for a significant fraction of the *Swift*-detected bursts.

Having both the Gamma-ray Burst Monitor (GBM; 8 KeV-40 MeV, Meegan et al. 2009), and the Large Area Telescope (LAT; 20 MeV-300 GeV, Atwood et al. 2009) onboard the *Fermi* Gamma-ray Space Telescope, it provides unprecedented spectral coverage of up to seven orders of magnitude in energy, and making it possible to fully assess all the current GRB spectral models (e.g., Abdo et al. 2009; Ryde et al. 2010; Axelsson et al. 2012; Guiriec et al. 2015; Li 2019a,b; Li et al. 2021). By May 2022, *Fermi* had completed 13 years of operation, in which at least 3000 GRBs had been observed, and contained at least 153 bursts with known redshifts, making it possible to study the GRB spectral-energy correlations with a large *Fermi* burst sample. There are several time-integrated and time-resolved spectral parameter catalogs of GRBs in the literature (e.g., von Kienlin et al. 2014; Gruber et al. 2014; von Kienlin et al. 2020; Narayana Bhat et al. 2016; Yu et al. 2016) based on the *Fermi* observations, but the majority of them focus on the parameter properties (e.g., parameter distributions and parameter correlations) in the GRB observer frame. A few studies (e.g., Poolakkil et al. 2021) based on the GBM data catalog have also presented their results in the GRB rest frame, however no relevant scientific research on the spectral parameters has yet been involved. Moreover, the frequentist method is the foundation for the majority of the earlier GBM catalogs (e.g., von Kienlin et al. 2014; Gruber et al. 2014; von Kienlin et al. 2020; Narayana Bhat et al. 2016; Yu et al. 2016). However, numerous recent studies (e.g., Yu et al. 2019; Li et al. 2021) have used a fully Bayesian approach. In light of this, it is important to perform independent analyses with a third party other than the official *Fermi*/GBM team and to revisit these correlations based on the *Fermi* observations with a large burst sample. Specifically, the establishment of a spectral-energy correlation for a full sGRB sample is required. Moreover, previous studies (e.g., Amati et al. 2002; Yonetoku et al. 2004; Ghirlanda et al. 2007; Amati et al. 2008; Nava et al. 2012; Qin & Chen 2013; Minaev & Pozanenko 2020) have not given much attention to the properties of GRB pulses. In the framework of the standard fireball shock model, each pulse on the lightcurve relates to the emission formed by the collision of two fast and slow relativistic shells ejected from the central engine as a result of the shock-waves. Different pulses reflect different properties from the central engine and possibly

also from the progenitor, such as some characteristic internal time and energy that is required to produce a pulse (Li et al. 2021). Therefore, revisiting the GRB spectral-energy correlations based on their pulse properties is of great interest. In addition, it is also important to note that the majority of previous studies (e.g., Nava et al. 2012; Qin & Chen 2013) have directly used the spectral parameters of a single spectral model (e.g., Band) provided by the satellite online catalog (e.g., *Fermi*/GBM). However, decades of observations have revealed that GRBs have diverse spectral properties that a single spectral model (e.g., Band-alone) cannot accurately characterize all the spectral shapes. For example, some GRB spectra can be well-fitted with a single non-thermal spectral component such as the Band-like component (e.g., 080916C, Abdo et al. 2009)², but some other GRBs may require a dominant thermal component in order to obtain an acceptable fit (e.g., 090902B, Ryde et al. 2010), and even some bursts exhibit a hybrid spectrum (e.g., 110721A, Iyyani et al. 2013), i.e., composited with a non-thermal component and a thermal component within a single GRB simultaneously. Moreover, the E_p obtained from the non-thermal spectral fit is clearly less than that from the best fit in the hybrid spectrum if the spectral component is fully attributed to the non-thermal component (Li 2019b). Furthermore, a recent study (Li 2022) suggests that inconsistent peaks (both α and E_p) of the spectral parameter distribution have been found between Band-like bursts and CPL-like bursts. In particular, the derived spectral parameters deviated significantly in the “Band (preferred)-to-CPL (misused)” case, but do not occur in the “CPL (preferred)-to-Band (misused)” case³.

Following these lines of argument, we will consider the following improvements in our investigations over earlier studies. (i) By using the broad spectral coverage of the *Fermi* data, the E_p of the prompt emission spectrum could accurately be measured for the majority of bursts. (ii) all of the E_p in our tasks is obtained from the best-model fits by performing detailed spectral analysis and model comparisons between various GRB spectral models and their hybrid versions. (iii) Using a “clean” sample of well-defined single-pulse GRBs and well-separated multi-pulse GRBs (Li et al. 2022, in prep.) to revisit the GRB spectral-energy correlations can in principle more directly reflect some internal properties of the central engine and predecessor stars. We will report our results in a series of papers using the *Fermi*-detected burst samples with distinct model and pulse properties. As the first paper in the series, we collect a complete GRB sample detected by *Fermi* with a measured redshift, and use the sample to revisit the GRB spectral-energy correlations, paying special attention to the Amati and Yonetoku relations. This effort is dedicated to achieving a “clean” model-based GRB spectral-energy correlation analysis.

The paper is organized as follows. The methodology are presented in Section 2. The results are summarized in Section 3. The discussions and conclusions are presented in Section 4 and Section 5, respectively. Throughout the paper, the standard Λ -CDM cosmology with the parameters $H_0 = 67.4 \text{ kms}^{-1} \text{ Mpc}^{-1}$, $\Omega_M = 0.315$, and $\Omega_\Lambda = 0.685$ are adopted (Planck Collaboration et al. 2018).

2. METHODOLOGY

In order to perform the model-wise analysis of the spectral-energy correlations of GRBs proposed in this paper, a nearly complete GRB sample detected by *Fermi* with a measured redshift was created via a dedicated search from the NASA/HEASARC database⁴ from July 2008 to May 2022, consisting of 153 such GRBs. Following the traditional GRB classification scheme according to their duration, 17 GRBs belong to short bursts ($t_{90} \lesssim 2 \text{ s}$) whereas 136 GRBs belong to long bursts ($t_{90} \gtrsim 2 \text{ s}$)⁵. Interestingly, with a time-dilation factor of $1/(1+z)$ corrected to the rest frame, the duration of six more GRBs (GRB 090423, GRB 110731A, GRB 130612A, GRB 140808A, GRB 141004A, and GRB 210610A) satisfy $t_{90}/(1+z) \lesssim 2 \text{ s}$. In order to obtain E_p , $E_{\gamma,\text{iso}}$, and $L_{p,\text{iso}}$, our data procedure invokes the following steps, which we briefly introduce here.

1. Using 3ML (the Multi-Mission Maximum Likelihood Framework, see Vianello et al. 2015), and following the standard practices (Li et al. 2019; Li 2019b; Yu et al. 2019; Burgess et al. 2019; Li 2020; Li & Zhang 2021; Li et al. 2021) provided by the *Fermi* team, including the selection of detectors, sources, and background intervals, we performed a detailed spectral analysis for each individual burst in our initial sample. In order to ensure consistency of the results across various algorithms, we utilize both the maximum-likelihood estimation (MLE)

² Recent studies (Guiriec et al. 2015; Vereshchagin et al. 2022) have shown that in order to obtain an acceptable fit to the spectral data of GRB 080916C, a thermal component needs to be added during the initial prompt emission of the burst.

³ Here the “Band (preferred)-to-CPL (misused)” case means that if a spectrum is statistically preferentially fitted to the Band, applying CPL to derive the spectral parameters, and vice versa the “CPL (preferred)-to-Band (misused)” case.

⁴ <https://heasarc.gsfc.nasa.gov/W3Browse/fermi/fermigbrst.html>

⁵ We notice that there are several bursts where we suspect that the duration reported by the GBM team may not be reliable. For instance, GRB 140506A880, GRB 191011192.

and a fully Bayesian analysis plus Markov Chain Monte Carlo (MCMC) algorithms to explore their best parameter space.

2. For a given burst in our target sample, we first attempted using the GRB model, known as the Band function (Band et al. 1993), to fit its time-integrated spectral data. The photon number spectrum of Band is defined as

$$N_{\text{Band}}(E) = A \begin{cases} \left(\frac{E}{E_{\text{piv}}}\right)^\alpha \exp\left(-\frac{E}{E_0}\right), & E < (\alpha - \beta)E_0 \\ \left[\frac{(\alpha - \beta)E_0}{E_{\text{piv}}}\right]^{(\alpha - \beta)} \exp(\beta - \alpha) \left(\frac{E}{E_{\text{piv}}}\right)^\beta, & E \geq (\alpha - \beta)E_0 \end{cases} \quad (1)$$

where A is the normalization factor in units of $\text{ph cm}^{-2}\text{keV}^{-1}\text{s}^{-1}$, E_{piv} is the pivot energy always fixed at 100 keV, E_0 is the break energy correlated with the peak energy of νF_ν spectrum (assuming $\beta < -2$) by $E_p = (2 + \alpha)E_0$, α and β are the low-energy and high-energy asymptotic power-law photon indices, respectively. There are two steps. (1) If all the model parameters from the Band fit are well-constrained, we then attempt to add a BB component to the Band. If an acceptable fit can still be obtained, we then obtain the E_p from the Band+BB fit. Otherwise, the Band-alone fit provides the E_p . The BB emission can be modified by Planck spectrum, which is given by the photon flux

$$N_{\text{BB}}(E, t) = A(t) \frac{E^2}{\exp\left[\frac{E}{kT(t)}\right] - 1}, \quad (2)$$

where A is the normalization, T is the temperature, and k is the Boltzmann constant. (2) Alternatively, if the model parameters from the Band fit are not well-constrained or Band- β is poorly constrained (have fairly large values and large uncertainties), we then try the CPL model (a power law with an exponential tail) to refit the same spectral data and possibly obtain equally good fits for α and cut-off energy E_c , and obtain the peak energy E_p of the νF_ν -spectrum through⁶ $E_p = (2 + \alpha)E_c$. The CPL (COMP) function is given by

$$N_{\text{CPL}}(E) = A \left(\frac{E}{E_{\text{piv}}}\right)^\alpha \exp\left(-\frac{E}{E_c}\right). \quad (3)$$

Repeat Step (1), we may obtain E_p from the CPL+BB fit in some cases. As a result, E_p in our analysis can be obtained from two single spectral models (Band-alone and CPL-alone) and two hybrid spectral models (Band+BB and CPL+BB). To evaluate different spectral models and select the preferred one, we adopted both the Akaike Information Criterion (AIC; Akaike 1974) and the Bayesian Information Criterion (BIC; Schwarz 1978). This is due to the fact that the BIC is recommended for nested models (e.g., Band against Band+BB) while the AIC is favored for models that are not nested (such as Band versus CPL). The preferred model is the one that provides the lowest AIC and BIC scores. It should also be noted that in some cases, even if we obtain the lowest AIC and BIC scores, some of the model parameters found in the ‘‘preferred’’ model cannot be constrained. Therefore, it is likely that we have found only the local minimum of the likelihood function rather than the global minimum. In this case, we need to reset the initial model parameters and repeat the fit until all model parameters are constrained and the minimum AIC and BIC scores are obtained.

3. Through Step 2, the E_p of the νF_ν prompt emission spectrum can be obtained from our refined spectral analysis, and its cosmological properties can be computed by

$$E_{p,z} = E_p(1 + z). \quad (4)$$

In addition, the energy flux F_γ ($\text{erg cm}^{-2}\text{s}^{-1}$) can be also obtained from spectral parameters, with a k -correction (k_c , $1\text{-}10^4$ keV) applied. In order to use the $E_{p,z}$ - L_p relation, a bolometric luminosity in a common cosmological rest-frame energy band ($1\text{-}10^4$ keV) is needed. It can be obtained by using the spectral parameters to conduct a k -correction extrapolating the observed energy band to $1\text{-}10^4$ keV. For a given burst, the k -correction factor (k_c) can be derived using the following procedure. The observed flux F^{obs} ($\text{erg cm}^{-2}\text{s}^{-1}$), in a fixed detector energy bandwidth $[e_1, e_2]$ (for instance, for the *Fermi*-GBM observation, $e_1=8$ keV, $e_2=40$ MeV), can be written as:

$$F_{[e_1, e_2]}^{\text{obs}} = \int_{e_1}^{e_2} EN(E)dE, \quad (5)$$

⁶ If the model parameters from the CPL model fit are not yet well-constrained, there may be two possibilities. (i) The lack of source photons in the analyzed bursts (e.g., $S < 20$), so that the spectral fit can not be well-determined; or (ii) the source photons in the analyzed bursts are sufficient (e.g., $S > 20$), but the model that best characterizes the spectral shape indeed is a simpler model than the CPL function (e.g., the simple power-law model).

where E is in units of keV, and $N(E)$ is a GRB photon number spectrum. The total luminosity emitted in the bandwidth $[e_1, e_2]$, defined in the cosmological rest-frame, is given by:

$$L_{[e_1(1+z), e_2(1+z)]} = 4\pi D_L^2(z) F_{[e_1, e_2]}^{\text{obs}}, \quad (6)$$

which $D_L(z)$ is the luminosity distance. To express the luminosity L in the cosmological rest-frame energy band, $[E_1=1 \text{ keV}, E_2=10^4 \text{ keV}]$, common to all sources, the Eq.(6) can be rewritten as:

$$L_{[E_1, E_2]} = 4\pi D_L^2 F_{\left[\frac{E_1}{1+z}, \frac{E_2}{1+z}\right]}^{\text{obs}} = 4\pi D_L^2 k[e_1, e_2, E_1, E_2, z] F_{[e_1, e_2]}^{\text{obs}}, \quad (7)$$

where the k -correction factor, k_c , is therefore defined as:

$$k_c = k[e_1, e_2, E_1, E_2, z] = \frac{F_{\left[\frac{E_1}{1+z}, \frac{E_2}{1+z}\right]}^{\text{obs}}}{F_{[e_1, e_2]}^{\text{obs}}} = \frac{\int_{E_1/(1+z)}^{E_2/(1+z)} EN(E)dE}{\int_{e_1}^{e_2} EN(E)dE}, \quad (8)$$

with k_c , F_γ , and redshift measurement, one can estimate the peak isotropic-equivalent luminosity as

$$L_{p, \text{iso}} = 4\pi D_L^2 F_{p, \gamma} k_c, \quad (9)$$

where D_L is the luminosity distance. Therefore, the fluence S_γ (erg cm^{-2}) during the source interval (ΔT_{src}) can be yielded by $S_\gamma = F_\gamma \Delta T_{\text{src}}$. With S_γ , and redshift measurement, one can estimate the isotropic-equivalent energy releases in γ -ray band

$$E_{\gamma, \text{iso}} = \frac{4\pi d_L^2 S_\gamma k_c}{(1+z)}. \quad (10)$$

3. RESULTS

3.1. Distributions of k_c , T_{90} ($T_{90, z}$), S_γ , $E_{p, z}$, $E_{\gamma, \text{iso}}$, and $L_{p, \text{iso}}$

We show the distributions of k_c , T_{90} ($T_{90, z}$), S_γ , $E_{p, z}$, $E_{\gamma, \text{iso}}$, and $L_{\gamma, \text{iso}}$ in Figure 1 for our complete sample described in Section 2. Figure 1a depicts the distributions of t_{90} for the cases both in the observed frame (cyan line) and rest-frame (shadow grey region), and one can see that they do not share the same distribution. With a time-dilation factor $1/(1+z)$ corrected, the peak of the distribution of $t_{90, z}$ at the cosmological rest-frame is smaller than that of the observed frame (see Table 5). The k -correction factor, k_c , is calculated as the flux ratio between the 1-10⁴ keV and GBM energy bands (8 keV-40 MeV) based on the time-integrated spectra of each burst in the sample. The distribution can be fitted with Gaussian functions ($\mathcal{N} = \mu \pm \sigma$), where μ is the average value and σ is the corresponding standard deviation. The best Gaussian fit for the distribution of k_c gives $k_c = 0.95 \pm 0.11$ (Figure 1b). This result ($k_c \approx 1$) is due to the GBM energy band being comparable to the k -correction energy band that we used. Similar results can also be found in Figure 1c, where we present the distributions of S_γ . The S_γ obtained in the GBM band is shown by the cyan line while that of in the bolometric (1-10⁴ keV) energy band is overlaid in gray. One can see that both share a similar distribution. The spectral parameters ($E_{p, z}$, $E_{\gamma, \text{iso}}$, and $L_{\gamma, \text{iso}}$) are derived from the model-wise spectral analysis (see Section 2). As presented in Section 2, $E_{p, z}$ can be obtained from both the time-integrated (see dashed line in Figure 1d) and (1-s) peak (see shadow grey region in Figure 1d) spectral analyses. However, $E_{\gamma, \text{iso}}$ is only obtained from the time-integrated spectral analysis (see dashed line in Figure 1e) whereas $L_{\gamma, \text{iso}}$ is only obtained from the (1-s) peak spectral analysis (see dashed line in Figure 1f). Detailed information about the best Gaussian fit of each distribution is presented in Table 5, along with the corresponding average values and standard deviations.

3.2. The model-wise $E_{p, z} - E_{\gamma, \text{iso}}$ (Amati) Correlation

With the refined spectral analysis described in Section 2, one hundred and nine GRBs have well-measured their time-integrated E_p , whereas thirty-eight GRBs have a low statistical significance⁷, resulting in poorly determined spectral fits and hence unmeasured E_p (see Column 8 in Table 1). The 109 GRBs with well-measured E_p provide a well-defined sample for studying the GRB time-integrated $E_{p, z} - E_{\gamma, \text{iso}}$ (Amati) correlation. Based on the time-integrated spectral

⁷ Note that there is a peculiar event (GRB 150727A). The event has a high statistical significance and a well-measured E_p . However, background photons cannot be properly subtracted, resulting in somewhat anomalous results. The spectral parameters ($\alpha = -1.12 \pm 0.13$, $E_c = 210_{-55}^{+75}$ keV) obtained from the CPL model (better than other models) fit, with redshift at $z = 0.313$, we obtain $E_{p, z} = 242_{-72}^{+93}$ keV and $E_{\gamma, \text{iso}} = (0.5_{-0.1}^{+0.2}) \times 10^{52}$ erg for this event.

analysis, we independently present all the fitted parameters (unless the model parameters cannot be well-constrained for some bursts) using two individual (standard) models (CPL and Band) in Table 2. The information given in Table 2 include GRB name (Column 1); The selected source interval $T_{\text{start}} \sim T_{\text{stop}}$ (Column 2); The corresponding significance S ; The best-fit parameters for the CPL model (normalization K , low-energy power-law index α , and cutoff energy E_c of the νF_ν spectrum) are listed in Columns (4-6); as well as the corresponding likelihood, AIC, and BIC; The derived rest-frame peak energy $E_{p,z}$ and the isotropic-bolometric-equivalent γ -ray emission energy $E_{\gamma,\text{iso}}$ are listed in Columns 8-9. The best-fit parameters for the Band model (normalization K , low-energy power-law index α , peak energy E_p of the νF_ν spectrum, and high-energy power-law index β) are listed in Columns (10-13), as well as the corresponding likelihood, AIC, and BIC; The derived $E_{p,z}$ and $E_{\gamma,\text{iso}}$ are listed in Columns (15-16); The difference of AIC between Band and CPL models, defined as $\Delta\text{AIC}=\text{AIC}_{\text{Band}}-\text{AIC}_{\text{CPL}}$, is listed in Column 17. By performing model-wise analysis following the Steps described in Section 2, we classify these bursts into four groups. To summarize, our sample is composed as follows.

- Band-like bursts. This group includes 64 GRBs (3 sGRBs and 61 lGRBs) in which the spectral data can be well fitted by the Band-alone model (see Column (8) of Table 1 and Column (17) of Table 2), and E_p can be directly obtained from the fits, being consistent with the previous studies (e.g., Amati et al. 2002).
- CPL-like bursts. This group consist of 45 GRBs (6 sGRBs and 39 lGRBs) that CPL-alone model can be well fitted the spectral data (see Column (8) of Table 1 and Column (17) of Table 2), and E_p is computed through $E_p=(2+\alpha)E_c$.
- Band+BB-like bursts. This group includes 6 lGRBs (0 sGRBs and 6 lGRBs) in which the spectral data require an additional thermal component based on the Band component, namely, the Band plus a BB model (see the upper panel of Table 4), and E_p can be directly obtained from the Band component.
- CPL+BB-like bursts. This group consist of 5 lGRBs (0 sGRBs and 5 lGRBs) that the spectral data still require an additional thermal component based on the CPL model, namely, CPL plus a BB component (see the upper panel of Table 4), and E_p is computed through $E_p=(2+\alpha)E_c$ from the CPL component.

To measure the E_p of the prompt emission spectra, the Band model (Band et al. 1993) has been used extensively in previous studies. Several recent statistical results (e.g., Yu et al. 2019; Li et al. 2021) based on *Fermi* observations show that the Band-like spectra dominate the time-integrated spectral properties, whereas the CPL-like spectra dominate the time-resolved spectral properties, regardless of whether it is a single-pulse (Yu et al. 2019) or multi-pulse (Li et al. 2021) burst. These two spectral models are widely used in practically all GRB literature and are the canonical models of GRBs. Furthermore, the deviations in the derived spectral parameters as a result of their misuse have also been thoroughly investigated in a recent study (Li 2022). Moreover, hybrid spectra (e.g., 110721A, Axelsson et al. 2012) can be observed in some other GRBs, and the E_p determined from the spectral fit deviates greatly from the intrinsic spectral shape if the spectral component is totally attributed to the non-thermal component (Li 2019b).

In light of the above arguments, it will be fascinating to see whether GRB spectrum-energy correlations are affected by the spectral model chosen. We first investigate the model-based properties of the $E_{p,z} - E_{\gamma,\text{iso}}$ (Amati) correlation. Similar to the method described in Nava et al. (2012), we modeled the distribution of data points for our lGRB sample by using a linear function in the $E_{p,z} - E_{\gamma,\text{iso}}$ logarithmic plane, and fitted the data using a nonlinear least-squares method using the Levenberg-Marquardt minimization algorithm (Newville et al. 2016). This option is motivated by the fact that there is no reason to assume either E_p or $E_{\gamma,\text{iso}}$ (or $L_{\gamma,\text{iso}}$) as an independent variable a priori, as well as by the high degree of dispersion in the data points. The slope and normalization errors are computed by fitting data points to their barycenters, which are uncorrelated. We estimate the Spearman's rank correlation coefficient and the associated chance probability for the samples, and provide these values in Table 6. To double-check our results, we also performed a correlation coefficient analysis using the Markov Chain Monte Carlo algorithm to evaluate the correlation between these parameters (see Appendix and Table A1).

In Figure 3, we present the (preferred) spectral-model-based $E_{p,z} - E_{\gamma,\text{iso}}$ (Amati) correlation analysis for our sample. The data points with magenta, cyan, orange, and grey colors indicate the Band-like, CPL-like, Band+BB-like, and CPL+BB-like bursts, receptively. We employ the power-law model $E_{p,z} = a \left(\frac{E_{\gamma,\text{iso}}}{E_{\gamma,\text{iso}}^{\text{div}}} \right)^b$ to fit the data, where a is the normalization, b is the power-law index, and $E_{\gamma,\text{iso}}^{\text{div}}$ is the pivot energy fixed at 2×10^{52} erg. The fits are

performed by using the python package *lmfit* (Newville et al. 2016) by applying a nonlinear least-squares method using the Levenberg-Marquardt minimization algorithm. The best power-law fit is shown by the grey line, while the shadow area represents the 2σ error zone. The power-law model fitted to our Band-like IGRBs using the Spearman correlation analysis gives

$$E_{p,z}/(\text{keV}) = (229 \pm 29) \left[\frac{E_{\gamma,\text{iso}}/(\text{erg})}{E_{\gamma,\text{iso}}^{\text{piv}}} \right]^{(0.42 \pm 0.05)}, \quad (11)$$

at 2σ confidence level, with the number of data points $N=61$, the Spearman's rank correlation coefficient of $R=0.71$, and a chance probability $p < 10^{-4}$. The power-law model fitted to our CPL-like IGRBs bursts gives

$$E_{p,z}/(\text{keV}) = (341 \pm 65) \left[\frac{E_{\gamma,\text{iso}}/(\text{erg})}{E_{\gamma,\text{iso}}^{\text{piv}}} \right]^{(0.25 \pm 0.12)}, \quad (12)$$

at 2σ confidence level, with the number of data points $N=39$, the Spearman's rank correlation coefficient of $R=0.11$, and a chance probability 0.67. Moreover, we found three Band-like short bursts and six CPL-like short bursts (see Column (8) in Table 1 and Column (17) of Table 2). Using mixed samples (sGRBs and IGRBs), we also attempted to do a similar model-wise analysis and reported our results in Table 6. For the Band-like cases, due to the small sample size (3 events), adding the sGRBs sample does not significantly affect the results. However, for the CPL-like case, the correlation changes significantly when the sGRB sample is included (see Table 6). Also, we note that due to the fact that the sample size for the hybrid spectral events is small, we are not able to do a relevant statistical analysis for these groups. A more detailed statistical analysis of hybrid spectra, will be possible in the future when *Fermi* observations accumulate more such cases.

Our analysis shows that Band-like bursts and CPL-like bursts may not have the same Amati correlation as shown in the $E_p - E_{\gamma,\text{iso}}$ plane (Figure 3), despite the fact that CPL-like events have a more significant dispersion and that data points have a larger error bar, and therefore, the results may not be statistically significant. More interestingly, the Band-like spectral-based Amati correlation remains consistent with previous studies without distinguishing between the spectral models. The CPL-like spectral-based Amati correlation, on the other hand, is inconsistent with the findings in previous samples and with the Band-like bursts, and a shallower power-law index is found. Individual parameter distributions (E_p and $E_{\gamma,\text{iso}}$) are shown in the upper panels of Figure 2. Compared to the Band-like bursts, one can see that CPL-like bursts show a smaller $E_{\gamma,\text{iso}}$ peak. However, CPL-like bursts and Band-like bursts appear to have similar peaks in the E_p distributions (Figure 2a). As a result, Band-like bursts and CPL-like bursts may not have the same Amati correlation. In addition, if the CPL-like spectra events can explain the outliers observed in the $E_{p,z} - E_{\gamma,\text{iso}}$ plane, they should dominate the low- $E_{\gamma,\text{iso}}$ and high- $E_{p,z}$ regions, as shown in Figure 3.

3.3. The model-wise $E_{p,z} - L_{p,\text{iso}}$ (Yonetoku) Correlation

Investigating the spectral-model-based properties of the Yonetoku correlation is equally intriguing. In order to investigate the $E_{p,z} - L_{p,\text{iso}}$ (Yonetoku) correlation, we need to obtain both the time-averaged $E_{p,z}$ and the peak luminosity $L_{p,\text{iso}}$ according to the definition of the previous studies (e.g., Yonetoku et al. 2010). In order to obtain the peak luminosity $L_{p,\text{iso}}$, we select the (1-s) peak spectrum of a given burst in our sample and repeat Steps 1-3 described in Section 2. In order to precisely identify the 1-s peak energy spectrum, we apply the ‘‘constant’’ binning method with a time slice $\Delta t=1$ to the TTE (Time-Tagged Events) light curve of the brightest NaI detector. We then calculate the counts for each time bin based on the ‘‘constant’’ time binning method and pick up the one with the maximum count value. Fifty-one GRBs were too faint to determine the peak luminosity based on their spectral parameters. The remaining 102 GRBs that can determine their spectral parameters could be further used to study the $E_{p,z} - L_{p,\text{iso}}$ (Yonetoku) correlation. Combined with the time-integrated spectral analysis studied in Section 3.2, a total of 92 GRBs were able to obtain both well-measured $E_{p,z}$ from the time-integrated spectrum and peak luminosity $L_{p,\text{iso}}$ from the 1-s peak spectrum, and can be divided into four groups based on their best-fit spectral models. Similarly, based on the 1-s peak spectral analysis, we also independently present all the fitted parameters from both CPL and Band models (Table 3). The derived peak luminosity $L_{p,\text{iso}}$ are listed in Column (8) and Column (14) for the CPL and Band models, respectively. The information remaining is the same as in Table 2.

- Band-like bursts. This group includes 55 GRBs (3 sGRBs and 52 lGRBs) in which the spectral data can be well fitted by the Band-alone model (see Column (8) of Table 1 and Column (17) of Table 3), and E_p can be directly obtained from the fit, being consistent with the previous studies (e.g., Yonetoku et al. 2010).
- CPL-like bursts. This group consist of 37 GRBs (2 sGRBs and 35 lGRBs) that CPL-alone model can be well fitted the spectral data (see Column (8) of Table 1 and Column (17) of Table 3), and E_p is computed through $E_p = (2+\alpha)E_c$.
- Band+BB-like bursts. This group includes 5 GRBs (0 sGRBs and 5 lGRBs) in which the spectral data require an additional thermal component based on the Band component, namely, the Band plus a BB model (see the lower panel of Table 4), and E_p can be directly obtained from the Band component.
- CPL+BB-like bursts. This group consist of 8 lGRBs (0 sGRBs and 8 lGRBs) that the spectral data still require an additional thermal component based on the CPL model, namely, CPL plus a BB component (see the lower panel of Table 4), and E_p is computed through $E_p = (2+\alpha)E_c$ from the CPL component.

Figure 4 shows the spectral model-dependent $E_p - L_{p,iso}$ (Yonetoku) correlation for 102 GRBs with a well-measured E_p using 1-s peak spectrum. The symbols and colors are the same as in Figure 3. Similarly, we employ the power-law model $E_{p,z} = a \left(\frac{L_{p,iso}}{L_{p,iso}^{piv}} \right)^b$ to fit the data, where a is the normalization, b is the power-law index, and $L_{p,iso}^{piv}$ is the pivot luminosity fixed at a typical value (see Table 6). We fit the Band-like 1-s peak spectra for our lGRB sample with the power-law model using the Spearman correlation analysis, and yield the following results

$$E_{p,z}/(\text{keV}) = (307 \pm 34) \left[\frac{L_{p,iso}/(\text{erg.s}^{-1})}{L_{p,iso}^{piv}} \right]^{(0.34 \pm 0.04)}, \quad (13)$$

at 2σ confidence level, with the number of data points $N=53$, the Spearman's rank correlation coefficient of $R=0.83$, and a chance probability $p < 10^{-4}$. Similar analysis is performed on the CPL-like lGRBs and come up with the following results

$$E_{p,z}/(\text{keV}) = (454 \pm 55) \left[\frac{L_{p,iso}/(\text{erg.s}^{-1})}{L_{p,iso}^{piv}} \right]^{(0.40 \pm 0.08)}, \quad (14)$$

at 2σ confidence level, with the number of data points $N=35$, the Spearman's rank correlation coefficient of $R=0.69$, and a chance probability $p < 10^{-4}$.

Based on the time-integrated spectral analysis and the 1-s peak spectral analysis, we found that the CPL-like lGRBs do not fall on the Band-like lGRB Yonetoku correlation, having a shallower slope, as shown in the $E_{p,z} - L_{p,iso}$ plane (Figure 4). This result is inconsistent with the findings (e.g., Amati 2006; Zhang et al. 2009; Ghirlanda et al. 2009; Guiriec et al. 2013) that short and long GRBs in the $E_{p,z} - L_{p,iso}$ plane are no longer well-separated. However, it is similar to the findings found in the $E_{p,z} - E_{\gamma,iso}$ plane in several previous studies that the short GRBs do not fall on the long GRB Amati relation (e.g., Zhang et al. 2009; Ghirlanda et al. 2009; Guiriec et al. 2013). Moreover, we also performed a similar model-wise analysis by adding the sGRBs to the lGRB sample (see Table 6). Due to the small sample size of the sGRBs for both the Band-like and CPL-like cases, we do not find a significant difference between the lGRB sample and entire (mixed) sample (sGRBs+lGRBs). We discover that the Band-like events have a larger dispersion than the CPL-like events, and that the power-law index is inconsistent with the CPL-like bursts with respect to their uncertainties. This may be due to the fact that the sample size of the Band-like event is not large enough to lead to missed low-luminosity events.

3.4. Outliers in the $E_{p,z}-E_{\gamma,iso}$ Plane

Interestingly, we discovered three notable outliers (GRB 110721A, GRB 130702A, and GRB 140606B) that are located outside the 3σ region of the lGRB Amati correlation, as shown in the $E_{p,z} - E_{\gamma,iso}$ plane, where all these events belong to the traditional classification of long-duration bursts (Figure 5). More interestingly, the CPL model presents the best fittings to GRB 130702A and GRB 140606B while the remaining one (GRB 110721A) is a Band+BB-like burst. These results motivated us to investigate whether spectral modeling could affect the results of the Amati

correlation and whether the selection of the spectral model could have contributed to the outliers in the $E_{p,z}-E_{\gamma,\text{iso}}$ plane. Apart from these outliers, several more events that either involve Band+BB-like spectra or CPL+BB-like spectra are also interesting to include. Together, these events are particularly useful for testing whether the outliers observed in the $E_{p,z}-E_{\gamma,\text{iso}}$ plane arise from the applied spectral model selection. We next compare the E_p , $E_{\gamma,\text{iso}}$, and $E_p - E_{\gamma,\text{iso}}$ correlations between the preferred model and the Band model by selecting several outliers from CPL-like, Band+BB-like, and CPL+BB-like bursts, as shown in Figure 5. The CPL model is statistically preferred for GRB 101213A, and GRB 140606B with respect to values of $\Delta\text{AIC}=2.0$ and 1.6 (see Column 17 of Table 2), respectively. Moreover, we discovered that $E_{\gamma,\text{iso}}$ did not change when alternative spectral models were used, since energy fluence (erg cm^{-2}) integrated from energy flux ($\text{erg cm}^{-2}\text{s}^{-1}$) between the same time period and energy range (e.g., 1-10⁴ keV) based on various spectral models varied very little (Li 2019b, 2022). For the other two cases (GRB 101213A and GRB 140606B), neither $E_{p,z}$ nor $E_{\gamma,\text{iso}}$ altered after Band model application, which corresponds to a recent study (Li 2022), where we found that the derived spectral parameters deviated significantly in the “Band (preferred)-to-CPL (misused)” case, but did not occur in the “CPL (preferred)-to-Band (misused)” case (Li 2022). Both the Band+BB-like and CPL+BB-like bursts invoke a hybrid spectrum, with a subdominant thermal component occupying the left shoulder (below E_p) of the Band or CPL component. For the Band+BB-like bursts, the Band+BB model is statistically preferred for GRB 110721A, GRB 150314A, and GRB 150403A with respect to values of $\Delta\text{BIC}=-7.9$, -14.5, and -115.6 (see Column 14 of Table 4), respectively. One notable outlier in the $E_p - E_{\gamma,\text{iso}}$ plane is GRB 110721A. While the derived E_p from the Band greatly differs from that of the Band+BB, it still does not fall back to the region dominated by the Amati relation. The E_p of GRB 150403A changed moderately, but neither Band+BB nor Band did not exhibit a significant outlier in the $E_{p,z} - E_{\gamma,\text{iso}}$ plane. The last case is GRB 150314A, which has a negligible alter in E_p and falls well in the 3σ region of the IGRB $E_p - E_{\gamma,\text{iso}}$ correlation. For the CPL+BB-like bursts, the CPL+BB model is statistically preferred for GRB 131231A, and GRB 181020A with respect to values of $\Delta\text{BIC}=-331.2$, and -3.9, respectively. Both cases show moderate alterations of E_p when the Band model is reused, and neither case has a substantial outlier in the $E_{p,z} - E_{\gamma,\text{iso}}$ plane.

Several possibilities have been proposed by some authors to explain the outliers of the Amati correlation holding for long cosmological GRBs (Amati et al. 2002). For instance, (i) due to viewing angle effects with off-axis scenarios; (ii) the existence of a class of nearby and intrinsically faint GRBs with different properties with respect to “standard” GRBs; (iii) several earlier studies (e.g., Amati 2006) also point out that the Amati correlation can be used as a pseudo-redshift estimator for testing possible selection effects of GRBs with unknown redshifts. We, therefore, briefly discuss here the possible reasons for the three outliers (GRB 110721A, GRB 130702A, and GRB 140606B) observed in the $E_{p,z}-E_{\gamma,\text{iso}}$ plane of our IGRB sample. Interestingly, Berger (2011) suggested two possible redshifts ($z = 0.382$ or $z = 3.512$) for GRB 110721A based on a candidate optical counterpart reported in Greiner et al. (2011), with the former being preferred. To investigate whether the outlier (GRB 110721A) is caused by a pseudo-redshift, we conducted the following tests. By performing the model comparisons, we found that the Band+BB model superiors other single (e.g., Band) and hybrid (e.g., CPL+BB) models. The rest-frame peak energy $E_{p,z}=(1+z)E_p$, as well as isotropic total energy $E_{\gamma,\text{iso}} = 4\pi d_L^2 S_\gamma k_c / (1+z)$, can be calculated using the spectral parameters obtained from the Band+BB model fit (Table 4). We then plot the evolution of the redshift from 0.01 to 10 in the $E_{p,z}-E_{\gamma,\text{iso}}$ plane for these outliers (see dashed lines in Figure 5). To directly compare the possible values of redshift for the burst falling in the $E_{p,z}-E_{\gamma,\text{iso}}$ region with the possible values of redshift in the non- $E_{p,z}-E_{\gamma,\text{iso}}$ region, we use gray, black, and red to denote the low (from 0.01 to 1), intermediate (from 1 to 3), and high redshift (from 3 to 10) regions, respectively. Conclusively, our analysis indicates that $z = 3.512$ could be a preferred redshift candidate for maintaining the validity of the $E_{p,z}-E_{\gamma,\text{iso}}$ correlation. However, the redshifts of both GRB 130702A (Singer et al. 2013) and GRB 140606B (Perley et al. 2014) have been firmly measured. As a result, the method applied to GRB 110721A may not be applicable to GRB 130702A and GRB 140606B. For GRB 130702A, our refined spectral analysis suggests that the CPL model is a superior model compared to other models. With a redshift at $z=0.145$ (it is at a fairly close distance) and the spectral parameters obtained from the best fitting, where $E_p = (2+\alpha)E_c$, and one can calculate its isotropic total energy as $E_{\gamma,\text{iso}}=2.9_{-1.4}^{+3.1} \times 10^{50}$ erg. The unique feature of the event is its extremely low isotropic bolometric emission energy. Specifically, the presence of a bright supernova associated with GRB 130702A (D’Elia et al. 2015) implies that it is a nearby event. GRB 140606B is another event similar to GRB 130702A. Its spectroscopically associated type Ic-BL SN was reported in Cano et al. (2015). The time-integrated spectrum can be fitted by the CPL model with $\alpha=-1.19\pm 0.05$ and $E_c=532_{-111}^{+141}$ keV. With a redshift measured ($z=0.384$), the rest-frame peak energy ($E_{p,z} = 597_{-130}^{+162}$ keV) and

isotropic bolometric emission energy ($E_{\gamma,\text{iso}} = 2.9_{-0.5}^{+0.7} \times 10^{51}$ erg) can be calculated. This event is thus located outside the 3σ region of the IGRB Amati correlation (see Figure 5).

4. DISCUSSIONS

4.1. Comparison with Previous Samples

Our sample selection criteria differ from previous sample studies (e.g., Amati et al. 2008; Yonetoku et al. 2010) in several major ways. (i) In order to fully evaluate the various current GRB spectral models, we focus on the bursts observed by *Fermi*-GBM. (ii) In order to allow a “clean” study of the pulse properties of the energy-spectral correlations, we focus on a sample of well-defined single-pulse GRBs and well-separated multi-pulse GRBs. (iii) In order to investigate the spectral model-dependent properties of the Amati and Yonetoku relations, the E_p for each burst in our sample was obtained using a preferred spectral model by examining several frequently used spectral models. Based on these criteria, our sample selection may have a bias. Thus, an interesting question is whether the spectral-energy parameters we obtained differ from the previous samples in terms of statistical distributions. Here, we address the question of whether or not the spectral-energy properties of our sample are similar to those of the previous samples.

We compare the distributions of $E_{p,z}$ (Fig.1d), $E_{\gamma,\text{iso}}$ (Fig.1e), and $L_{p,\text{iso}}$ (Fig.1f), between our sample and the samples in Amati et al. (2008) and Yonetoku et al. (2010). Our sample is shown by the cyan dashed line while the sample defined in Amati et al. (2008) or Yonetoku et al. (2010) is displayed by the grey shaded area. The best Gaussian fit for each distribution, including the corresponding average values and standard deviations are summarized in Table 5. We find that both $E_{p,z}$ and $E_{\gamma,\text{iso}}$ in the sample defined in Amati et al. (2008) are approximately double for our sample. Using the 1-s peak spectral properties, we also compare the distributions of the $L_{p,\text{iso}}$ (Fig.1f) between our sample and the sample defined in Yonetoku et al. (2010). We find that $L_{p,\text{iso}}$ is similar between the samples (see Table 5). By using 2-dimensional plots, we also compare the samples in the $E_{p,z} - E_{\gamma,\text{iso}}$ and $E_{p,z} - L_{p,\text{iso}}$ planes (Figure 6). As shown in Figure 6, the amplitudes and slopes remain similar between our samples and the samples defined in Amati et al. (2008)(Figure 6d) and Yonetoku et al. (2010)(Figure 6e).

In order to perform an evaluation of consistency with previous studies to show quantitative consistency and/or validity between our study and the results present in the *Fermi*/GBM catalog. In Figure 6, we present the parameter comparison between our study and the results in Poolakkil et al. (2021) by using 2-dimensional plots. Three relevant parameters ($E_{p,z}$, $E_{\gamma,\text{iso}}$, and $L_{p,\text{iso}}$) representing the GRB rest frame properties were selected to be compared. We find that both $E_{p,z}$ (Figure 6a) and $L_{p,\text{iso}}$ (Figure 6c) are generally the same. However, $E_{\gamma,\text{iso}}$ (Figure 6b) found in Poolakkil et al. (2021) are systemically greater than that in our sample. This may be due to the fact that we have probably selected a slightly different duration from those in Poolakkil et al. (2021), which is the likely explanation of both $E_{p,z}$ and $L_{p,\text{iso}}$ being the same while the $E_{\gamma,\text{iso}}$ is different.

4.2. Possible explanations for the physical origins of the Band-like and CPL-like spectral-energy correlations

Despite these spectral-energy correlations have been widely studied in understanding the nature of GRBs, their physical origin is still under debate. Several possible explanations have been proposed in previous studies (i) the result of instrumental selection effects suggested by some authors (e.g., Nakar & Piran 2005; Band & Preece 2005; Butler et al. 2007; Kocevski 2012); This possibility was ruled out by some other authors (e.g., Nava et al. 2012) since the time-resolved $E_{p,z}-E_{\gamma,\text{iso}}$ and $E_{p,z}-L_{\gamma,\text{iso}}$ correlations found within individual GRBs are similar to each other (Liang et al. 2004; Frontera et al. 2012; Lu et al. 2012; Guiriec et al. 2013), and are also comparable to the $E_{p,z}-E_{\gamma,\text{iso}}$ and $E_{p,z}-L_{\gamma,\text{iso}}$ correlation described by the time-integrated spectral properties of different bursts. (ii) Moreover, a recent study (Xue 2021) shows in theory the universal correlations among GRBs’ spectral peak, total energy, luminosity and time duration T_{90} , provided that GRBs central engines are attributed to gravitational collapses of a massive stellar core or a binary coalescence.

We find that CPL-like GRBs and Band-like GRBs exhibit different Amati and Yonetoku correlations, suggesting that their radiation processes may be different. Several possible scenarios may be used to explain these results. First, due to the different spectral shapes. The spectral shape directly determines $E_{p,z}$ and $E_{\gamma,\text{iso}}$ ($L_{\gamma,\text{iso}}$), which leads to different spectral-energy correlations. Despite the CPL function being defined as the first part of the Band function, it is still highly debated whether CPL and Band functions have the same physical origins or whether CPL is just an approximation of Band at $\beta \ll 0$ (e.g., Li 2022). Based on the observed properties of the different distributions of β between the Band-like and CPL-like time-resolved spectra using a multipulse GRB sample (Li et al. 2021), Li (2022)

argues that Band and CPL may invoke different radiation mechanisms. Second, individual parameter changes. If CPL is just an approximation of Band at $\beta \ll 0$, this means that both CPL and Band should have the same E_p for a given spectrum. This possibility is also supported by some observational evidence (see Figure 9 in Li 2022). In this case, E_p is equally fixed since it is intrinsically the same in both the models, while $E_{\gamma, \text{iso}}$ changes due to the different spectral shapes that occur on the CPL and Band in the high-energy β segments, resulting in a different flux integral in the observed energy bands, which we call the β effect. For a given observed spectrum, the earlier the spectrum cuts, the less E_p will be observed, and the $E_{\gamma, \text{iso}}^{\text{cut}}$ will be smaller than the $E_{\gamma, \text{iso}}^{\text{Band}}$ due to $S_{\gamma}^{\text{cut}} < S_{\gamma}^{\text{Band}}$, where $E_{\gamma, \text{iso}}^{\text{cut}}$ and $E_{\gamma, \text{iso}}^{\text{Band}}$ are the $E_{\gamma, \text{iso}}$ that integrates the energy flux of the 1-10⁴ keV based on the CPL-like and Band-like spectra, respectively. In contrast, if the cut comes later, the E_p would be larger, and $E_{\gamma, \text{iso}}^{\text{cut}}$ will be closer to $E_{\gamma, \text{iso}}^{\text{Band}}$. That would result in a flatter increment of the CPL-like bursts than the Band-like bursts as observed in the $E_{p,z}$ - $E_{\gamma, \text{iso}}$ plane. Alternatively, if the Band-like and CPL-like spectra come from different physical origins, the CPL- E_p and Band- E_p may not be intrinsically the same, so both E_p and $E_{\gamma, \text{iso}}$ may be different. In this case, all possible cases ($E_{p,z} \propto E_{\gamma, \text{iso}}^{\delta}$ with $\delta_{\text{CPL}} < \delta_{\text{Band}}$, $\delta_{\text{CPL}} > \delta_{\text{Band}}$, and $\delta_{\text{CPL}} \simeq \delta_{\text{Band}}$) in the E_p - $E_{\gamma, \text{iso}}$ plane may be observed. The observations (see Figure 3 and Figure 4), however, are only consistent with the first case ($\delta_{\text{CPL}} < \delta_{\text{Band}}$). Nevertheless, we still cannot rule out the possibility that the CPL and Band originate from different physical origins. In this scenario, a natural interpretation is that the power law of the apparent CPL spectrum is a superposition of the convolution of multiple blackbody spectra in photospheres, and the exponential tail of the apparent CPL spectrum corresponds to the highest temperature of the blackbody spectrum (e.g., Ryde et al. 2010). The corresponding physical picture is that the photosphere photons observed at a given time interval, corresponding to one time bin in the spectral analysis, are assumed to be emitted from different thin shells, which is given by considering the fireball optical depth falling to a unity. Therefore, the photosphere blackbody spectrum at the given time interval determine the properties of the corresponding shells, and the entire CPL spectrum is conjugated by the photosphere emission from a sequence of such shells.

5. CONCLUSIONS

In this paper, we have studied the model-wise properties of GRB spectral-energy correlations by gathering all *Fermi*-detected GRBs with known redshift from July 2008 to May 2022. A complete GRB sample was created, consisting of 153 bursts (17 sGRBs and 136 lGRBs). Our analysis focuses on two important empirical correlations: the relation between the rest-frame peak energy $E_{p,z}$ and isotropic bolometric emission energy $E_{\gamma, \text{iso}}$ (the Amati relation), and the relation between the rest-frame peak energy $E_{p,z}$ and peak luminosity $L_{p, \text{iso}}$ (the Yonetoku relation). In order to investigate the model-wise properties of GRB spectral-energy correlations, we examined various frequently used spectral models by performing a detailed spectral analysis and model comparisons between various GRB spectral models and their hybrid versions, and all of the E_p are obtained from the best-modeled fits.

Using refined time-integrated spectral analysis and model comparison analysis, we selected 109 GRBs (including 9 sGRBs and 100 lGRBs) with well-measured E_p and measured redshift to investigate the model-wise Amati correlation. Via a spectral model-dependent analysis, we found 64 Band-like bursts, 45 CPL-like bursts, 6 Band+BB-like bursts, 5 CPL+BB-like bursts. For the sample as a whole, we found a tight correlation between rest-frame peak energy $E_{p,z}$ and isotropic bolometric emission energy $E_{\gamma, \text{iso}}$ ($E_{p,z} \propto E_{\gamma, \text{iso}}^{0.41 \pm 0.06}$) for our Band-like burst sample (sGRBs+lGRBs), while the CPL-like burst sample (sGRBs+lGRBs) in the $E_{p,z}$ - $E_{\gamma, \text{iso}}$ plane ($E_{p,z} \propto E_{\gamma, \text{iso}}^{0.00 \pm 0.13}$) do not follow the same correlation found in the Band-like burst sample, pointing toward the fact that the Amati correlation is tightly reliant on the model-wise properties. Similar results were also found between the Band-like lGRB sample ($E_{p,z} \propto E_{\gamma, \text{iso}}^{0.42 \pm 0.05}$) and the CPL-like lGRB sample ($E_{p,z} \propto E_{\gamma, \text{iso}}^{0.25 \pm 0.12}$).

By selecting the 1-s peak spectrum, we then repeated our analysis for the Yonetoku correlation as was done for the Amati correlation. We selected 92 GRBs (5 sGRBs and 87 lGRBs) with well-measured E_p and peak luminosity $L_{p, \text{iso}}$ to investigate the model-wise Yonetoku correlation. Via a spectral model-dependent analysis, we found 55 Band-like bursts, 37 CPL-like bursts, 5 Band+BB-like bursts, 8 CPL+BB-like bursts. We discovered that the Band-like burst samples and the CPL-like burst samples were still well-separated in the $E_{p,z}$ - $L_{p, \text{iso}}$ plane, which takes the form of $E_{p,z} \propto L_{p, \text{iso}}^{0.36 \pm 0.04}$ for the entire Band-like burst sample (sGRBs+lGRBs) and $E_{p,z} \propto L_{p, \text{iso}}^{0.40 \pm 0.12}$ for the full CPL-like burst sample (sGRBs+lGRBs); and $E_{p,z} \propto L_{p, \text{iso}}^{0.34 \pm 0.04}$ for the Band-like lGRB sample and $E_{p,z} \propto L_{p, \text{iso}}^{0.40 \pm 0.08}$ for the CPL-like lGRB sample, which may not be in line with earlier studies (Yonetoku et al. 2010) without distinguishing between the models.

The CPL-like bursts do not fall on the Band-like Amati and Yonetoku relations, suggesting distinct radiation processes. We then discussed several possible explanations, and suggested that the Band-like spectra could originate from a non-thermal emission component (such as synchrotron radiation), that the CPL-like spectra, on the other hand, could be attributed to a superposition of the convolution of multiple blackbody spectra in photospheres, and that the exponential tail of the apparent CPL spectrum corresponds to the highest temperature of the blackbody spectrum. This is also supported by several pieces of additional evidence. For example, an independent β distribution is found between the Band-like and CPL-like time-resolved spectral analysis (Li 2022).

We also found three notable outliers (GRB 110721A, GRB 130702A, and GRB 140606B) in the $E_{p,z}-E_{\gamma,iso}$ plane and discussed several possibilities, such as whether the selection of the spectral model could have contributed to the outliers in the $E_{p,z}-E_{\gamma,iso}$ plane. In order to maintain the validity of the $E_{p,z}-E_{\gamma,iso}$ correlation, the redshift candidate of $z = 3.512$ is the more trustworthy between the two redshift candidates ($z = 0.382$ and $z = 3.512$) of GRB 110721A as suggested by Berger (2011). We also found that GRB 130702A is consistent with the existence of a class of nearby and intrinsically faint GRBs with different properties with respect to “standard” GRBs as first found in Amati et al. (2002).

ACKNOWLEDGMENTS

I thank the anonymous referee for valuable comments and suggestions. I also thank Maria Dainotti, Rahim Moradi, J.-L. Atteia, and the ICRANet members for many helpful discussions on GRB physics and phenomena. This research is made use of the High Energy Astrophysics Science Archive Research Center (HEASARC) Online Service at the NASA/Goddard Space Flight Center (GSFC).

Facilities: *Fermi*/GBM

Software: 3ML (Vianello et al. 2015), matplotlib (Hunter 2007), NumPy (Harris et al. 2020; van der Walt et al. 2011), SciPy (Virtanen et al. 2020), *lmfit* (Newville et al. 2016), astropy (Astropy Collaboration et al. 2013), pandas (Reback et al. 2022), seaborn (Waskom et al. 2017), PyMC3 (Salvatier et al. 2016)

REFERENCES

- Abdo, A. A., Ackermann, M., Arimoto, M., et al. 2009, *Science*, 323, 1688
- Akaike, H. 1974, *IEEE Transactions on Automatic Control*, 19, 716
- Amati, L. 2006, *MNRAS*, 372, 233
- . 2010, arXiv e-prints, arXiv:1002.2232
- Amati, L., Guidorzi, C., Frontera, F., et al. 2008, *MNRAS*, 391, 577
- Amati, L., Frontera, F., Tavani, M., et al. 2002, *A&A*, 390, 81
- Astropy Collaboration, Robitaille, T. P., Tollerud, E. J., et al. 2013, *A&A*, 558, A33
- Atwood, W. B., Abdo, A. A., Ackermann, M., et al. 2009, *ApJ*, 697, 1071
- Axelsson, M., Baldini, L., Barbiellini, G., et al. 2012, *ApJL*, 757, L31
- Band, D., Matteson, J., Ford, L., et al. 1993, *ApJ*, 413, 281
- Band, D. L., & Preece, R. D. 2005, *ApJ*, 627, 319
- Barthelmy, S. D., Barbier, L. M., Cummings, J. R., et al. 2005, *SSRv*, 120, 143
- Berger, E. 2011, *GRB Coordinates Network*, 12193, 1
- Burgess, J. M., Greiner, J., Bégué, D., & Berlato, F. 2019, *MNRAS*, 490, 927
- Butler, N. R., Kocevski, D., Bloom, J. S., & Curtis, J. L. 2007, *ApJ*, 671, 656
- Cano, Z., de Ugarte Postigo, A., Perley, D., et al. 2015, *MNRAS*, 452, 1535
- Chib, S., & Winkelmann, R. 2001, *Journal of Business & Economic Statistics*, 19, 428
- Dainotti, M., Del Vecchio, R., & Tarnopolski, M. 2016, arXiv e-prints, arXiv:1612.00618
- Dainotti, M., Petrosian, V., Willingale, R., et al. 2015, *MNRAS*, 451, 3898
- Dainotti, M. G., & Amati, L. 2018, *PASP*, 130, 051001
- Dainotti, M. G., Cardone, V. F., & Capozziello, S. 2008, *MNRAS*, 391, L79
- Dainotti, M. G., & Del Vecchio, R. 2017, *NewAR*, 77, 23
- Dainotti, M. G., Nagataki, S., Maeda, K., Postnikov, S., & Pian, E. 2017, *A&A*, 600, A98

- Dainotti, M. G., Petrosian, V., Singal, J., & Ostrowski, M. 2013, *ApJ*, 774, 157
- Dainotti, M. G., Willingale, R., Capozziello, S., Fabrizio Cardone, V., & Ostrowski, M. 2010, *ApJL*, 722, L215
- D’Elia, V., Pian, E., Melandri, A., et al. 2015, *A&A*, 577, A116
- Frontera, F., Amati, L., Guidorzi, C., Landi, R., & in’t Zand, J. 2012, *ApJ*, 754, 138
- Ghirlanda, G., Bosnjak, Z., Ghisellini, G., Tavecchio, F., & Firmani, C. 2007, *MNRAS*, 379, 73
- Ghirlanda, G., Ghisellini, G., & Celotti, A. 2004, *A&A*, 422, L55
- Ghirlanda, G., Nava, L., Ghisellini, G., Celotti, A., & Firmani, C. 2009, *A&A*, 496, 585
- Greiner, J., Updike, A. C., Kruehler, T., & Sudilovsky, V. 2011, *GRB Coordinates Network*, 12192, 1
- Gruber, D., Goldstein, A., Weller von Ahlefeld, V., et al. 2014, *ApJS*, 211, 12
- Guiriec, S., Daigne, F., Hascoët, R., et al. 2013, *ApJ*, 770, 32
- Guiriec, S., Kouveliotou, C., Daigne, F., et al. 2015, *ApJ*, 807, 148
- Harris, C. R., Millman, K. J., van der Walt, S. J., et al. 2020, *Nature*, 585, 357
- Heussaff, V., Atteia, J. L., & Zolnierowski, Y. 2013, *A&A*, 557, A100
- Hunter, J. D. 2007, *Computing in Science and Engineering*, 9, 90
- Iyyani, S., Ryde, F., Axelsson, M., et al. 2013, *MNRAS*, 433, 2739
- Kocevski, D. 2012, *ApJ*, 747, 146
- Kouveliotou, C., Meegan, C. A., Fishman, G. J., et al. 1993, *ApJL*, 413, L101
- Li, L. 2019a, *ApJS*, 242, 16
- . 2019b, *ApJS*, 245, 7
- . 2020, *ApJ*, 894, 100
- . 2022, *ApJ*, 941, 27
- Li, L., Ryde, F., Pe’er, A., Yu, H.-F., & Acuner, Z. 2021, *ApJS*, 254, 35
- Li, L., & Zhang, B. 2021, *ApJS*, 253, 43
- Li, L., Geng, J.-J., Meng, Y.-Z., et al. 2019, *ApJ*, 884, 109
- Liang, E., & Zhang, B. 2005, *ApJ*, 633, 611
- Liang, E. W., Dai, Z. G., & Wu, X. F. 2004, *ApJL*, 606, L29
- Lu, R.-J., Wei, J.-J., Liang, E.-W., et al. 2012, *ApJ*, 756, 112
- Meegan, C., Lichti, G., Bhat, P. N., et al. 2009, *ApJ*, 702, 791
- Minaev, P. Y., & Pozanenko, A. S. 2020, *MNRAS*, 492, 1919
- Nakar, E., & Piran, T. 2005, *MNRAS*, 360, L73
- Narayana Bhat, P., Meegan, C. A., von Kienlin, A., et al. 2016, *ApJS*, 223, 28
- Nava, L., Salvaterra, R., Ghirlanda, G., et al. 2012, *MNRAS*, 421, 1256
- Newville, M., Stensitzki, T., Allen, D. B., et al. 2016, *ascl*
- Pe’er, A., Mészáros, P., & Rees, M. J. 2006, *ApJ*, 642, 995
- Perley, D. A., Cao, Y., Kasliwal, M., & Kirby, E. 2014, *GRB Coordinates Network*, 16365, 1
- Planck Collaboration, Aghanim, N., Akrami, Y., et al. 2018, *arXiv e-prints*, arXiv:1807.06209
- Poolakkil, S., Preece, R., Fletcher, C., et al. 2021, *ApJ*, 913, 60
- Qin, Y.-P., & Chen, Z.-F. 2013, *MNRAS*, 430, 163
- Reback, J., jbrockmendel, McKinney, W., et al. 2022, *pandas-dev/pandas: Pandas 1.4.2*, Zenodo, doi:10.5281/zenodo.3509134
- Rees, M. J., & Meszaros, P. 1994, *ApJL*, 430, L93
- Rees, M. J., & Mészáros, P. 2005, *ApJ*, 628, 847
- Ryde, F., Axelsson, M., Zhang, B. B., et al. 2010, *ApJL*, 709, L172
- Salvatier, J., Wiecki, T. V., & Fonnesbeck, C. 2016, *PyMC3: Python probabilistic programming framework*, *Astrophysics Source Code Library*, , , ascl:1610.016
- Schwarz, G. 1978, *Annals of Statistics*, 6, 461
- Singer, L. P., Cenko, S. B., Kasliwal, M. M., et al. 2013, *ApJL*, 776, L34
- van der Walt, S., Colbert, S. C., & Varoquaux, G. 2011, *Computing in Science and Engineering*, 13, 22
- Vereshchagin, G., Li, L., & Bégué, D. 2022, *MNRAS*, 512, 4846
- Vianello, G., Lauer, R. J., Younk, P., et al. 2015, *arXiv e-prints*, arXiv:1507.08343
- Virtanen, P., Gommers, R., Oliphant, T. E., et al. 2020, *Nature Methods*, 17, 261
- von Kienlin, A., Meegan, C. A., Paciesas, W. S., et al. 2014, *ApJS*, 211, 13
- . 2020, *ApJ*, 893, 46
- Wang, F. Y., Dai, Z. G., & Liang, E. W. 2015, *NewAR*, 67, 1
- Waskom, M., Botvinnik, O., O’Kane, D., et al. 2017, *Mwaskom/Seaborn: V0.8.1 (September 2017)*, Zenodo, v.v0.8.1, Zenodo, doi:10.5281/zenodo.883859
- Xu, F., Tang, C.-H., Geng, J.-J., et al. 2021, *ApJ*, 920, 135
- Xu, M., & Huang, Y. F. 2012, *A&A*, 538, A134
- Xue, S.-S. 2021, *JCAP*, 2021, 044
- Yonetoku, D., Murakami, T., Nakamura, T., et al. 2004, *ApJ*, 609, 935

- Yonetoku, D., Murakami, T., Tsutsui, R., et al. 2010, PASJ, 62, 1495
- Yu, H.-F., Dereli-Bégué, H., & Ryde, F. 2019, ApJ, 886, 20
- Yu, H.-F., Preece, R. D., Greiner, J., et al. 2016, A&A, 588, A135
- Zhang, B. 2018, The Physics of Gamma-Ray Bursts, doi:10.1017/9781139226530
- Zhang, B., Zhang, B.-B., Virgili, F. J., et al. 2009, ApJ, 703, 1696
- Zhang, F.-W., Shao, L., Yan, J.-Z., & Wei, D.-M. 2012, ApJ, 750, 88
- Zhang, Z. B., Zhang, C. T., Zhao, Y. X., et al. 2018, PASP, 130, 054202

Table 1. Global Properties of the Sample

GRB	z	T_{90}	$T_{90}/(1+z)$	S_γ	Detectors	$[\Delta T_{(bkg,1)}, \Delta T_{(bkg,2)}]$	Averaged Spectrum	Classified
(1)	(2)	(s)	(s)	(erg.cm^{-2})	(6)	(s)	(E_p)	(9)
(1)	(2)	(3)	(4)	(5)	(6)	(7)	(8)	(9)
sGRBs								
080905(499)	0.1218	0.960±0.345	0.86±0.31	$(8.50\pm0.46)\times10^{-7}$	n3(n6)n7b0	(-20 to -10, 20 to 40)	Unconstrained	Short
090510(016)	0.903	0.960±0.138	0.50±0.07	$(3.37\pm0.04)\times10^{-6}$	(n6)n7n9b1	(-20 to -10, 20 to 40)	CPL	Short
090927(422)	1.37	0.512±0.231	0.22±0.10	$(3.03\pm0.18)\times10^{-7}$	n2n9(na)b1	(-20 to -10, 40 to 60)	Unconstrained	Short
100117A(879)	0.92	0.256±0.834	0.13±0.43	$(4.23\pm0.69)\times10^{-7}$	n3(n4)n8b0	(-20 to -10, 20 to 50)	CPL	Short
100206A(563)	0.4068	0.176±0.072	0.13±0.05	$(7.57\pm0.11)\times10^{-7}$	(n0)n1n3b0	(-20 to -10, 30 to 60)	CPL	Short
100625A(773)	0.452	0.240±0.276	0.17±0.19	$(5.63\pm0.25)\times10^{-7}$	(n4)b0	(-20 to -10, 20 to 40)	CPL	Short
100816A(026)	0.8049	2.045±0.229	1.13±0.13	$(3.65\pm0.05)\times10^{-6}$	n7n8(nb)b1	(-20 to -10, 40 to 60)	Band	Short
101224AS(227)	0.7180	1.728±1.680	1.01±0.98	$(1.91\pm0.27)\times10^{-7}$	n3n4(n5)b0	(-20 to -10, 20 to 40)	Unconstrained	Short
111117A(510)	2.211	0.432±0.082	0.13±0.03	$(5.64\pm0.13)\times10^{-7}$	n6n7(n9)b1	(-20 to -10, 20 to 40)	CPL	Short
131004A(904)	0.717	1.152±0.590	0.67±0.34	$(5.10\pm0.19)\times10^{-7}$	n9(na)b1	(-20 to -10, 20 to 40)	Unconstrained	Short
141004A(973)	0.573	2.560±0.607	1.63±0.39	$(1.18\pm0.03)\times10^{-6}$	n9(na)b0	(-40 to -10, 30 to 60)	CPL	Short
150101B(641)	0.134	0.080±0.928	0.07±0.82	$(2.38\pm0.15)\times10^{-7}$	n6(n7)n9b1	(-20 to -10, 20 to 40)	Unconstrained	Short
160624A(477)	0.483	0.384±0.405	0.26±0.27	$(3.92\pm0.08)\times10^{-7}$	n2n9nab1	(-20 to -10, 20 to 40)	Unconstrained	Short
160821B(937)	0.16	1.088±0.977	0.94±0.84	$(1.95\pm0.20)\times10^{-7}$	n7(n9)n1b1	(-20 to -10, 20 to 40)	Unconstrained	Short
170817A(529)	0.009783	2.048±0.466	2.03±0.46	$(2.79\pm0.17)\times10^{-7}$	n1(n2)n5b0	(-50 to -10, 10 to 50)	Unconstrained	Short
200826A(187)	0.7481	1.136±0.132	0.65±0.08	$(4.26\pm0.02)\times10^{-6}$	n6n7(n8)n9b1	(-20 to -10, 40 to 60)	Band	Short
201221D(963)	1.046	0.144±0.066	0.07±0.03	$(6.34\pm0.24)\times10^{-7}$	n6n7(n8)b1	(-25 to -5, 5 to 30)	Band	Short
IGRBs								
080810(549)	3.35	75.201±3.638	17.29±0.83	$(9.44\pm0.05)\times10^{-6}$	n7(nb)b1	(-25 to -5, 100 to 150)	Unconstrained	M
080905(705)	2.374	105.984±6.802	31.41±2.02	$(2.91\pm0.04)\times10^{-6}$	n7n8(nb)b1	(-25 to -5, 120 to 200)	Unconstrained	M
080916(406)	0.689	46.337±7.173	27.43±4.25	$(7.81\pm0.08)\times10^{-6}$	n7(n8)b1	(-30 to -10, 80 to 120)	CPL	M
080928(628)	1.692	14.336±4.007	5.33±1.49	$(1.17\pm0.04)\times10^{-6}$	(n3)n6n7b0	(-25 to -5, 40 to 80)	Unconstrained	M
081109(293)	0.9787	58.369±5.221	29.50±2.64	$(6.55\pm0.06)\times10^{-6}$	n2n9(na)b1	(-20 to -10, 80 to 120)	Unconstrained	S
081121(858)	2.512	41.985±8.510	11.95±2.42	$(1.53\pm0.02)\times10^{-5}$	(na)nbb1	(-30 to -10, 60 to 100)	CPL	S
081221(681)	2.26	29.697±0.410	9.11±0.13	$(3.00\pm0.01)\times10^{-5}$	n1(n2)b0	(-30 to -10, 60 to 100)	CPL	M
081222(204)	2.77	18.880±2.318	5.01±0.61	$(1.19\pm0.01)\times10^{-5}$	n0(n1)n2b0	(-30 to -10, 50 to 100)	Band	S
090102(122)	1.547	26.624±0.810	10.45±0.32	$(2.79\pm0.01)\times10^{-5}$	n9na(nb)b1	(-30 to -10, 60 to 120)	CPL	M
090113(778)	1.7493	17.408±3.238	6.34±1.18	$(1.57\pm0.05)\times10^{-6}$	n0(n1)n9b1	(-30 to -10, 40 to 80)	Unconstrained	M
090323(002)	3.57	133.890±0.572	29.30±0.13	$(1.08\pm0.0004)\times10^{-4}$	n7(n9)nbb1	(-20 to -5, 150 to 200)	Band	M
090328(401)	0.736	61.697±1.810	35.54±1.04	$(4.20\pm0.006)\times10^{-5}$	n6n7(n8)b1	(-30 to -5, 100 to 200)	CPL	M
090423(330)	8.26	7.168±2.415	0.77±0.26	$(8.16\pm0.72)\times10^{-7}$	n2(n9)nab1	(-25 to -5, 50 to 100)	Unconstrained	M
090424(592)	0.544	14.144±0.264	9.16±0.17	$(4.63\pm0.003)\times10^{-5}$	(n7)n8nbb1	(-25 to -10, 40 to 80)	CPL+BB	M
090516(353)	4.109	123.138±2.064	24.10±0.40	$(1.63\pm0.008)\times10^{-5}$	n0(n3)b0	(-25 to -10, 150 to 200)	Unconstrained	M
090529(564)	2.625	9.853±0.179	2.72±0.05	$(8.69\pm0.03)\times10^{-6}$	n3(n4)n8b1	(-20 to -10, 40 to 60)	CPL	M
090618(353)	0.54	112.386±1.086	72.98±0.71	$(2.68\pm0.01)\times10^{-4}$	(n4)b0	(-25 to -5, 200 to 250)	CPL+BB	M
090902B(462)	1.822	19.328±0.286	6.85±0.10	$(2.22\pm0.003)\times10^{-4}$	n0(n1)n9b0	(-25 to -10, 50 to 100)	CPL+BB	S
090926(181)	2.1062	13.760±0.286	4.43±0.09	$(1.47\pm0.003)\times10^{-4}$	n3n6(n7)b1	(-25 to -5, 40 to 80)	Band	M
090926B(914)	1.24	64.001±1.557	28.57±0.70	$(1.05\pm0.01)\times10^{-5}$	n7(n8)nbb1	(-25 to -5, 100 to 150)	Band	S
091003(191)	0.8969	20.224±0.362	10.66±0.19	$(2.33\pm0.008)\times10^{-5}$	n3(n6)b1	(-25 to -5, 40 to 80)	CPL	M
091020(900)	1.71	24.256±7.973	8.95±2.94	$(8.35\pm0.15)\times10^{-6}$	n2(n5)b0	(-30 to -10, 60 to 100)	CPL	S
091024(372)	1.092	93.954±5.221	44.91±2.50	$(8.56\pm0.06)\times10^{-6}$	(nb)b1	(-20 to -5, 100 to 150)	Unconstrained	S
091127(976)	0.49	8.701±0.571	5.84±0.38	$(2.07\pm0.003)\times10^{-5}$	(n6)n7n9b1	(-20 to -5, 20 to 60)	Band	M
091208B(410)	1.063	12.480±5.018	6.05±2.43	$(6.19\pm0.19)\times10^{-6}$	(n9)nab1	(-20 to -5, 20 to 100)	CPL	M
100414A(097)	1.368	26.497±2.073	11.19±0.88	$(8.85\pm0.02)\times10^{-5}$	n7n9(nb)b1	(-25 to -10, 40 to 60)	CPL	S
100615A(083)	1.398	37.377±0.979	15.59±0.41	$(8.72\pm0.08)\times10^{-6}$	n6n7(n8)b1	(-30 to -10, 50 to 100)	CPL	M
100728A(095)	1.567	165.378±2.896	64.43±1.13	$(1.28\pm0.006)\times10^{-4}$	n0(n1)b0	(-25 to -5, 220 to 250)	CPL+BB	M
100728B(439)	2.106	10.240±1.846	3.30±0.59	$(3.34\pm0.06)\times10^{-6}$	n6(n7)n8b1	(-15 to -5, 30 to 60)	CPL	S

Table 1 continued on next page

Table 1 (continued)

GRB	z	T_{90}	$T_{90}/(1+z)$	S_{γ}	Detectors	$[\Delta T_{(\text{bkg},1)}, \Delta T_{(\text{bkg},2)}]$	Averaged Spectrum	Classified
(1)	(2)	(s)	(s)	($\text{erg}\cdot\text{cm}^{-2}$)	(6)	(s)	(E_p)	(9)
100814A(160)	1.44	150.530±1.619	61.69±0.66	(1.49±0.01)×10 ⁻⁵	n7(n8)b1	(-20 to -5, 200 to 250)	CPL	M
100906A(576)	1.727	110.594±2.828	40.56±1.04	(2.33±0.006)×10 ⁻⁵	(nb)b1	(-25 to -5, 150 to 200)	Band	M
101213A(451)	0.414	45.057±1.950	31.86±1.38	(7.40±0.10)×10 ⁻⁶	n2(n5)b0	(-20 to -10, 100 to 200)	CPL	S
101219B(686)	0.55	51.009±1.775	32.91±1.15	(3.99±0.05)×10 ⁻⁶	n3n6(n7)b1	(-25 to -5, 60 to 100)	Unconstrained	M
110106B(893)	0.618	35.521±3.612	21.95±2.23	(4.11±0.06)×10 ⁻⁶	n9na(nb)b1	(-25 to -5, 50 to 100)	Unconstrained	M
110128A(073)	2.339	12.160±4.971	3.64±1.49	(1.43±0.10)×10 ⁻⁶	n6(n7)n9b1	(-25 to -5, 50 to 100)	Unconstrained	S
110213A(220)	1.46	34.305±1.639	13.95±0.67	(9.37±0.05)×10 ⁻⁶	n3(n4)b0	(-20 to -5, 50 to 100)	CPL	M
110721A(200)	0.3820	21.822±0.572	15.79±0.41	(3.70±0.004)×10 ⁻⁵	(n6)n7n9b1	(-30 to -10, 40 to 60)	Band+BB	S
110731A(465)	2.83	7.485±0.572	1.95±0.15	(2.29±0.006)×10 ⁻⁵	(n0)n3b0	(-20 to -10, 40 to 60)	Band	S
110818A(860)	3.36	67.073±3.916	15.38±0.90	(5.15±0.03)×10 ⁻⁶	n7n8(nb)b1	(-50 to -20, 100 to 150)	CPL	S
111107A(035)	2.893	12.032±0.923	3.09±0.24	(9.07±0.35)×10 ⁻⁷	n4(n8)b1	(-25 to -10, 50 to 100)	Unconstrained	M
111228A(657)	0.714	99.842±2.111	58.25±1.23	(1.81±0.01)×10 ⁻⁵	n7(n8)b1	(-30 to -20, 80 to 120)	Band	M
120118B(709)	2.943	37.825±12.586	9.59±3.19	(2.66±0.05)×10 ⁻⁶	(n6)n8b1	(-40 to -10, 60 to 100)	Unconstrained	S
120119A(170)	1.728	55.297±6.229	20.27±2.28	(3.87±0.01)×10 ⁻⁵	n9na(nb)b1	(-30 to -5, 100 to 150)	Band	S
120326A(056)	1.798	11.776±1.810	4.21±0.65	(3.26±0.05)×10 ⁻⁶	n0(n1)n2b1	(-25 to -10, 30 to 60)	Band	S
120624B(933)	2.1974	271.364±4.580	84.87±1.43	(1.92±0.002)×10 ⁻⁴	n1(n2)nab0	(-25 to -10, 40 to 100)	CPL	M
120711A(115)	1.405	44.033±0.724	18.31±0.52	(1.94±0.01)×10 ⁻⁴	(n2)nab0	(-25 to -10, 150 to 200)	CPL	M
120712A(571)	4.1745	22.528±5.431	4.35±1.05	(4.43±0.05)×10 ⁻⁶	(n3)n6n7b1	(-50 to -10, 50 to 100)	Band	S
120716A(712)	2.486	226.048±1.056	64.84±0.30	(1.27±0.01)×10 ⁻⁵	(n9)nanbb1	(-30 to -5, 50 to 150)	CPL	M
120729A(456)	0.80	25.472±2.612	14.15±1.45	(5.08±0.05)×10 ⁻⁶	n1(n2)b0	(-50 to -20, 40 to 80)	Band	S
120811C(649)	2.671	14.336±6.557	3.91±1.79	(3.45±0.21)×10 ⁻⁶	n4(n8)b1	(-30 to -10, 20 to 100)	Unconstrained	S
120907A(017)	0.970	5.760±1.778	2.92±0.90	(8.09±0.41)×10 ⁻⁷	(n4)b0	(-20 to -10, 40 to 60)	Unconstrained	S
120909A(070)	3.93	112.066±10.419	22.73±2.11	(9.85±0.15)×10 ⁻⁶	n6n7(n8)b1	(-25 to -5, 150 to 200)	Band	M
121128A(212)	2.20	17.344±0.923	5.42±0.29	(9.30±0.11)×10 ⁻⁶	n3(n4)b0	(-50 to -10, 50 to 100)	Band	M
121211A(574)	1.023	5.632±1.717	2.78±0.85	(6.41±0.39)×10 ⁻⁷	(n3)n4n5b0	(-50 to -10, 50 to 100)	Unconstrained	M
130215A(063)	0.597	143.746±13.029	90.01±8.16	(1.86±0.03)×10 ⁻⁵	n1(n2)nab0	(-100 to -50, 150 to 200)	Band	S
130420A(313)	1.297	104.962±8.809	45.70±3.84	(1.16±0.02)×10 ⁻⁵	n2(na)b1	(-100 to -50, 50 to 100)	CPL	S
130427A(324)	0.3399	138.242±3.238	103.17±2.42	(2.46±0.001)×10 ⁻³	n6(n9)nab1	(-30 to -10, 80 to 100)	Band	M
130518A(580)	2.488	48.577±0.916	13.93±0.26	(9.46±0.02)×10 ⁻⁵	(n3)n6n7b1	(-50 to -20, 100 to 150)	Band	M
130610A(133)	2.092	21.760±1.639	7.04±0.53	(3.54±0.05)×10 ⁻⁶	n7(n8)b1	(-100 to -50, 50 to 200)	CPL	S
130612A(141)	2.006	7.424±6.192	2.47±2.06	(6.80±0.63)×10 ⁻⁷	n6n7(n9)b1	(-40 to -10, 30 to 60)	Unconstrained	S
130702A(004)	0.145	58.881±6.192	51.42±5.41	(5.72±0.12)×10 ⁻⁶	n6n7(n8)b1	(-100 to -10, 100 to 200)	...	S
130925A(173)	0.347	215.555±1.810	160.03±1.34	(8.48±0.03)×10 ⁻⁵	n6(n7)n9b1	(-120 to -50, 300 to 320)	Band	M
131011A(741)	1.874	77.057±2.996	26.81±1.04	(8.88±0.06)×10 ⁻⁶	n9na(nb)b1	(-100 to -50, 100 to 150)	Band	S
131105A(087)	1.686	112.642±0.462	41.94±0.17	(2.38±0.01)×10 ⁻⁵	n6(n7)n8b1	(-50 to -10, 150 to 200)	CPL	M
131108A(862)	2.40	18.176±0.572	5.35±0.17	(3.57±0.01)×10 ⁻⁵	n3(n6)n7b1	(-40 to -10, 40 to 80)	Band	M
131231A(198)	0.642	31.232±0.572	19.02±0.35	(1.52±0.001)×10 ⁻⁴	n0(n3)n4b0	(-50 to -10, 100 to 150)	CPL+BB	M
140206A(275)	2.73	146.690±4.419	39.33±1.18	(1.23±0.01)×10 ⁻⁴	n0(n1)n3b0	(-50 to -10, 70 to 100)	Band	M
140213A(807)	1.2076	18.624±0.716	8.44±0.32	(2.12±0.01)×10 ⁻⁵	n0(n1)n2b0	(-40 to -10, 40 to 80)	Band	M
140423A(356)	3.26	95.233±11.585	22.36±2.72	(1.81±0.01)×10 ⁻⁵	n6(n9)b1	(-20 to -5, 100 to 200)	Unconstrained	M
140506A(880)	0.889	64.128±2.005	33.95±1.06	(6.59±0.12)×10 ⁻⁶	(n2)n5b0	(-100 to -10, 20 to 100)	Band	S
140508A(128)	1.027	44.288±0.231	21.85±0.11	(6.14±0.01)×10 ⁻⁵	(na)b1	(-40 to -10, 80 to 120)	Band	M
140512A(814)	0.725	147.970±2.360	85.78±1.37	(2.93±0.01)×10 ⁻⁵	n0(n1)n3b0	(-50 to -10, 200 to 240)	CPL	M
140606B(133)	0.384	22.784±2.064	16.46±1.49	(7.59±0.04)×10 ⁻⁶	n3(n4)n7b0	(-50 to -10, 40 to 100)	CPL	S
140620A(219)	2.04	45.825±12.130	15.07±3.99	(6.15±0.06)×10 ⁻⁶	n8(nb)b1	(-100 to -50, 60 to 100)	Band	S
140623A(224)	1.92	111.104±3.999	38.05±1.37	(3.22±0.05)×10 ⁻⁶	(n0)n1n9b1	(-40 to -10, 150 to 200)	Unconstrained	M
140703A(026)	3.14	83.969±2.996	20.28±0.72	(7.57±0.05)×10 ⁻⁶	n0(n1)n3b1	(-50 to -10, 100 to 150)	CPL	S
140801A(792)	1.32	7.168±0.572	3.09±0.25	(1.24±0.004)×10 ⁻⁵	n1(n2)nab0	(-40 to -10, 20 to 50)	Band	M
140808A(038)	3.29	4.477±0.362	1.04±0.08	(3.21±0.03)×10 ⁻⁶	(n3)n4b0	(-40 to -10, 40 to 70)	Band	S
140907A(672)	1.21	35.841±5.473	16.22±2.48	(6.45±0.06)×10 ⁻⁶	n0n1(n3)b0	(-50 to -10, 60 to 100)	CPL	S
141028A(455)	2.33	31.489±2.429	9.46±0.73	(3.48±0.01)×10 ⁻⁵	(n6)n7n9b1	(-100 to -50, 50 to 100)	Band	S
141220A(252)	1.3195	7.616±0.923	3.28±0.40	(5.34±0.04)×10 ⁻⁶	n0(n3)n4b0	(-40 to -10, 30 to 60)	CPL	S

Table 1 continued on next page

Table 1 (continued)

GRB	z	T_{90}	$T_{90}/(1+z)$	S_{γ}	Detectors	$[\Delta T_{(\text{bkg},1)}, \Delta T_{(\text{bkg},2)}]$	Averaged Spectrum	Classified
(1)	(2)	(s)	(s)	(erg.cm^{-2})	(6)	(s)	(E_p)	(9)
141221A(338)	1.452	23.808±1.717	9.71±0.70	(4.07±0.06)×10 ⁻⁶	(n1)n2b0	(-100 to -50, 100 to 150)	CPL	M
141225A(959)	0.915	56.320±4.891	29.41±2.55	(3.73±0.04)×10 ⁻⁶	(na)nab1	(-50 to -10, 100 to 150)	Band	S
150301B(818)	1.5169	13.312±1.557	5.29±0.62	(3.09±0.03)×10 ⁻⁶	n3n6(n7)b0	(-40 to -10, 50 to 100)	CPL	S
150314A(205)	1.758	10.688±0.143	3.88±0.05	(8.16±0.01)×10 ⁻⁵	n1(n9)b1	(-40 to -10, 30 to 60)	Band+BB	S
150403A(913)	2.06	22.272±0.810	7.28±0.26	(5.47±0.006)×10 ⁻⁵	(n3)n4b0	(-50 to -10, 50 to 150)	Band+BB	S
150514A(774)	0.807	10.813±1.072	5.98±0.59	(4.74±0.05)×10 ⁻⁶	n0(n3)n4b0	(-50 to -10, 50 to 100)	Band	S
150727A(793)	0.313	49.409±3.974	37.63±3.03	(4.42±0.06)×10 ⁻⁶	(n3)n4n6b0	(-50 to -40)	Unconstrained	S
150821A(406)	0.755	103.426±5.753	58.93±3.28	(5.21±0.03)×10 ⁻⁵	(n9)nab1	(-50 to -20, 160 to 200)	Band	M
151027A(166)	0.81	123.394±1.145	68.17±0.63	(1.41±0.01)×10 ⁻⁵	(n0)n1n2b0	(-50 to -10, 200 to 250)	CPL	M
160509A(374)	1.17	369.670±0.810	170.35±0.37	(1.79±0.01)×10 ⁻⁴	(n0)n1n3b0	(-50 to -20, 200 to 240)	Band+BB	M
160623A(209)	0.367	107.776±8.693	78.84±6.36	(3.96±0.07)×10 ⁻⁶	n7(n8)b1	(-50 to -10, 100 to 150)	Unconstrained	S
160625B(945)	1.406	453.385±0.572	188.44±0.24	(6.43±0.01)×10 ⁻⁴	(n6)n7n9b1	(-50 to -20, 80 to 120)	Band+BB	M
160629A(930)	3.332	64.769±0.923	14.95±0.21	(1.31±0.004)×10 ⁻⁵	(n7)n8nbb1	(-50 to -10, 100 to 150)	CPL	M
160804A(065)	0.736	131.586±21.723	75.80±12.51	(1.62±0.02)×10 ⁻⁵	n3(n4)n8b0	(-130 to -90, 100 to 150)	CPL	S
161014A(522)	2.823	36.609±1.493	9.58±0.39	(6.10±0.05)×10 ⁻⁶	(n9)nanbb1	(-60 to -20, 80 to 120)	CPL	M
161017A(745)	2.013	37.888±10.861	12.57±3.60	(4.86±0.06)×10 ⁻⁶	(n5)b0	(-100 to -10, 100 to 200)	CPL	S
161117A(066)	1.549	122.178±0.659	47.93±0.26	(3.12±0.01)×10 ⁻⁵	n1(n2)b0	(-100 to -20, 200 to 250)	CPL	M
161129A(300)	0.645	36.096±0.724	21.94±0.44	(6.54±0.04)×10 ⁻⁶	n3(n4)n8b0	(-80 to -10, 100 to 250)	Band	M
170113A(420)	1.968	49.152±4.136	16.56±1.39	(2.04±0.08)×10 ⁻⁶	(n8)nbb1	(-100 to -10, 100 to 200)	Unconstrained	M
170214A(649)	2.53	122.882±0.724	34.81±0.21	(1.77±0.001)×10 ⁻⁴	n0(n1)n9b0	(-120 to -80, 180 to 300)	Band	M
170405A(777)	3.510	78.593±0.572	17.43±0.13	(7.40±0.007)×10 ⁻⁵	n7(n8)nbb1	(-80 to -20, 100 to 150)	Band	M
170607A(971)	0.557	20.928±2.096	13.44±1.35	(9.41±0.06)×10 ⁻⁶	(n2)n5b0	(-50 to -10, 40 to 80)	Band	S
170705A(115)	2.010	22.781±1.377	7.57±0.46	(1.34±0.01)×10 ⁻⁵	n8(nb)b1	(-50 to -10, 40 to 80)	Band	M
171010A(792)	0.3285	107.266±0.810	80.74±0.61	(6.33±0.001)×10 ⁻⁴	(n8)nbb1	(-50 to -10, 200 to 250)	Band	M
171222A(684)	2.409	80.384±4.615	23.58±1.35	(3.19±0.04)×10 ⁻⁶	n0(n3)n4b0	(-50 to -20, 100 to 150)	Unconstrained	M
180205A(184)	1.409	15.360±1.448	6.38±0.60	(2.06±0.10)×10 ⁻⁶	n7n8(nb)b1	(-50 to -10, 100 to 150)	Unconstrained	M
180620B(660)	1.1175	46.721±1.332	22.06±0.63	(9.10±0.09)×10 ⁻⁶	n4(n8)b0	(-50 to -20, 100 to 150)	Unconstrained	M
180703A(876)	0.6678	20.736±1.557	12.43±0.93	(1.63±0.004)×10 ⁻⁵	n6(n7)n8b1	(-50 to -10, 50 to 100)	Band	S
180720B(598)	0.654	48.897±0.362	29.56±0.22	(2.99±0.001)×10 ⁻⁴	n6(n7)nbb1	(-30 to -10, 80 to 100)	Band	M
180728A(728)	0.117	6.400±0.362	5.73±0.32	(5.59±0.01)×10 ⁻⁵	n3(n7)b1	(-40 to -10, 40 to 80)	CPL	M
181010A(247)	1.39	9.728±2.187	4.07±0.92	(7.76±0.73)×10 ⁻⁷	n9(na)b1	(-50 to -10, 100 to 150)	CPL	S
181020A(792)	2.938	15.104±0.572	3.84±0.15	(2.81±0.003)×10 ⁻⁵	(n7)nbb1	(-50 to -10, 50 to 100)	CPL+BB	S
190114C(873)	0.425	116.354±2.563	81.65±1.80	(4.43±0.005)×10 ⁻⁴	n3(n4)n7n8b0	(-40 to -10, 120 to 160)	CPL+BB	M
190530A(430)	<2.2	18.432±0.362	5.76±0.11	(3.71±0.01)×10 ⁻⁴	(n0)n5b0	(-30 to -10, 60 to 80)	Band	M
190613A(172)	2.78	17.149±1.493	4.53±0.39	(3.20±0.05)×10 ⁻⁶	n1(n3)b0	(-50 to -10, 30 to 60)	Unconstrained	S
190719C(624)	2.469	175.620±3.083	50.63±0.89	(7.12±0.07)×10 ⁻⁸	na(nb)b1	(-50 to -10, 200 to 250)	Unconstrained	M
190829A(830)	0.0785	59.393±0.572	55.07±0.53	(1.54±0.01)×10 ⁻⁵	(n6)n9b1	(-40 to -10, 80 to 120)	Band	M
191011A(192)	1.722	25.088±4.352	9.22±1.60	(8.52±0.45)×10 ⁻⁷	n6(n9)b1	(-100 to -10, 50 to 150)	Unconstrained	S
200524A(211)	1.256	37.761±6.209	16.74±2.75	(1.40±0.01)×10 ⁻⁵	(n1)n3b0	(-20 to -5, 60 to 80)	Band	S
200613A(229)	1.22	478.026±3.168	215.33±1.43	(4.89±0.02)×10 ⁻⁵	(n0)n1b0	(-100 to -10, 100 to 200)	Band	S
200829A(582)	1.25	6.912±0.362	3.07±0.16	(2.14±0.01)×10 ⁻⁴	(n4)n8b0	(-50 to -10, 50 to 100)	Band	M
201020A(241)	2.903	21.504±3.114	5.51±0.80	(1.56±0.02)×10 ⁻⁶	(n1)n5b0	(-50 to -10, 50 to 100)	Band	S
201020B(732)	0.804	15.872±0.362	8.80±0.20	(3.41±0.01)×10 ⁻⁵	n6(n7)nbb1	(-10 to -5, 30 to 50)	Band	M
201021C(852)	1.070	35.328±2.202	17.07±1.06	(1.68±0.04)×10 ⁻⁶	(n7)nbb1	(-50 to -10, 50 to 100)	Unconstrained	S
201216C(963)	1.10	29.953±0.572	14.26±0.27	(1.36±0.001)×10 ⁻⁴	(na)nbb1	(-50 to -10, 80 to 120)	Band	M
210204A(270)	0.876	206.852±2.290	110.26±1.22	(7.57±0.01)×10 ⁻⁵	n7(nb)b1	(-50 to -20, 80 to 120)	CPL	M
210610A(628)	3.54	8.192±2.064	1.80±0.46	(1.28±0.04)×10 ⁻⁶	(n9)nab1	(-40 to -10, 30 to 60)	Band	S
210610B(827)	1.13	55.041±0.724	25.84±0.34	(1.10±0.001)×10 ⁻⁴	n6(nb)b1	(-100 to -20, 150 to 200)	Band	S
210619B(999)	1.937	54.785±0.572	18.65±0.19	(3.02±0.001)×10 ⁻⁴	n3n4n7(n8)b0	(-50 to -10, 100 to 150)	Band+BB	M
210722A(871)	1.145	61.953±11.337	28.88±5.29	(4.37±0.06)×10 ⁻⁶	n4(n8)b1	(-100 to -10, 80 to 120)	CPL	S
210731A(931)	1.2525	25.857±5.278	11.48±2.34	(3.05±0.06)×10 ⁻⁶	n8(na)nbb1	(-100 to -10, 60 to 100)	Unconstrained	S
211023A(546)	0.3906	79.106±0.572	56.89±0.41	(9.13±0.01)×10 ⁻⁵	n4(n7)b1	(-100 to -50, 200 to 250)	CPL	M

Table 1 continued on next page

Table 1 (*continued*)

GRB	z	T_{90}	$T_{90}/(1+z)$	S_{γ}	Detectors	$[\Delta T_{(\text{bkg},1)}, \Delta T_{(\text{bkg},2)}]$	Averaged Spectrum	Classified
(1)	(2)	(s)	(s)	($\text{erg}\cdot\text{cm}^{-2}$)	(6)	(s)	(E_p)	(9)
220101A(215)	4.618	128.259 ± 15.79	222.83 ± 2.81	$(6.04 \pm 0.02) \times 10^{-5}$	n6(n7)b1	(-130 to -80, 200 to 250)	Band	M
220107A(615)	1.246	33.025 ± 0.572	14.70 ± 0.25	$(1.80 \pm 0.01) \times 10^{-5}$	n7(n8)b1	(-50 to -10, 50 to 100)	CPL	M
220527A(387)	0.857	10.496 ± 0.362	5.65 ± 0.19	$(5.18 \pm 0.003) \times 10^{-5}$	(n6)n8b1	(-40 to -10, 40 to 80)	Band	M

NOTE—(1) GRB name. (2) Redshift. (3) t_{90} , in units of s. (4) The rest-frame $t_{90,z}$, in units of s. (5) The γ -ray fluence S_{γ} , in units of $\text{erg}\cdot\text{cm}^{-2}$. (6) The GBM trigger detectors. (7) The used background intervals. (8) The preferred spectral models for the averaged (time-integrated) spectrum. (9) The classified burst populations. “Short”: short GRBs; “S”: single-peak pulse long GRBs; “M”: multi-peak pulse long GRBs. Note that (i) the background spectrum of GRB 130702A can not be well measured; (ii) In order to obtain an acceptable fit, several special bursts require an additional thermal component either in the time-integrated spectrum (GRB 110721200, GRB 150314205, GRB150403913, and GRB160509374 from the Band+BB model fit and GRB 090902462, GRB 131231198, GRB 181020792, GRB 190114873 from the CPL+BB model fit) or in the 1-s peak spectrum (GRB 090926181, GRB 110721200, GRB 150314205, GRB 150403913, GRB 160625945, GRB 180720598, GRB 210619999 from the Band+BB model fit and GRB 090424592, GRB 090618353, GRB 090902462, GRB 131108862, GRB 170214649, GRB 190114873, GRB 190530430, GRB 201020732, GRB 220527387 from the CPL+BB model), see Table 4 for details.

Table 2. Time-integrated Spectral Fit Results

ID	$t_{\text{start}} \sim t_{\text{stop}}$ (s)	Time from T_0			COMP			Band			Difference					
		(1)	(2)	(3)	(4)	(5)	(6)	(7)	(8)	(9)	(10)	(11)	(12)	(13)	(14)	(15)
		K	K	E_c (keV)	likeli/AIC/BIC	E_{rest}^p (keV)	$E_{\gamma, \text{iso}}$ (erg)	K	α	E_p (keV)	β	likeli/AIC/BIC	E_{rest}^p (keV)	$E_{\gamma, \text{iso}}$ (erg)	ΔAIC	
080916406	-1~50	28	$(0.8 \pm 0.2) \times 10^{-2}$	-1.04 ± 0.10	124 ± 24	2729/5464/5475	201 ± 44	$(0.6 \pm 0.2) \times 10^{52}$	$(0.8 \pm 0.1) \times 10^{-2}$	-1.04 ± 0.09	-5.00 ± 0.59	119 ± 11	119 ± 11	$(0.6 \pm 0.1) \times 10^{52}$	2.1	
081121858	-1~30	27	$(1.4 \pm 0.1) \times 10^{-2}$	-0.79 ± 0.09	211 ± 33	2029/4065/4075	899 ± 155	$(6.8 \pm 1.5) \times 10^{52}$	$(1.4 \pm 0.1) \times 10^{-2}$	-0.79 ± 0.06	-4.88 ± 0.68	255 ± 1	255 ± 1	$(6.9 \pm 0.4) \times 10^{52}$	2.0	
081221681	-1~40	133	$(7.1 \pm 0.3) \times 10^{-2}$	-0.84 ± 0.03	74 ± 2	2669/5343/5355	280 ± 10	$(1.8 \pm 0.1) \times 10^{53}$	$(7.3 \pm 0.4) \times 10^{-2}$	-0.83 ± 0.03	-3.81 ± 0.57	85 ± 2	85 ± 2	$(1.2 \pm 0.1) \times 10^{53}$	1.5	
081222204	-1~20	57	$(2.2 \pm 0.2) \times 10^{-2}$	-0.90 ± 0.04	147 ± 12	3059/6124/6137	611 ± 39	$(5.0 \pm 0.6) \times 10^{52}$	$(2.3 \pm 0.2) \times 10^{-2}$	-0.83 ± 0.05	-2.51 ± 0.18	145 ± 8	145 ± 8	$(6.0 \pm 0.9) \times 10^{52}$	-3.2	
090102122	-1~40	68	$(1.2 \pm 0.03) \times 10^{-2}$	-1.00 ± 0.02	480 ± 34	3345/6697/6709	1238 ± 92	$(9.9 \pm 0.7) \times 10^{52}$	$(1.2 \pm 0.03) \times 10^{-2}$	-1.00 ± 0.02	-5.00 ± 0.01	488 ± 27	488 ± 27	$(9.9 \pm 0.6) \times 10^{52}$	2.1	
090323002	-1~145	19	$(1.1 \pm 0.1) \times 10^{-2}$	-0.85 ± 0.09	472 ± 136	4375/8757/8769	2482 ± 740	$(8.4 \pm 3.0) \times 10^{53}$	$(1.3 \pm 0.1) \times 10^{-2}$	-0.75 ± 0.10	-1.73 ± 0.06	380 ± 106	380 ± 106	$(9.8 \pm 2.3) \times 10^{53}$	-1.0	
090328401	-1~70	71	$(0.9 \pm 0.02) \times 10^{-2}$	-1.14 ± 0.02	849 ± 84	3761/7529/7541	1267 ± 128	$(6.0 \pm 0.6) \times 10^{52}$	$(0.9 \pm 0.02) \times 10^{-2}$	-1.14 ± 0.02	-3.06 ± 0.05	724 ± 62	724 ± 62	$(6.4 \pm 0.6) \times 10^{52}$	1.2	
090424592	-1~15	110	$(1.0 \pm 0.02) \times 10^{-1}$	-0.98 ± 0.02	184 ± 6	3499/7003/7016	290 ± 11	$(2.5 \pm 0.1) \times 10^{52}$	$(1.1 \pm 0.03) \times 10^{-1}$	-0.95 ± 0.02	-2.84 ± 0.16	176 ± 5	176 ± 5	$(2.9 \pm 0.2) \times 10^{52}$	-10.6	
090510016	-1~2	22	$(9.0 \pm 0.4) \times 10^{-3}$	-0.90 ± 0.04	4784 ± 695	1978/3962/3975	10014 ± 1309	$(2.1 \pm 0.3) \times 10^{52}$	$(0.9 \pm 0.04) \times 10^{-2}$	-0.90 ± 0.04	-3.40 ± 0.14	5200 ± 574	5200 ± 574	$(2.1 \pm 0.2) \times 10^{52}$	1.6	
090529564	-1~11	48	$(1.8 \pm 0.1) \times 10^{-2}$	-1.15 ± 0.05	281 ± 37	2901/5809/5821	866 ± 123	$(4.1 \pm 0.5) \times 10^{52}$	$(1.8 \pm 0.1) \times 10^{-2}$	-1.15 ± 0.05	-5.00 ± 0.05	239 ± 24	239 ± 24	$(4.1 \pm 0.5) \times 10^{52}$	2.1	
090618353	-1~110	196	$(5.8 \pm 0.1) \times 10^{-2}$	-1.23 ± 0.01	250 ± 10	2681/5368/5378	296 ± 12	$(1.2 \pm 0.1) \times 10^{53}$	$(9.8 \pm 0.4) \times 10^{-2}$	-0.92 ± 0.03	-2.16 ± 0.02	118 ± 3	118 ± 3	$(1.7 \pm 0.1) \times 10^{53}$	-265.6	
090926181	-1~18	252	$(1.6 \pm 0.01) \times 10^{-1}$	-0.77 ± 0.01	283 ± 5	3750/7506/7518	1081 ± 19	$(5.6 \pm 0.1) \times 10^{53}$	$(1.6 \pm 0.02) \times 10^{-1}$	-0.74 ± 0.01	-2.60 ± 0.06	322 ± 5	322 ± 5	$(6.4 \pm 0.2) \times 10^{53}$	-70.7	
090926914	-1~30	31	$(6.7 \pm 1.5) \times 10^{-2}$	0.15 ± 0.13	46 ± 4	3360/6725/6737	222 ± 25	$(1.8 \pm 0.3) \times 10^{52}$	$(9.2 \pm 2.4) \times 10^{-2}$	0.33 ± 0.15	-4.30 ± 0.31	92 ± 4	92 ± 4	$(1.5 \pm 0.5) \times 10^{52}$	-2.1	
091003191	-1~24	91	$(2.4 \pm 0.1) \times 10^{-2}$	-1.05 ± 0.02	451 ± 33	2476/4958/4970	812 ± 65	$(4.8 \pm 0.3) \times 10^{52}$	$(2.4 \pm 0.1) \times 10^{-2}$	-1.04 ± 0.02	-2.58 ± 0.32	400 ± 29	400 ± 29	$(5.5 \pm 0.8) \times 10^{52}$	1.2	
091120900	-1~20	30	$(0.8 \pm 0.1) \times 10^{-2}$	-1.32 ± 0.07	417 ± 108	2318/4642/4654	767 ± 263	$(2.3 \pm 0.6) \times 10^{52}$	$(1.0 \pm 0.3) \times 10^{-2}$	-1.15 ± 0.15	-1.91 ± 0.12	156 ± 54	156 ± 54	$(3.3 \pm 1.6) \times 10^{52}$	-2.1	
091127976	-1~10	154	$(3.8 \pm 0.1) \times 10^{-2}$	-1.81 ± 0.02	320 ± 29	2782/5570/5582	91 ± 12	$(2.3 \pm 0.5) \times 10^{52}$	$(2.3 \pm 0.4) \times 10^{-2}$	-1.35 ± 0.09	-2.18 ± 0.02	2312 ± 114	2312 ± 114	$(1.2 \pm 0.1) \times 10^{52}$	-78.4	
091208410	-1~15	35	$(1.2 \pm 0.1) \times 10^{-2}$	-1.36 ± 0.06	228 ± 43	2179/4364/4375	301 ± 64	$(1.0 \pm 0.2) \times 10^{52}$	$(1.2 \pm 0.2) \times 10^{-2}$	-1.33 ± 0.07	-2.45 ± 0.36	131 ± 19	131 ± 19	$(1.3 \pm 0.3) \times 10^{52}$	0.7	
100117879	0.0~0.2	7	$(2.1 \pm 1.2) \times 10^{-2}$	-0.31 ± 0.34	176 ± 63	278/562/574	570 ± 349	$(0.8 \pm 0.5) \times 10^{51}$	$(2.8 \pm 0.9) \times 10^{-2}$	-0.31 ± 0.29	-4.69 ± 2.51	298 ± 88	298 ± 88	$(0.3 \pm 0.2) \times 10^{51}$	2.0	
100206563	0.0~0.2	15	$(4.2 \pm 0.5) \times 10^{-2}$	-0.46 ± 0.14	405 ± 127	315/632/644	878 ± 286	$(0.3 \pm 0.3) \times 10^{51}$	$(4.3 \pm 0.3) \times 10^{-2}$	-0.42 ± 0.14	-2.67 ± 0.95	$312/632/649$	584 ± 133	$(0.4 \pm 0.2) \times 10^{51}$	0.9	
100414097	-1~28	98	$(3.2 \pm 0.4) \times 10^{-2}$	-0.50 ± 0.02	416 ± 15	3544/7094/7106	1475 ± 52	$(2.4 \pm 0.2) \times 10^{52}$	$(3.2 \pm 0.4) \times 10^{-2}$	-0.50 ± 0.02	-5.00 ± 0.26	622 ± 14	622 ± 14	$(2.4 \pm 0.1) \times 10^{53}$	2.1	
100615083	-1~50	38	$(0.7 \pm 0.1) \times 10^{-2}$	-1.30 ± 0.06	161 ± 28	3551/7108/7120	271 ± 53	$(0.7 \pm 0.1) \times 10^{-2}$	$(0.7 \pm 0.1) \times 10^{-2}$	-1.30 ± 0.06	-3.70 ± 1.34	112 ± 9	112 ± 9	$(2.6 \pm 0.1) \times 10^{52}$	1.9	
100625773	-1~2	7	$(0.4 \pm 0.1) \times 10^{-2}$	-0.99 ± 0.27	1044 ± 679	944/1893/1903	1532 ± 1076	$(0.1 \pm 0.1) \times 10^{52}$	$(0.4 \pm 0.1) \times 10^{-2}$	-0.99 ± 0.29	-4.97 ± 0.47	1068 ± 521	1068 ± 521	$(1.0 \pm 0.3) \times 10^{51}$	2.1	
100728095	-1~190	61	$(1.5 \pm 0.1) \times 10^{-2}$	-0.65 ± 0.04	235 ± 15	3604/7213/7225	814 ± 59	$(3.5 \pm 0.3) \times 10^{53}$	$(1.6 \pm 0.1) \times 10^{-2}$	-0.60 ± 0.05	-2.64 ± 0.34	$3602/7213/7228$	292 ± 20	$(3.9 \pm 0.7) \times 10^{53}$	-0.5	
100728439	-1~10	22	$(1.2 \pm 0.3) \times 10^{-2}$	-1.05 ± 0.12	148 ± 15	3054/6114/6127	438 ± 146	$(1.1 \pm 0.3) \times 10^{52}$	$(1.3 \pm 0.4) \times 10^{-2}$	-0.94 ± 0.11	-2.22 ± 0.25	$3053/6115/6131$	113 ± 22	$(1.5 \pm 0.5) \times 10^{52}$	0.4	
100814160	-1~50	25	$(1.4 \pm 0.3) \times 10^{-2}$	-0.37 ± 0.13	97 ± 14	2877/5759/5771	383 ± 71	$(2.3 \pm 0.8) \times 10^{52}$	$(1.9 \pm 0.7) \times 10^{-2}$	-0.22 ± 0.21	-2.26 ± 0.38	$2876/5760/5775$	136 ± 22	$(3.4 \pm 3.7) \times 10^{52}$	0.4	
100816026	-1~3	41	$(6.9 \pm 0.7) \times 10^{-2}$	-0.45 ± 0.06	98 ± 8	2127/4260/4272	273 ± 25	$(0.4 \pm 0.1) \times 10^{52}$	$(7.8 \pm 0.9) \times 10^{-2}$	-0.39 ± 0.07	-2.70 ± 0.24	$2123/4255/4271$	141 ± 7	$(0.5 \pm 0.1) \times 10^{52}$	-4.7	
100906576	-1~130	42	$(0.5 \pm 0.1) \times 10^{-2}$	-1.44 ± 0.06	436 ± 191	2216/4439/4449	665 ± 213	$(1.0 \pm 0.3) \times 10^{53}$	$(0.6 \pm 0.3) \times 10^{-2}$	-1.35 ± 0.12	-1.89 ± 0.12	146 ± 65	146 ± 65	$(1.5 \pm 0.5) \times 10^{53}$	-0.7	
101213451	-1~45	19	$(0.6 \pm 0.1) \times 10^{-2}$	-1.28 ± 0.11	404 ± 131	2961/5927/5939	411 ± 205	$(0.8 \pm 0.2) \times 10^{52}$	$(0.6 \pm 0.1) \times 10^{-2}$	-1.28 ± 0.10	-2.77 ± 0.21	292 ± 72	292 ± 72	$(0.5 \pm 0.1) \times 10^{52}$	2.0	
110213220	-5~40	38	$(0.9 \pm 0.2) \times 10^{-2}$	-1.49 ± 0.08	147 ± 37	2816/5638/5649	184 ± 49	$(2.9 \pm 0.6) \times 10^{52}$	$(0.9 \pm 0.2) \times 10^{-2}$	-1.46 ± 0.09	-2.75 ± 0.33	$2816/5639/5655$	71 ± 8	$(3.3 \pm 0.9) \times 10^{52}$	1.6	
110721200	-1~20	92	$(2.3 \pm 0.4) \times 10^{-2}$	-1.12 ± 0.02	945 ± 89	3177/6361/6373	3754 ± 365	$(3.4 \pm 0.3) \times 10^{53}$	$(2.6 \pm 0.1) \times 10^{-2}$	-1.02 ± 0.02	-4.62 ± 0.42	302 ± 42	302 ± 42	$(4.5 \pm 0.4) \times 10^{53}$	-99.3	
110731465	-1~20	80	$(4.5 \pm 0.2) \times 10^{-2}$	-0.98 ± 0.03	323 ± 25	2223/4451/4463	1260 ± 147	$(1.0 \pm 0.1) \times 10^{53}$	$(4.7 \pm 0.2) \times 10^{-2}$	-0.95 ± 0.04	-2.55 ± 0.25	462 ± 43	462 ± 43	$(1.1 \pm 0.1) \times 10^{53}$	-0.9	
110818860	-10~60	18	$(0.3 \pm 0.1) \times 10^{-2}$	-1.24 ± 0.14	319 ± 127	3800/7605/7617	1059 ± 462	$(5.1 \pm 1.8) \times 10^{52}$	$(0.3 \pm 0.1) \times 10^{-2}$	-1.22 ± 0.13	-2.11 ± 0.28	218 ± 67	218 ± 67	$(6.4 \pm 2.3) \times 10^{52}$	0.5	
111117510	0.0~0.5	8	$(1.8 \pm 0.3) \times 10^{-2}$	-0.56 ± 0.24	376 ± 225	674/1354/1366	1737 ± 1079	$(0.8 \pm 0.3) \times 10^{52}$	$(1.5 \pm 0.3) \times 10^{-2}$	-0.56 ± 0.20	-4.60 ± 2.46	542 ± 179	542 ± 179	$(0.3 \pm 0.1) \times 10^{52}$	2.0	
120128657	-15~13	58	$(0.9 \pm 0.1) \times 10^{-2}$	-1.76 ± 0.05	189 ± 33	3222/6450/6463	75 ± 21	$(1.0 \pm 0.1) \times 10^{52}$	$(0.9 \pm 0.1) \times 10^{-2}$	-1.74 ± 0.05	-2.65 ± 0.23	$3220/6449/6465$	43 ± 3	$(1.1 \pm 0.2) \times 10^{52}$	-1.5	
120119170	-1~60	86	$(1.9 \pm 0.1) \times 10^{-2}$	-1.02 ± 0.03	223 ± 14	3723/7453/7465	595 ± 41	$(1.9 \pm 0.1) \times 10^{53}$	$(2.3 \pm 0.1) \times 10^{-2}$	-0.98 ± 0.03	-1.97 ± 1.1	$2790/7448/7465$	19 ± 11	$(1.4 \pm 0.1) \times 10^{53}$	-4.8	
120326056	-1~12	32	$(1.4 \pm 0.3) \times 10^{-2}$	-1.34 ± 0.09	96 ± 19	2790/5587/5599	176 ± 42	$(1.1 \pm 0.3) \times 10^{52}$	$(2.3 \pm 0.1) \times 10^{-2}$	-1.12 ± 0.21	-2.44 ± 0.16	$2789/5585/5602$	51 ± 7	$(1.3 \pm 0.1) \times 10^{52}$	-1.6	
120624933	-1~30	58	$(1.4 \pm 0.04) \times 10^{-2}$	-1.00 ± 0.03	626 ± 65	3502/7010/7023	2002 ± 201	$(1.1 \pm 0.2) \times 10^{53}$	$(1.4 \pm 0.04) \times 10^{-2}$	-1.00 ± 0.03	-2.69 ± 0.49	607 ± 60	607 ± 60	$(1.7 \pm 0.2) \times 10^{53}$	0.5	
120711115	0~120	77	$(1.4 \pm 0.02) \times 10^{-2}$	-1.05 ± 0.01	1775 ± 129	3512/7031/7042										

Table 2 (continued)

ID	$t_{\text{start}} \sim t_{\text{stop}}$ (s)	COMP	K (ph.s $^{-1}$.cm $^{-2}$ keV $^{-1}$)	α	E_c (keV)	likeli/AIC/BIC	E_{rest}^p (keV)	$E_{\gamma, \text{iso}}$ (erg)	K (ph.s $^{-1}$.cm $^{-2}$ keV $^{-1}$)	α	E_p (keV)	β	likeli/AIC/BIC	E_{rest}^p (keV)	$E_{\gamma, \text{iso}}$ (erg)	ΔAIC
120716712	1-~215	16	(0.3 $^{+0.1}_{-0.1}$) $\times 10^{-2}$	-1.02 $^{+0.14}_{-0.14}$	162 $^{+54}_{-40}$	4177/8360/8373	554 $^{+202}_{-157}$	(6.4 $^{+2.7}_{-1.0}$) $\times 10^{52}$	(0.3 $^{+0.1}_{-0.1}$) $\times 10^{-2}$	-1.00 $^{+0.14}_{-0.15}$	154 $^{+29}_{-24}$	-2.97 $^{+0.81}_{-0.35}$	4177/8362/8379	154 $^{+29}_{-24}$	(7.1 $^{+3.1}_{-2.3}$) $\times 10^{52}$	1.9
120729456	1-~6	16	(1.7 $^{+0.7}_{-0.7}$) $\times 10^{-2}$	0.19 $^{+0.33}_{-0.33}$	63 $^{+17}_{-17}$	2383/4773/4784	250 $^{+77}_{-36}$	(0.1 $^{+0.1}_{-0.1}$) $\times 10^{52}$	(1.5 $^{+0.3}_{-0.3}$) $\times 10^{-2}$	-0.76 $^{+0.11}_{-0.11}$	172 $^{+36}_{-36}$	-5.00 $^{+0.01}_{-0.01}$	1544/3097/3112	172 $^{+36}_{-36}$	(0.2 $^{+0.1}_{-0.1}$) $\times 10^{52}$	-1675.8
120909070	5-~120	18	(0.3 $^{+0.1}_{-0.1}$) $\times 10^{-2}$	-1.02 $^{+0.11}_{-0.11}$	279 $^{+114}_{-114}$	4262/8530/8542	1346 $^{+567}_{-409}$	(1.2 $^{+0.5}_{-0.5}$) $\times 10^{53}$	(0.4 $^{+0.1}_{-0.1}$) $\times 10^{-2}$	-0.91 $^{+0.12}_{-0.12}$	198 $^{+45}_{-45}$	-1.90 $^{+0.14}_{-0.14}$	4259/8527/8543	198 $^{+45}_{-45}$	(1.6 $^{+0.5}_{-0.5}$) $\times 10^{53}$	-3.0
121128212	2-~30	53	(2.1 $^{+0.3}_{-0.3}$) $\times 10^{-2}$	-1.12 $^{+0.08}_{-0.08}$	85 $^{+11}_{-11}$	2477/4960/4971	237 $^{+38}_{-38}$	(3.7 $^{+0.5}_{-0.5}$) $\times 10^{52}$	(2.4 $^{+0.5}_{-0.5}$) $\times 10^{-2}$	-1.04 $^{+0.10}_{-0.10}$	69 $^{+5}_{-5}$	-2.87 $^{+0.33}_{-0.33}$	2475/4958/4974	69 $^{+5}_{-5}$	(4.2 $^{+1.3}_{-1.3}$) $\times 10^{52}$	-1.3
130215063	1-~60	31	(0.4 $^{+0.02}_{-0.02}$) $\times 10^{-2}$	-1.38 $^{+0.04}_{-0.04}$	2383 $^{+925}_{-925}$	3523/7053/7065	2359 $^{+929}_{-929}$	(2.1 $^{+0.5}_{-0.5}$) $\times 10^{52}$	(0.6 $^{+0.1}_{-0.1}$) $\times 10^{-2}$	-1.09 $^{+0.13}_{-0.13}$	207 $^{+72}_{-72}$	-1.72 $^{+0.06}_{-0.06}$	3521/7051/7067	207 $^{+72}_{-72}$	(1.2 $^{+0.7}_{-0.7}$) $\times 10^{52}$	-1.7
130420313	1-~30	20	(2.5 $^{+1.0}_{-1.0}$) $\times 10^{-2}$	-0.90 $^{+0.24}_{-0.25}$	49 $^{+10}_{-10}$	2360/4726/4737	124 $^{+46}_{-39}$	(1.1 $^{+0.9}_{-0.9}$) $\times 10^{52}$	(2.8 $^{+1.2}_{-1.1}$) $\times 10^{-2}$	-0.84 $^{+0.21}_{-0.21}$	53 $^{+3}_{-3}$	-3.51 $^{+0.83}_{-0.73}$	2360/4727/4742	53 $^{+3}_{-3}$	(2.1 $^{+0.7}_{-0.7}$) $\times 10^{52}$	1.4
130427324	1-10~25.5	569	(5.1 $^{+0.01}_{-0.01}$) $\times 10^{-1}$	-0.84 $^{+0.01}_{-0.01}$	692 $^{+4}$	6974/13955/13967	1075 $^{+7}$	(4.3 $^{+0.03}_{-0.03}$) $\times 10^{53}$	(5.2 $^{+0.01}_{-0.01}$) $\times 10^{-1}$	-0.82 $^{+0.01}_{-0.01}$	747 $^{+4}$	-3.07 $^{+0.03}_{-0.03}$	6680/13367/13384	747 $^{+4}$	(4.5 $^{+0.03}_{-0.03}$) $\times 10^{53}$	-587.7
130518580	1-~50	133	(3.0 $^{+0.1}_{-0.1}$) $\times 10^{-2}$	-0.85 $^{+0.01}_{-0.01}$	373 $^{+15}_{-15}$	3793/7591/7604	1490 $^{+59}_{-56}$	(4.0 $^{+0.2}_{-0.2}$) $\times 10^{53}$	(3.3 $^{+0.1}_{-0.1}$) $\times 10^{-2}$	-0.79 $^{+0.02}_{-0.02}$	349 $^{+14}_{-14}$	-1.12 $^{+0.05}_{-0.05}$	3763/7535/7551	349 $^{+14}_{-14}$	(5.3 $^{+0.3}_{-0.3}$) $\times 10^{53}$	-56.6
130610133	10-~30	21	(0.3 $^{+0.1}_{-0.1}$) $\times 10^{-2}$	-1.43 $^{+0.10}_{-0.10}$	423 $^{+222}_{-222}$	2595/5196/5208	745 $^{+311}_{-311}$	(2.5 $^{+0.8}_{-0.8}$) $\times 10^{52}$	(0.3 $^{+0.05}_{-0.05}$) $\times 10^{-2}$	-1.43 $^{+0.09}_{-0.09}$	241 $^{+67}_{-67}$	-5.00 $^{+0.12}_{-0.12}$	2595/5198/5213	241 $^{+67}_{-67}$	(2.4 $^{+0.5}_{-0.5}$) $\times 10^{52}$	2.1
130925173	1-~200	139	(1.1 $^{+0.04}_{-0.04}$) $\times 10^{-2}$	-1.58 $^{+0.02}_{-0.02}$	240 $^{+16}_{-16}$	4767/9541/9553	136 $^{+11}_{-11}$	(2.4 $^{+0.1}_{-0.1}$) $\times 10^{52}$	(4.1 $^{+0.3}_{-0.3}$) $\times 10^{-2}$	-1.05 $^{+0.03}_{-0.03}$	41 $^{+2}$	-1.95 $^{+0.01}_{-0.01}$	4668/9344/9361	41 $^{+2}$	(3.9 $^{+0.4}_{-0.4}$) $\times 10^{52}$	-196.3
131105087	1-~120	40	(0.4 $^{+0.03}_{-0.03}$) $\times 10^{-2}$	-0.96 $^{+0.06}_{-0.06}$	266 $^{+45}_{-45}$	4039/8085/8097	796 $^{+144}_{-124}$	(3.5 $^{+0.7}_{-0.7}$) $\times 10^{52}$	(1.0 $^{+0.2}_{-0.2}$) $\times 10^{-2}$	-0.84 $^{+0.14}_{-0.14}$	201 $^{+72}_{-72}$	-1.99 $^{+0.20}_{-0.20}$	3178/6363/6380	201 $^{+72}_{-72}$	(4.8 $^{+0.2}_{-0.2}$) $\times 10^{52}$	-2.7
131108862	1-~20	92	(3.1 $^{+0.1}_{-0.1}$) $\times 10^{-2}$	-1.32 $^{+0.04}_{-0.04}$	383 $^{+61}_{-61}$	3180/6366/6378	698 $^{+118}_{-118}$	(7.7 $^{+1.0}_{-1.0}$) $\times 10^{52}$	(0.4 $^{+0.03}_{-0.03}$) $\times 10^{-2}$	-1.32 $^{+0.04}_{-0.04}$	261 $^{+33}_{-33}$	-3.30 $^{+0.18}_{-0.18}$	4039/8087/8103	261 $^{+33}_{-33}$	(8.3 $^{+1.1}_{-1.1}$) $\times 10^{52}$	1.9
131231198	0.1~40	355	(8.5 $^{+0.1}_{-0.1}$) $\times 10^{-2}$	-0.90 $^{+0.02}_{-0.02}$	366 $^{+19}_{-19}$	3067/6141/6153	1367 $^{+75}_{-75}$	(1.7 $^{+0.1}_{-0.1}$) $\times 10^{53}$	(3.2 $^{+0.1}_{-0.1}$) $\times 10^{-2}$	-0.88 $^{+0.02}_{-0.02}$	371 $^{+17}_{-17}$	-2.47 $^{+0.14}_{-0.14}$	3062/6132/6148	371 $^{+17}_{-17}$	(1.9 $^{+0.1}_{-0.1}$) $\times 10^{53}$	-8.8
140206275	1-~50	162	(3.5 $^{+0.1}_{-0.1}$) $\times 10^{-2}$	-1.24 $^{+0.01}_{-0.01}$	286 $^{+6}$	4729/9465/9477	358 $^{+8}$	(1.0 $^{+0.02}_{-0.02}$) $\times 10^{53}$	(1.12 $^{+0.02}_{-0.02}$) $\times 10^{-1}$	-1.08 $^{+0.01}_{-0.01}$	149 $^{+3}$	-2.15 $^{+0.02}_{-0.02}$	4562/9132/9149	149 $^{+3}$	(1.3 $^{+0.04}_{-0.04}$) $\times 10^{53}$	-332.1
140506880	1-~3	21	(3.5 $^{+0.2}_{-0.2}$) $\times 10^{-2}$	-1.23 $^{+0.02}_{-0.02}$	136 $^{+6}$	2919/5844/5857	230 $^{+11}_{-11}$	(4.9 $^{+0.2}_{-0.2}$) $\times 10^{53}$	(4.6 $^{+0.2}_{-0.2}$) $\times 10^{-2}$	-0.93 $^{+0.02}_{-0.02}$	220 $^{+11}$	-1.97 $^{+0.03}_{-0.03}$	4231/8470/8487	220 $^{+11}$	(5.9 $^{+0.4}_{-0.4}$) $\times 10^{53}$	-128.4
140508128	1-~54	114	(2.5 $^{+0.1}_{-0.1}$) $\times 10^{-2}$	-0.89 $^{+0.16}_{-0.16}$	138 $^{+30}_{-30}$	1359/2725/2736	289 $^{+76}_{-76}$	(0.3 $^{+0.1}_{-0.1}$) $\times 10^{52}$	(3.8 $^{+1.1}_{-1.1}$) $\times 10^{-2}$	-0.80 $^{+0.18}_{-0.18}$	138 $^{+19}_{-19}$	-2.62 $^{+0.42}_{-0.42}$	1358/2725/2740	138 $^{+19}_{-19}$	(0.4 $^{+0.2}_{-0.2}$) $\times 10^{52}$	-0.3
140512814	1-~160	41	(0.3 $^{+0.01}_{-0.01}$) $\times 10^{-2}$	-1.11 $^{+0.02}_{-0.02}$	328 $^{+21}_{-21}$	1828/3662/3672	592 $^{+39}_{-39}$	(5.8 $^{+0.6}_{-0.6}$) $\times 10^{52}$	(2.7 $^{+0.1}_{-0.1}$) $\times 10^{-2}$	-1.08 $^{+0.03}_{-0.03}$	265 $^{+15}_{-15}$	-2.44 $^{+0.14}_{-0.14}$	1823/3655/3668	265 $^{+15}_{-15}$	(1.2 $^{+0.1}_{-0.1}$) $\times 10^{53}$	-7.5
140606133	1-~12	34	(1.1 $^{+0.1}_{-0.1}$) $\times 10^{-2}$	-1.33 $^{+0.04}_{-0.04}$	1608 $^{+762}_{-762}$	4617/9239/9252	1860 $^{+888}_{-888}$	(0.3 $^{+0.01}_{-0.01}$) $\times 10^{-2}$	(0.3 $^{+0.01}_{-0.01}$) $\times 10^{-2}$	-1.33 $^{+0.04}_{-0.04}$	1072 $^{+353}_{-353}$	-5.00 $^{+0.19}_{-0.19}$	4617/9241/9258	1072 $^{+353}_{-353}$	(5.8 $^{+1.1}_{-1.1}$) $\times 10^{52}$	2.1
140620219	1-~30	30	(0.8 $^{+0.1}_{-0.1}$) $\times 10^{-2}$	-1.29 $^{+0.09}_{-0.09}$	167 $^{+41}_{-41}$	2324/4654/4666	367 $^{+130}_{-130}$	(2.6 $^{+0.6}_{-0.6}$) $\times 10^{52}$	(1.7 $^{+0.6}_{-0.6}$) $\times 10^{-2}$	-0.95 $^{+0.17}_{-0.17}$	74 $^{+12}_{-12}$	-2.17 $^{+0.37}_{-0.37}$	2884/4776/5792	74 $^{+12}_{-12}$	(3.2 $^{+0.3}_{-0.3}$) $\times 10^{52}$	-0.8
140703026	5-~85	20	(0.4 $^{+0.1}_{-0.1}$) $\times 10^{-2}$	-1.16 $^{+0.11}_{-0.11}$	172 $^{+41}_{-41}$	3944/7894/7907	600 $^{+161}_{-161}$	(4.8 $^{+1.3}_{-1.3}$) $\times 10^{52}$	(0.4 $^{+0.1}_{-0.1}$) $\times 10^{-2}$	-1.16 $^{+0.12}_{-0.12}$	142 $^{+20}_{-20}$	-3.31 $^{+0.99}_{-0.99}$	3944/7896/7913	142 $^{+20}_{-20}$	(5.2 $^{+1.3}_{-1.3}$) $\times 10^{52}$	1.9
140801792	1-~10	54	(1.1 $^{+0.1}_{-0.1}$) $\times 10^{-1}$	-0.43 $^{+0.05}_{-0.05}$	79 $^{+3}$	2237/4481/4493	288 $^{+14}_{-14}$	(2.5 $^{+0.2}_{-0.2}$) $\times 10^{52}$	(1.2 $^{+0.1}_{-0.1}$) $\times 10^{-1}$	-0.40 $^{+0.05}_{-0.05}$	121 $^{+3}$	-3.56 $^{+0.37}_{-0.37}$	2236/4480/4496	121 $^{+3}_{-3}$	(2.7 $^{+0.3}_{-0.3}$) $\times 10^{52}$	-4.8
140808038	1-~35	35	(5.7 $^{+0.9}_{-0.9}$) $\times 10^{-2}$	-0.40 $^{+0.09}_{-0.09}$	79 $^{+7}$	1587/3179/3191	515 $^{+60}_{-60}$	(1.7 $^{+0.3}_{-0.3}$) $\times 10^{52}$	(6.8 $^{+1.2}_{-1.2}$) $\times 10^{-2}$	-0.31 $^{+0.11}_{-0.11}$	111 $^{+6}$	-2.82 $^{+0.27}_{-0.27}$	1583/3175/3190	111 $^{+6}_{-6}$	(2.0 $^{+0.5}_{-0.5}$) $\times 10^{52}$	-4.8
140907672	1-~35	24	(0.9 $^{+0.1}_{-0.1}$) $\times 10^{-2}$	-0.94 $^{+0.10}_{-0.10}$	114 $^{+20}_{-20}$	3378/6762/6774	267 $^{+46}_{-46}$	(1.1 $^{+0.2}_{-0.2}$) $\times 10^{52}$	(0.9 $^{+0.2}_{-0.2}$) $\times 10^{-2}$	-0.94 $^{+0.10}_{-0.10}$	120 $^{+8}$	-5.00 $^{+0.01}_{-0.01}$	3378/6764/6780	120 $^{+8}_{-8}$	(1.1 $^{+0.3}_{-0.3}$) $\times 10^{52}$	2.1
141004973	0~2	21	(1.2 $^{+1.0}_{-0.3}$) $\times 10^1$	-1.46 $^{+0.20}_{-0.20}$	215 $^{+211}_{-215}$	920/1847/1858	182 $^{+192}_{-192}$	(0.1 $^{+0.1}_{-0.1}$) $\times 10^{52}$	(1.4 $^{+0.5}_{-0.5}$) $\times 10^{-2}$	-1.46 $^{+0.21}_{-0.21}$	115 $^{+9}$	-5.00 $^{+2.74}_{-2.74}$	920/1849/1864	115 $^{+9}_{-9}$	(1.0 $^{+0.2}_{-0.2}$) $\times 10^{51}$	2.0
141028455	1-~40	78	(1.6 $^{+0.4}_{-0.4}$) $\times 10^{-2}$	-0.91 $^{+0.02}_{-0.02}$	386 $^{+22}_{-22}$	3391/6788/6801	1402 $^{+87}_{-87}$	(1.8 $^{+0.1}_{-0.1}$) $\times 10^{53}$	(1.9 $^{+0.1}_{-0.1}$) $\times 10^{-2}$	-0.81 $^{+0.03}_{-0.03}$	306 $^{+21}$	-1.99 $^{+0.06}_{-0.06}$	3367/6742/6758	306 $^{+21}_{-21}$	(2.2 $^{+0.2}_{-0.2}$) $\times 10^{53}$	-46.5
141220252	1-~5	43	(3.6 $^{+0.4}_{-0.4}$) $\times 10^{-2}$	-0.66 $^{+0.07}_{-0.07}$	125 $^{+13}_{-13}$	2172/4350/4362	390 $^{+44}_{-44}$	(0.6 $^{+0.2}_{-0.2}$) $\times 10^{52}$	(1.1 $^{+0.02}_{-0.02}$) $\times 10^{-2}$	-1.55 $^{+0.01}_{-0.01}$	154150 $^{+1}$	-2.07 $^{+0.10}_{-0.10}$	2351/4711/4727	154150 $^{+1}_{-1}$	(2.4 $^{+0.1}_{-0.1}$) $\times 10^{52}$	361.0
141221338	1-~25	18	(0.5 $^{+0.2}_{-0.2}$) $\times 10^{-2}$	-1.06 $^{+0.18}_{-0.18}$	144 $^{+61}_{-61}$	2314/4634/4645	333 $^{+127}_{-127}$	(0.8 $^{+0.3}_{-0.3}$) $\times 10^{52}$	(0.6 $^{+0.2}_{-0.2}$) $\times 10^{-2}$	-0.97 $^{+0.02}_{-0.02}$	117 $^{+25}$	-2.39 $^{+0.39}_{-0.39}$	2314/4635/4650	117 $^{+25}_{-25}$	(1.0 $^{+0.5}_{-0.5}$) $\times 10^{52}$	1.7
141225959	1-~60	14	(0.3 $^{+0.1}_{-0.1}$) $\times 10^{-2}$	-0.83 $^{+0.19}_{-0.19}$	198 $^{+68}_{-68}$	2675/5356/5368	442 $^{+249}_{-249}$	(0.8 $^{+0.4}_{-0.4}$) $\times 10^{52}$	(0.5 $^{+0.2}_{-0.2}$) $\times 10^{-2}$	-0.55 $^{+0.24}_{-0.24}$	154 $^{+33}$	-2.05 $^{+0.20}_{-0.20}$	2673/5355/5370	154 $^{+33}_{-33}$	(1.1 $^{+0.9}_{-0.9}$) $\times 10^{52}$	-1.8
150301818	1-~15	21	(0.2 $^{+0.1}_{-0.1}$) $\times 10^{-2}$	-1.16 $^{+0.09}_{-0.09}$	239 $^{+66}_{-66}$	2802/5609/5622	506 $^{+148}_{-148}$	(1.0 $^{+0.3}_{-0.3}$) $\times 10^{52}$	(0.7 $^{+0.1}_{-0.1}$) $\times 10^{-2}$	-1.13 $^{+0.09}_{-0.09}$	184 $^{+32}$	-2.26 $^{+0.17}_{-0.17}$	2801/5610/5627	184 $^{+32}_{-32}$	(1.3 $^{+0.4}_{-0.4}$) $\times 10^{52}$	0.8
150314205	1															

Table 2 (continued)

Time from T_0		COMP										Band				Difference	
ID	$t_{\text{start}} \sim t_{\text{stop}}$ (s)	K (ph.s $^{-1}$.cm $^{-2}$ keV $^{-1}$)	α	E_c (keV)	likeli/AIC/BIC	E_{rest}^p (keV)	$E_{\gamma, \text{iso}}$ (erg)	K (ph.s $^{-1}$.cm $^{-2}$ keV $^{-1}$)	α	E_p (keV)	β	likeli/AIC/BIC	E_{rest}^p (keV)	$E_{\gamma, \text{iso}}$ (erg)	ΔAIC		
(1)	(2)	(3)	(4)	(5)	(6)	(7)	(8)	(9)	(10)	(11)	(12)	(13)	(14)	(15)	(16)	(17)	
161117066	-1~150	77	(2.3 $^{+0.2}_{-0.2}$) $\times 10^{-2}$	-0.88 $^{+0.05}_{-0.05}$	7 $^{+5}_{-5}$	3168/6342/6353	204 $^{+18}_{-15}$	(8.9 $^{+1.2}_{-1.0}$) $\times 10^{52}$	(2.3 $^{+0.2}_{-0.2}$) $\times 10^{-2}$	-0.88 $^{+0.05}_{-0.05}$	80 $^{+2}_{-2}$	-5.00 $^{+0.06}_{-0.06}$	3168/6344/6359	80 $^{+2}_{-2}$	(9.0 $^{+1.1}_{-1.0}$) $\times 10^{52}$	2.1	
161129300	-1~50	20	(0.3 $^{+0.1}_{-0.1}$) $\times 10^{-2}$	-0.55 $^{+0.15}_{-0.15}$	118 $^{+26}_{-26}$	3523/7052/7064	281 $^{+61}_{-56}$	(0.5 $^{+0.1}_{-0.1}$) $\times 10^{52}$	(1.0 $^{+0.3}_{-0.3}$) $\times 10^{-2}$	-0.40 $^{+0.20}_{-0.20}$	144 $^{+21}_{-21}$	-2.37 $^{+0.33}_{-0.33}$	3521/7051/7067	144 $^{+21}_{-21}$	(0.7 $^{+0.3}_{-0.3}$) $\times 10^{52}$	-0.6	
170214649	-1~150	143	(1.9 $^{+0.03}_{-0.03}$) $\times 10^{-2}$	-1.04 $^{+0.01}_{-0.01}$	518 $^{+23}_{-23}$	5220/10446/10458	1758 $^{+81}_{-78}$	(9.2 $^{+0.5}_{-0.5}$) $\times 10^{53}$	(2.0 $^{+0.04}_{-0.04}$) $\times 10^{-2}$	-1.03 $^{+0.02}_{-0.02}$	461 $^{+20}_{-20}$	-2.47 $^{+0.14}_{-0.14}$	5213/10434/10450	461 $^{+20}_{-20}$	(1.1 $^{+0.1}_{-0.1}$) $\times 10^{54}$	-11.9	
170405777	-1~100	83	(1.8 $^{+0.1}_{-0.1}$) $\times 10^{-2}$	-0.79 $^{+0.02}_{-0.02}$	274 $^{+14}_{-14}$	4173/8351/8364	1497 $^{+81}_{-77}$	(5.2 $^{+0.4}_{-0.4}$) $\times 10^{53}$	(2.0 $^{+0.1}_{-0.1}$) $\times 10^{-2}$	-0.72 $^{+0.03}_{-0.03}$	287 $^{+13}_{-13}$	-2.31 $^{+0.10}_{-0.10}$	4163/8335/8351	287 $^{+13}_{-13}$	(6.0 $^{+0.5}_{-0.5}$) $\times 10^{53}$	-16.9	
170607971	-1~20	50	(4.1 $^{+0.2}_{-0.2}$) $\times 10^{-2}$	-1.39 $^{+0.06}_{-0.06}$	209 $^{+33}_{-33}$	2186/4379/4391	198 $^{+37}_{-37}$	(0.2 $^{+0.1}_{-0.1}$) $\times 10^{52}$	(1.9 $^{+0.3}_{-0.3}$) $\times 10^{-2}$	-1.24 $^{+0.07}_{-0.07}$	97 $^{+9}_{-9}$	-2.34 $^{+0.11}_{-0.11}$	4182/4372/4387	97 $^{+9}_{-9}$	(0.7 $^{+0.2}_{-0.2}$) $\times 10^{52}$	-7.4	
170705115	-1~25	60	(2.1 $^{+0.2}_{-0.2}$) $\times 10^{-2}$	-1.11 $^{+0.05}_{-0.05}$	156 $^{+14}_{-14}$	2290/4587/4598	418 $^{+45}_{-45}$	(4.9 $^{+0.5}_{-0.5}$) $\times 10^{52}$	(2.6 $^{+0.4}_{-0.4}$) $\times 10^{-2}$	-1.01 $^{+0.07}_{-0.07}$	117 $^{+10}_{-10}$	-2.48 $^{+0.18}_{-0.18}$	2289/4585/4601	117 $^{+10}_{-10}$	(5.8 $^{+1.2}_{-1.1}$) $\times 10^{52}$	-1.7	
171010792	-1~150	555	(1.1 $^{+0.01}_{-0.01}$) $\times 10^{-1}$	-1.22 $^{+0.00}_{-0.00}$	271 $^{+3}_{-3}$	4421/8847/8859	282 $^{+4}_{-4}$	(1.5 $^{+0.02}_{-0.02}$) $\times 10^{53}$	(1.2 $^{+0.01}_{-0.01}$) $\times 10^{-1}$	-1.19 $^{+0.01}_{-0.01}$	190 $^{+2}_{-2}$	-2.43 $^{+0.03}_{-0.03}$	4335/8679/8694	190 $^{+2}_{-2}$	(1.8 $^{+0.04}_{-0.04}$) $\times 10^{53}$	-168.2	
180703876	-1~25	49	(1.1 $^{+0.04}_{-0.04}$) $\times 10^{-2}$	-0.88 $^{+0.03}_{-0.03}$	459 $^{+46}_{-46}$	3096/6198/6211	857 $^{+102}_{-88}$	(1.5 $^{+0.3}_{-0.3}$) $\times 10^{52}$	(1.2 $^{+0.1}_{-0.1}$) $\times 10^{-2}$	-0.82 $^{+0.04}_{-0.04}$	410 $^{+44}_{-44}$	-2.07 $^{+0.12}_{-0.12}$	3091/6191/6207	410 $^{+44}_{-44}$	(2.4 $^{+0.4}_{-0.4}$) $\times 10^{52}$	-7.2	
180720598	-1~60	172	(6.3 $^{+0.1}_{-0.1}$) $\times 10^{-2}$	-1.13 $^{+0.01}_{-0.01}$	895 $^{+33}_{-33}$	4588/9183/9195	1288 $^{+50}_{-50}$	(3.2 $^{+0.1}_{-0.1}$) $\times 10^{53}$	(6.5 $^{+0.1}_{-0.1}$) $\times 10^{-2}$	-1.11 $^{+0.01}_{-0.01}$	682 $^{+20}_{-20}$	-2.35 $^{+0.04}_{-0.04}$	4503/9013/9030	682 $^{+20}_{-20}$	(3.6 $^{+0.1}_{-0.1}$) $\times 10^{53}$	-169.7	
180728728	-1.6~20	266	(6.1 $^{+0.1}_{-0.1}$) $\times 10^{-2}$	-1.71 $^{+0.01}_{-0.01}$	339 $^{+16}_{-16}$	2409/4825/4836	109 $^{+7}_{-7}$	(0.2 $^{+0.01}_{-0.01}$) $\times 10^{52}$	(6.1 $^{+0.1}_{-0.1}$) $\times 10^{-2}$	-1.71 $^{+0.01}_{-0.01}$	97 $^{+2}_{-2}$	-5.00 $^{+0.01}_{-0.01}$	2409/4827/4842	97 $^{+2}_{-2}$	(0.2 $^{+0.01}_{-0.01}$) $\times 10^{52}$	2.0	
181010247	-1~5	5	(0.3 $^{+0.1}_{-0.1}$) $\times 10^{-2}$	-1.13 $^{+0.34}_{-0.34}$	365 $^{+710}_{-240}$	1525/3055/3067	758 $^{+1506}_{-581}$	(0.2 $^{+0.4}_{-0.4}$) $\times 10^{52}$	(3.0 $^{+0.4}_{-0.4}$) $\times 10^{-3}$	-1.13 $^{+0.19}_{-0.19}$	315 $^{+1}$	-5.00 $^{+0.21}_{-0.21}$	1525/3057/3073	315 $^{+1}$	(0.2 $^{+0.04}_{-0.04}$) $\times 10^{52}$	2.0	
181020792	-1~20	79	(2.2 $^{+0.1}_{-0.1}$) $\times 10^{-2}$	-0.77 $^{+0.03}_{-0.03}$	386 $^{+26}_{-26}$	2271/4549/4560	1867 $^{+134}_{-134}$	(1.8 $^{+0.2}_{-0.2}$) $\times 10^{53}$	(2.3 $^{+0.1}_{-0.1}$) $\times 10^{-2}$	-0.73 $^{+0.03}_{-0.03}$	430 $^{+34}_{-34}$	-2.40 $^{+0.21}_{-0.21}$	2268/4544/4560	430 $^{+34}_{-34}$	(2.0 $^{+0.2}_{-0.2}$) $\times 10^{53}$	-4.2	
190530430	-1~30	373	(1.2 $^{+0.01}_{-0.01}$) $\times 10^{-1}$	-1.06 $^{+0.01}_{-0.01}$	1092 $^{+17}_{-17}$	4508/9022/9034	3286 $^{+51}_{-51}$	(2.1 $^{+0.03}_{-0.03}$) $\times 10^{54}$	(1.22 $^{+0.01}_{-0.01}$) $\times 10^{-1}$	-1.06 $^{+0.01}_{-0.01}$	1024 $^{+13}_{-13}$	-4.10 $^{+0.31}_{-0.31}$	4505/9018/9033	1024 $^{+13}_{-13}$	(2.1 $^{+0.02}_{-0.02}$) $\times 10^{54}$	-4.7	
190829830	-1~60	65	(3.0 $^{+0.1}_{-0.1}$) $\times 10^{-3}$	-2.23 $^{+0.05}_{-0.05}$	634 $^{+588}_{-628}$	2833/5672/5683	157 $^{+150}_{-129}$	(0.4 $^{+0.1}_{-0.1}$) $\times 10^{51}$	(1.0 $^{+0.1}_{-0.1}$) $\times 10^{-2}$	-1.03 $^{+0.03}_{-0.03}$	14 $^{+1}$	-2.38 $^{+0.03}_{-0.03}$	2602/5211/5226	14 $^{+1}$	(0.3 $^{+0.1}_{-0.1}$) $\times 10^{51}$	-460.5	
200524211	-1~40	36	(1.0 $^{+0.1}_{-0.1}$) $\times 10^{-2}$	-0.95 $^{+0.06}_{-0.06}$	300 $^{+52}_{-52}$	2852/5710/5721	711 $^{+153}_{-129}$	(3.8 $^{+0.8}_{-0.8}$) $\times 10^{52}$	(4.3 $^{+0.2}_{-0.2}$) $\times 10^{-2}$	-0.61 $^{+0.13}_{-0.13}$	158 $^{+24}_{-24}$	-1.83 $^{+0.06}_{-0.06}$	2842/5692/5707	158 $^{+24}_{-24}$	(6.0 $^{+1.6}_{-1.6}$) $\times 10^{52}$	-17.8	
200613229	-1~45	150	(3.6 $^{+0.1}_{-0.1}$) $\times 10^{-2}$	-1.15 $^{+0.02}_{-0.02}$	147 $^{+6}_{-6}$	2836/5678/5690	277 $^{+13}_{-13}$	(0.4 $^{+0.04}_{-0.04}$) $\times 10^{52}$	(1.7 $^{+0.3}_{-0.3}$) $\times 10^{-1}$	-1.06 $^{+0.02}_{-0.02}$	106 $^{+3}_{-3}$	-2.65 $^{+0.08}_{-0.08}$	2612/5232/5247	106 $^{+3}_{-3}$	(8.2 $^{+0.5}_{-0.5}$) $\times 10^{52}$	-446.6	
200826187	-1~2	52	(1.0 $^{+0.1}_{-0.1}$) $\times 10^{-1}$	-0.77 $^{+0.04}_{-0.04}$	97 $^{+6}_{-6}$	2826/5657/5671	210 $^{+14}_{-14}$	(4.6 $^{+0.1}_{-0.1}$) $\times 10^{53}$	(1.00 $^{+0.01}_{-0.01}$) $\times 10^{-1}$	-0.71 $^{+0.01}_{-0.01}$	414 $^{+9}_{-9}$	-2.56 $^{+0.06}_{-0.06}$	2866/6540/6555	414 $^{+9}_{-9}$	(5.3 $^{+0.2}_{-0.2}$) $\times 10^{53}$	-86.9	
200829882	-5~30	171	(9.4 $^{+0.1}_{-0.1}$) $\times 10^{-2}$	-0.76 $^{+0.01}_{-0.01}$	369 $^{+8}_{-8}$	3310/6627/6638	1030 $^{+25}_{-22}$	(4.6 $^{+0.1}_{-0.1}$) $\times 10^{53}$	(3.5 $^{+0.1}_{-0.1}$) $\times 10^{-2}$	-0.75 $^{+0.02}_{-0.02}$	27 $^{+4}$	-2.37 $^{+0.18}_{-0.18}$	2254/4516/4531	27 $^{+4}$	(1.1 $^{+1.3}_{-1.3}$) $\times 10^{52}$	-4.2	
201020241	-10~10	16	(0.3 $^{+0.2}_{-0.2}$) $\times 10^{-2}$	-1.79 $^{+0.29}_{-0.29}$	154 $^{+315}_{-315}$	2257/4520/4531	125 $^{+532}_{-222}$	(1.6 $^{+2.0}_{-2.0}$) $\times 10^{52}$	(3.3 $^{+2.0}_{-2.0}$) $\times 10^{-2}$	-0.75 $^{+0.02}_{-0.02}$	27 $^{+4}$	-2.37 $^{+0.18}_{-0.18}$	2254/4516/4531	27 $^{+4}$	(1.1 $^{+1.3}_{-1.3}$) $\times 10^{52}$	-4.2	
201020732	-1~20	99	(6.0 $^{+0.2}_{-0.2}$) $\times 10^{-2}$	-0.89 $^{+0.02}_{-0.02}$	182 $^{+8}_{-8}$	3484/6973/6986	366 $^{+16}_{-16}$	(3.7 $^{+0.2}_{-0.2}$) $\times 10^{52}$	(7.3 $^{+0.4}_{-0.4}$) $\times 10^{-2}$	-0.77 $^{+0.03}_{-0.03}$	165 $^{+7}$	-2.23 $^{+0.07}_{-0.07}$	3467/6941/6958	165 $^{+7}$	(5.2 $^{+0.5}_{-0.5}$) $\times 10^{52}$	-32.1	
201221963	0.0~0.2	29	(7.9 $^{+3.3}_{-3.3}$) $\times 10^{-1}$	-0.42 $^{+0.23}_{-0.23}$	48 $^{+8}_{-8}$	137/280/290	235 $^{+45}_{-45}$	(0.1 $^{+0.1}_{-0.1}$) $\times 10^{52}$	(0.7 $^{+0.4}_{-0.4}$) $\times 10^{-2}$	0.81 $^{+0.40}_{-0.40}$	100 $^{+13}_{-13}$	-2.92 $^{+0.47}_{-0.47}$	135/278/292	100 $^{+13}_{-13}$	(0.1 $^{+0.1}_{-0.1}$) $\times 10^{52}$	-1.7	
210204270	-1~270	58	(0.7 $^{+0.04}_{-0.04}$) $\times 10^{-2}$	-1.51 $^{+0.03}_{-0.03}$	358 $^{+62}_{-62}$	3562/7130/7142	330 $^{+59}_{-59}$	(1.1 $^{+0.1}_{-0.1}$) $\times 10^{53}$	(0.7 $^{+0.1}_{-0.1}$) $\times 10^{-2}$	-1.46 $^{+0.05}_{-0.05}$	144 $^{+22}_{-22}$	-2.26 $^{+0.19}_{-0.19}$	3562/7132/7147	144 $^{+22}_{-22}$	(1.3 $^{+0.2}_{-0.2}$) $\times 10^{53}$	1.4	
210610628	0~5	11	(0.5 $^{+0.1}_{-0.1}$) $\times 10^{-2}$	-1.39 $^{+0.16}_{-0.16}$	551 $^{+871}_{-871}$	1589/3183/3195	1525 $^{+2443}_{-994}$	(0.9 $^{+0.7}_{-0.7}$) $\times 10^{52}$	(0.6 $^{+0.2}_{-0.2}$) $\times 10^{-2}$	-1.27 $^{+0.20}_{-0.20}$	179 $^{+51}_{-51}$	-3.67 $^{+1.47}_{-1.47}$	1410/2829/2844	179 $^{+51}_{-51}$	(0.7 $^{+0.3}_{-0.3}$) $\times 10^{52}$	-354.3	
210610827	-1~100	110	(3.0 $^{+0.1}_{-0.1}$) $\times 10^{-2}$	-0.66 $^{+0.02}_{-0.02}$	218 $^{+8}_{-8}$	3151/6309/6320	622 $^{+26}_{-26}$	(2.0 $^{+0.1}_{-0.1}$) $\times 10^{53}$	(3.2 $^{+0.1}_{-0.1}$) $\times 10^{-2}$	-0.62 $^{+0.03}_{-0.03}$	269 $^{+10}$	-2.58 $^{+0.16}_{-0.16}$	3146/6300/6315	269 $^{+10}$	(2.4 $^{+0.2}_{-0.2}$) $\times 10^{53}$	-9.4	
210619999	-1~70	358	(8.4 $^{+0.1}_{-0.1}$) $\times 10^{-2}$	-1.08 $^{+0.01}_{-0.01}$	366 $^{+7}_{-7}$	6270/12547/12560	990 $^{+23}_{-23}$	(1.1 $^{+0.02}_{-0.02}$) $\times 10^{54}$	(1.1 $^{+0.2}_{-0.2}$) $\times 10^{-2}$	-0.89 $^{+0.01}_{-0.01}$	198 $^{+4}$	-1.97 $^{+0.01}_{-0.01}$	5953/11913/11931	198 $^{+4}$	(1.4 $^{+0.04}_{-0.04}$) $\times 10^{54}$	-633.7	
210722871	-1~50	14	(0.6 $^{+0.3}_{-0.3}$) $\times 10^{-2}$	-0.87 $^{+0.22}_{-0.22}$	111 $^{+52}_{-52}$	2684/5373/5385	268 $^{+137}_{-137}$	(0.9 $^{+0.7}_{-0.7}$) $\times 10^{52}$	(0.6 $^{+0.1}_{-0.1}$) $\times 10^{-2}$	-0.86 $^{+0.01}_{-0.01}$	125 $^{+1}$	-5.00 $^{+0.02}_{-0.02}$	2684/5375/5391	125 $^{+1}$	(0.8 $^{+0.2}_{-0.2}$) $\times 10^{52}$	2.1	
211023546	-1~150	193	(1.5 $^{+0.03}_{-0.03}$) $\times 10^{-2}$	-1.80 $^{+0.01}_{-0.01}$	637 $^{+66}_{-66}$	3413/6832/6844	177 $^{+191}_{-191}$	(5.0 $^{+0.2}_{-0.2}$) $\times 10^{52}$	(1.5 $^{+0.03}_{-0.03}$) $\times 10^{-2}$	-1.80 $^{+0.01}_{-0.01}$	129 $^{+7}$	-5.00 $^{+0.02}_{-0.02}$	3413/6834/6850	129 $^{+7}$	(5.0 $^{+0.2}_{-0.2}$) $\times 10^{52}$	2.1	
220101215	-1~180	57	(9.0 $^{+0.4}_{-0.4}$) $\times 10^{-3}$	-0.98 $^{+0.04}_{-0.04}$	308 $^{+30}_{-30}$	3403/6812/6824	1764 $^{+197}_{-180}$	(5.7 $^{+0.7}_{-0.7}$) $\times 10^{53}$	(1.0 $^{+0.1}_{-0.1}$) $\times 10^{-2}$	-0.93 $^{+0.04}_{-0.04}$	266 $^{+25}_{-24}$	-2.14 $^{+0.14}_{-0.14}$	3399/6807/6822	266 $^{+25}_{-24}$	(6.5 $^{+0.8}_{-0.8}$) $\times 10^{53}$	-5.5	
220107615	-1~40	56	(1.4 $^{+0.1}_{-0.1}$) $\times 10^{-2}$	-0.76 $^{+0.04}_{-0.04}$	210 $^{+10}_{-10}$	2538/5082/5094	584 $^{+99}_{-99}$	(4.0 $^{+0.3}_{-0.3}$) $\times 10^{52}$	(1.4 $^{+0.1}_{-0.1}$) $\times 10^{-2}$	-0.76 $^{+0.04}_{-0.04}$	259 $^{+16}$	-5.00 $^{+0.02}_{-0.02}$	2538/5084/5100	259 $^{+16}$	(4.0 $^{+0.3}_{-0.3}$) $\times 10^{52}$	2.1	
220527387	-1~20	195	(1.0 $^{+0.02}_{-0.02}$) $\times 10^{-1}$	-0.85 $^{+0.02}_{-0.02}$	160 $^{+4}_{-4$												

Table 3. (1-s Peak) Spectral Fit Results

ID	$t_{\text{start}} \sim t_{\text{stop}}$ (s)	Time from T_0	COMP					Band					Difference	
			S	K ($\text{ph.s}^{-1} \cdot \text{cm}^{-2} \cdot \text{keV}^{-1}$)	α	E_c (keV)	likeli/AIC/BIC	$L_{p,\text{iso}}$ (erg.s^{-1})	K ($\text{ph.s}^{-1} \cdot \text{cm}^{-2} \cdot \text{keV}^{-1}$)	α	E_p (keV)	β		likeli/AIC/BIC
(1)	(2)	(3)	(4)	(5)	(6)	(7)	(8)	(9)	(10)	(11)	(12)	(13)	(14)	(15)
080916406	2~3	14	$(3.7^{+1.0}_{-0.8}) \times 10^{-2}$	$-0.27^{+0.20}_{-0.21}$	120^{+30}_{-24}	701/1408/1420	$(0.2^{+0.1}_{-0.1}) \times 10^{52}$	$(3.7^{+0.9}_{-0.9}) \times 10^{-2}$	$-0.27^{+0.20}_{-0.19}$	207^{+25}_{-26}	$-5.00^{+0.28}_{-0.04}$	701/1410/1425	$(0.2^{+0.1}_{-0.1}) \times 10^{52}$	2.1
081121858	17~18	10	$(3.2^{+1.8}_{-1.1}) \times 10^{-2}$	$-0.69^{+0.34}_{-0.32}$	145^{+88}_{-58}	507/1019/1030	$(4.1^{+4.7}_{-2.2}) \times 10^{52}$	$(3.9^{+1.8}_{-1.5}) \times 10^{-2}$	$-0.58^{+0.34}_{-0.29}$	165^{+35}_{-36}	$-2.31^{+0.37}_{-0.50}$	506/1020/1035	$(5.3^{+4.0}_{-2.8}) \times 10^{52}$	0.6
081221681	21~22	72	$(4.5^{+0.5}_{-0.7}) \times 10^{-1}$	$-0.14^{+0.07}_{-0.08}$	58^{+3}_{-3}	749/1505/1516	$(1.0^{+0.2}_{-0.2}) \times 10^{53}$	$(5.2^{+0.7}_{-0.7}) \times 10^{-1}$	$-0.06^{+0.08}_{-0.08}$	103^{+3}_{-3}	$-3.51^{+0.29}_{-0.48}$	746/1500/1516	$(1.1^{+0.2}_{-0.2}) \times 10^{53}$	-4.2
081222204	3~4	34	$(5.7^{+0.6}_{-0.6}) \times 10^{-2}$	$-0.86^{+0.08}_{-0.08}$	163^{+25}_{-22}	965/1936/1948	$(1.0^{+0.2}_{-0.2}) \times 10^{53}$	$(5.7^{+0.6}_{-0.6}) \times 10^{-2}$	$-0.86^{+0.07}_{-0.07}$	185^{+15}_{-15}	$-5.00^{+0.01}_{-0.01}$	965/1938/1954	$(1.0^{+0.2}_{-0.2}) \times 10^{53}$	2.1
090102122	14~15	34	$(5.5^{+0.3}_{-0.3}) \times 10^{-2}$	$-0.16^{+0.08}_{-0.08}$	214^{+21}_{-18}	891/1788/1801	$(5.6^{+1.2}_{-1.1}) \times 10^{52}$	$(5.5^{+0.3}_{-0.4}) \times 10^{-2}$	$-0.15^{+0.08}_{-0.09}$	394^{+23}_{-21}	$-4.52^{+2.05}_{-0.04}$	891/1790/1807	$(6.1^{+1.6}_{-1.0}) \times 10^{52}$	2.0
090323002	66~67	21	$(6.2^{+0.7}_{-0.6}) \times 10^{-2}$	$-0.27^{+0.11}_{-0.11}$	193^{+29}_{-26}	1415/2837/2849	$(3.5^{+1.3}_{-0.9}) \times 10^{53}$	$(6.3^{+0.6}_{-0.6}) \times 10^{-2}$	$-0.26^{+0.11}_{-0.11}$	333^{+30}_{-30}	$-4.13^{+1.88}_{-0.35}$	1415/2839/2855	$(3.9^{+1.2}_{-0.7}) \times 10^{53}$	2.0
090328401	24~25	44	$(5.6^{+0.3}_{-0.3}) \times 10^{-2}$	$-0.84^{+0.05}_{-0.04}$	382^{+43}_{-42}	911/1829/1841	$(1.0^{+0.2}_{-0.1}) \times 10^{52}$	$(5.6^{+0.3}_{-0.3}) \times 10^{-2}$	$-0.84^{+0.05}_{-0.04}$	441^{+33}_{-37}	$-4.03^{+1.82}_{-0.17}$	911/1831/1847	$(1.1^{+0.3}_{-0.2}) \times 10^{52}$	2.0
090424592	4~5	133	$(5.0^{+0.7}_{-0.7}) \times 10^{-1}$	$-0.65^{+0.02}_{-0.02}$	148^{+5}_{-5}	1676/3358/3370	$(1.5^{+0.1}_{-0.1}) \times 10^{52}$	$(5.4^{+0.2}_{-0.2}) \times 10^{-1}$	$-0.60^{+0.04}_{-0.04}$	186^{+5}_{-5}	$-3.00^{+0.19}_{-0.19}$	1670/3347/3364	$(1.7^{+0.1}_{-0.1}) \times 10^{52}$	-10.1
090510016	0~1	33	$(2.4^{+0.1}_{-0.1}) \times 10^{-2}$	$-0.84^{+0.03}_{-0.03}$	3949^{+413}_{-372}	1297/2601/2613	$(7.3^{+0.8}_{-0.8}) \times 10^{52}$	$(2.4^{+0.1}_{-0.1}) \times 10^{-2}$	$-0.83^{+0.03}_{-0.03}$	4299^{+454}_{-428}	$-2.76^{+0.40}_{-0.41}$	1296/2599/2616	$(7.2^{+0.7}_{-0.7}) \times 10^{52}$	-1.3
090529564	9~10	52	$(1.1^{+0.1}_{-0.1}) \times 10^{-1}$	$-0.78^{+0.05}_{-0.05}$	165^{+17}_{-16}	1287/2581/2593	$(1.7^{+0.3}_{-0.3}) \times 10^{53}$	$(1.4^{+0.2}_{-0.2}) \times 10^{-1}$	$-0.61^{+0.09}_{-0.09}$	158^{+14}_{-15}	$-2.29^{+0.15}_{-0.15}$	1285/2578/2595	$(2.2^{+0.4}_{-0.4}) \times 10^{53}$	-2.8
090618353	63~64	103	$(1.8^{+0.1}_{-0.1}) \times 10^{-1}$	$-1.03^{+0.03}_{-0.03}$	576^{+43}_{-43}	653/1311/1321	$(2.0^{+0.2}_{-0.2}) \times 10^{52}$	$(1.8^{+0.1}_{-0.1}) \times 10^{-1}$	$-1.02^{+0.03}_{-0.03}$	552^{+31}_{-31}	$-3.61^{+0.77}_{-0.71}$	652/1313/1326	$(2.1^{+0.2}_{-0.1}) \times 10^{52}$	1.6
090902462	9~10	135	$(1.7^{+0.2}_{-0.2}) \times 10^{-1}$	$-1.21^{+0.01}_{-0.01}$	2640^{+154}_{-148}	2117/4239/4252	$(8.5^{+0.3}_{-0.3}) \times 10^{53}$	$(1.7^{+0.2}_{-0.2}) \times 10^{-1}$	$-1.21^{+0.01}_{-0.01}$	2087^{+103}_{-107}	$-5.00^{+0.14}_{-0.14}$	2117/4241/4258	$(8.5^{+0.2}_{-0.2}) \times 10^{53}$	2.0
090926181	4~5	143	$(3.4^{+0.1}_{-0.1}) \times 10^{-1}$	$-0.65^{+0.02}_{-0.02}$	278^{+9}_{-9}	1679/3365/3377	$(6.6^{+0.3}_{-0.3}) \times 10^{53}$	$(4.3^{+0.2}_{-0.2}) \times 10^{-1}$	$-0.48^{+0.03}_{-0.03}$	276^{+10}_{-10}	$-2.17^{+0.04}_{-0.04}$	1603/3213/3230	$(8.0^{+0.5}_{-0.5}) \times 10^{53}$	-151.1
090926914	19~20	14	$(4.8^{+2.5}_{-1.6}) \times 10^{-2}$	$-0.42^{+0.27}_{-0.26}$	77^{+24}_{-24}	974/1954/1966	$(0.4^{+0.4}_{-0.4}) \times 10^{52}$	$(4.8^{+1.8}_{-1.9}) \times 10^{-2}$	$-0.42^{+0.24}_{-0.25}$	120^{+14}_{-14}	$-3.38^{+1.06}_{-0.97}$	974/1956/1972	$(0.5^{+0.4}_{-0.4}) \times 10^{52}$	1.6
091003191	18~19	64	$(1.0^{+0.4}_{-0.4}) \times 10^{-1}$	$-0.73^{+0.04}_{-0.04}$	366^{+31}_{-31}	876/1758/1769	$(3.2^{+0.4}_{-0.4}) \times 10^{52}$	$(1.0^{+0.1}_{-0.1}) \times 10^{-1}$	$-0.69^{+0.05}_{-0.05}$	426^{+34}_{-35}	$-2.60^{+0.28}_{-0.29}$	874/1756/1771	$(3.7^{+0.6}_{-0.5}) \times 10^{52}$	-2.1
091020900	3~4	16	$(1.7^{+0.4}_{-0.3}) \times 10^{-2}$	$-1.21^{+0.15}_{-0.15}$	425^{+337}_{-188}	742/1490/1502	$(2.0^{+1.4}_{-0.8}) \times 10^{52}$	$(2.7^{+1.2}_{-1.4}) \times 10^{-2}$	$-0.93^{+0.26}_{-0.29}$	160^{+73}_{-62}	$-1.90^{+0.15}_{-0.19}$	740/1489/1504	$(2.4^{+2.2}_{-1.3}) \times 10^{52}$	-1.3
091127976	0~1	124	$(2.3^{+0.1}_{-0.1}) \times 10^{-1}$	$-1.26^{+0.03}_{-0.03}$	142^{+8}_{-8}	1197/2400/2412	$(0.56^{+0.04}_{-0.04}) \times 10^{52}$	$(1.1^{+0.2}_{-0.2}) \times 10^{-0}$	$-0.55^{+0.10}_{-0.10}$	56^{+3}_{-3}	$-2.23^{+0.03}_{-0.03}$	1132/2272/2289	$(0.7^{+0.2}_{-0.2}) \times 10^{52}$	-127.2
091208410	0~1	19	$(2.9^{+0.5}_{-0.7}) \times 10^{-2}$	$-1.05^{+0.15}_{-0.15}$	171^{+50}_{-50}	743/1491/1503	$(0.5^{+0.3}_{-0.2}) \times 10^{52}$	$(3.6^{+1.3}_{-1.5}) \times 10^{-2}$	$-0.94^{+0.20}_{-0.22}$	131^{+41}_{-35}	$-2.19^{+0.29}_{-0.36}$	741/1491/1506	$(0.7^{+0.6}_{-0.4}) \times 10^{52}$	-0.5
100206563	0~1	8	$(0.8^{+0.2}_{-0.2}) \times 10^{-2}$	$-0.40^{+0.28}_{-0.28}$	357^{+213}_{-135}	1090/2186/2198	$(0.1^{+0.1}_{-0.03}) \times 10^{52}$	$(0.8^{+0.1}_{-0.1}) \times 10^{-2}$	$-0.40^{+0.26}_{-0.26}$	575^{+163}_{-171}	$-5.00^{+0.10}_{-0.02}$	1090/2188/2204	$(0.1^{+0.03}_{-0.02}) \times 10^{52}$	2.0
100414097	23~24	48	$(7.3^{+0.3}_{-0.3}) \times 10^{-2}$	$-0.69^{+0.04}_{-0.04}$	395^{+39}_{-35}	1222/2451/2463	$(7.5^{+1.2}_{-1.0}) \times 10^{52}$	$(7.6^{+0.4}_{-0.4}) \times 10^{-2}$	$-0.67^{+0.05}_{-0.05}$	481^{+47}_{-47}	$-2.68^{+0.44}_{-0.43}$	1221/2451/2467	$(8.5^{+1.7}_{-1.3}) \times 10^{52}$	-0.1
100615083	10~11	26	$(3.4^{+0.9}_{-0.3}) \times 10^{-2}$	$-1.11^{+0.13}_{-0.13}$	139^{+43}_{-46}	848/1702/1714	$(1.0^{+0.4}_{-0.4}) \times 10^{52}$	$(7.1^{+4.3}_{-4.3}) \times 10^{-2}$	$-0.76^{+0.29}_{-0.30}$	78^{+20}_{-20}	$-2.11^{+0.15}_{-0.15}$	845/1698/1714	$(1.4^{+1.5}_{-1.1}) \times 10^{52}$	-3.6
100728095	82~83	28	$(4.4^{+0.3}_{-0.3}) \times 10^{-2}$	$-0.48^{+0.08}_{-0.08}$	307^{+46}_{-46}	834/1674/1686	$(5.8^{+1.4}_{-1.4}) \times 10^{52}$	$(4.7^{+0.5}_{-0.5}) \times 10^{-2}$	$-0.41^{+0.10}_{-0.10}$	416^{+50}_{-50}	$-2.52^{+0.36}_{-0.33}$	833/1674/1689	$(6.7^{+1.5}_{-1.5}) \times 10^{52}$	-0.8
100728439	2~3	17	$(3.1^{+1.2}_{-0.9}) \times 10^{-2}$	$-0.94^{+0.19}_{-0.19}$	116^{+51}_{-34}	1423/2852/2864	$(2.0^{+1.2}_{-0.8}) \times 10^{52}$	$(4.8^{+3.0}_{-3.1}) \times 10^{-2}$	$-0.73^{+0.31}_{-0.32}$	92^{+27}_{-25}	$-2.10^{+0.24}_{-0.24}$	1421/2851/2867	$(2.8^{+3.2}_{-2.0}) \times 10^{52}$	-1.0
100816026	0.5~1.5	40	$(1.6^{+0.2}_{-0.2}) \times 10^{-1}$	$-0.34^{+0.07}_{-0.07}$	99^{+8}_{-7}	1195/2397/2409	$(0.7^{+0.1}_{-0.1}) \times 10^{52}$	$(2.0^{+0.3}_{-0.3}) \times 10^{-1}$	$-0.22^{+0.09}_{-0.09}$	138^{+7}_{-7}	$-2.62^{+0.19}_{-0.19}$	1190/2389/2405	$(0.9^{+0.2}_{-0.2}) \times 10^{52}$	-7.9
100906576	10~11	39	$(7.2^{+1.0}_{-0.9}) \times 10^{-2}$	$-0.86^{+0.09}_{-0.08}$	190^{+36}_{-30}	587/1180/1190	$(4.7^{+1.2}_{-0.9}) \times 10^{52}$	$(7.2^{+0.9}_{-0.9}) \times 10^{-2}$	$-0.86^{+0.09}_{-0.08}$	217^{+22}_{-23}	$-4.98^{+2.81}_{-0.46}$	587/1182/1196	$(5.3^{+1.8}_{-1.0}) \times 10^{52}$	2.1
101213451	1~2	9	$(1.7^{+0.3}_{-0.3}) \times 10^{-2}$	$-0.72^{+0.25}_{-0.25}$	234^{+82}_{-82}	942/1889/1901	$(0.05^{+0.02}_{-0.02}) \times 10^{52}$	$(1.7^{+0.4}_{-0.4}) \times 10^{-2}$	$-0.72^{+0.25}_{-0.25}$	300^{+75}_{-75}	$-4.99^{+0.58}_{-0.58}$	942/1891/1907	$(0.05^{+0.02}_{-0.02}) \times 10^{52}$	2.1
110213220	18~19	37	$(1.0^{+0.3}_{-0.2}) \times 10^{-1}$	$-0.96^{+0.12}_{-0.12}$	81^{+14}_{-14}	847/1699/1711	$(1.8^{+0.6}_{-0.5}) \times 10^{52}$	$(1.3^{+0.4}_{-0.4}) \times 10^{-1}$	$-0.84^{+0.15}_{-0.15}$	76^{+8}_{-8}	$-2.79^{+0.36}_{-0.37}$	845/1698/1714	$(1.9^{+1.0}_{-0.7}) \times 10^{52}$	-0.9
110721200	2~3	74	$(1.1^{+0.4}_{-0.4}) \times 10^{-1}$	$-0.90^{+0.03}_{-0.03}$	389^{+30}_{-30}	1201/2407/2420	$(8.5^{+0.9}_{-0.8}) \times 10^{53}$	$(14.7^{+1.0}_{-1.1}) \times 10^{-2}$	$-0.69^{+0.05}_{-0.05}$	258^{+20}_{-20}	$-2.01^{+0.05}_{-0.05}$	1172/2351/2368	$(1.2^{+0.2}_{-0.1}) \times 10^{54}$	-56.3
110731465	1~2	37	$(8.4^{+1.2}_{-1.0}) \times 10^{-2}$	$-0.87^{+0.09}_{-0.09}$	154^{+25}_{-22}	912/1831/1843	$(1.5^{+0.3}_{-0.3}) \times 10^{53}$	$(1.6^{+0.5}_{-0.5}) \times 10^{-1}$	$-0.50^{+0.18}_{-0.18}$	116^{+15}_{-15}	$-2.23^{+0.13}_{-0.13}$	908/1824/1840	$(1.8^{+0.9}_{-0.7}) \times 10^{53}$	-6.7
120119170	14~15	42	$(5.9^{+0.4}_{-0.4}) \times 10^{-2}$	$-0.90^{+0.04}_{-0.04}$	291^{+45}_{-45}	954/1914/1926	$(6.2^{+1.1}_{-0.7}) \times 10^{52}$	$(6.3^{+0.6}_{-0.6}) \times 10^{-2}$	$-0.86^{+0.06}_{-0.06}$	292^{+36}_{-36}	$-2.58^{+0.43}_{-0.43}$	953/1915/1931	$(7.3^{+2.9}_{-2.9}) \times 10^{52}$	1.0
120326056	1~2	20	$(4.5^{+1.2}_{-1.2}) \times 10^{-2}$	$-1.04^{+0.16}_{-0.16}$	72^{+18}_{-18}	1036/2078/2091	$(1.3^{+0.4}_{-0.4}) \times 10^{52}$	$(4.5^{+1.3}_{-1.3}) \times 10^{-2}$	$-1.04^{+0.15}_{-0.15}$	70^{+6}_{-6}	$-5.00^{+0.03}_{-0.03}$	1036/2080/2097	$(1.3^{+0.4}_{-0.4}) \times 10^{52}$	2.0
120624933	11~12	43	$(5.1^{+0.2}_{-0.2}) \times 10^{-2}$	$-0.77^{+0.05}_{-0.05}$	592^{+78}_{-78}	1190/2386/2399	$(2.5^{+0.5}_{-0.4}) \times 10^{53}$	$(5.6^{+0.4}_{-0.4}) \times 10^{-2}$	$-0.69^{+0.06}_{-0.06}$	567^{+84}_{-86}	$-2.11^{+0.16}_{-0.15}$	1184/2376/2393	$(2.6^{+0.5}_{-0.5}) \times 10^{53}$	-9.9
120711115	95~96	46	$(5.8^{+0.1}_{-0.1}) \times 10^{-2}$	$-0.98^{+0.03}_{-0.03}$	2441^{+289}_{-270}	920/1846/1858	$(2.5^{+0.3}_{-0.2}) \times 10^{53}$	$(6.0^{+0.2}_{-0.2}) \times 10^{-2}$	$-0.92^{+0.03}_{-0.03}$	1800^{+243}_{-229}	$-2.30^{+0.14}_{-0.15}$	907/1822/1837	$(2.3^{+0.3}_{-0.3}) \times 10^{53}$	-24.3

Table 3 continued on next page

Table 3 (continued)

ID	$t_{\text{start}} \sim t_{\text{stop}}$ (s)	Time from T_0	COMP			Band			Difference					
			S	K	α	$L_{p,\text{iso}}$ ($\text{ph.s}^{-1} \cdot \text{cm}^{-2} \text{keV}^{-1}$)	K	α	E_p (keV)	likeli/AIC/BIC	$L_{p,\text{iso}}$ (erg.s^{-1})	ΔAIC		
(1)	(2)	(3)	(4)	(5)	(6)	(7)	(8)	(9)	(10)	(11)	(12)	(13)	(14)	(15)
120716712	0~1	23	$(4.5^{+0.8}_{-0.7}) \times 10^{-2}$	$-0.83^{+0.11}_{-0.11}$	143^{+29}_{-24}	764/1534/1546	$(5.3^{+1.6}_{-1.5}) \times 10^{52}$	$(1.2^{+0.7}_{-0.8}) \times 10^{-1}$	$-0.30^{+0.31}_{-0.31}$	99^{+20}_{-21}	$-2.11^{+0.14}_{-0.14}$	759/1526/1543	$(7.2^{+7.2}_{-4.8}) \times 10^{52}$	-7.8
121128212	8~9	47	$(1.8^{+0.3}_{-0.3}) \times 10^{-1}$	$-0.50^{+0.10}_{-0.10}$	80^{+9}_{-8}	703/1411/1423	$(6.8^{+1.5}_{-1.5}) \times 10^{52}$	$(1.8^{+0.3}_{-0.2}) \times 10^{-1}$	$-0.49^{+0.09}_{-0.09}$	119^{+5}_{-6}	$-5.00^{+0.65}_{-0.65}$	703/1413/1428	$(6.8^{+1.4}_{-1.3}) \times 10^{52}$	2.1
130427324	10~11	424	$(1.5^{+0.01}_{-0.01}) \times 10^0$	$-0.63^{+0.01}_{-0.01}$	610^{+7}_{-7}	3098/6201/6214	$(1.1^{+0.02}_{-0.02}) \times 10^{53}$	$(1.6^{+0.1}_{-0.1}) \times 10^{-1}$	$-0.57^{+0.01}_{-0.01}$	731 ^{±8}	$-2.97^{+0.04}_{-0.04}$	2914/5836/5852	$(1.1^{+0.02}_{-0.02}) \times 10^{53}$	-365.4
130518580	25~26	94	$(1.3^{+0.03}_{-0.03}) \times 10^{-1}$	$-0.76^{+0.02}_{-0.02}$	515^{+36}_{-33}	1172/2351/2363	$(7.6^{+0.7}_{-0.7}) \times 10^{53}$	$(1.5^{+0.1}_{-0.1}) \times 10^{-1}$	$-0.69^{+0.03}_{-0.03}$	505^{+36}_{-36}	$-2.16^{+0.08}_{-0.08}$	1147/2303/2319	$(8.2^{+0.7}_{-0.7}) \times 10^{53}$	-48.0
130610133	8~9	9	$(0.9^{+0.4}_{-0.3}) \times 10^{-2}$	$-1.26^{+0.24}_{-0.25}$	344^{+463}_{-193}	665/1335/1347	$(1.6^{+1.5}_{-0.8}) \times 10^{52}$	$(1.3^{+0.8}_{-0.5}) \times 10^{-2}$	$-1.04^{+0.38}_{-0.24}$	139^{+42}_{-48}	$-5.00^{+0.39}_{-0.13}$	581/1171/1186	$(1.0^{+0.9}_{-0.6}) \times 10^{52}$	-164.3
130925173	83~84	33	$(2.1^{+0.3}_{-0.3}) \times 10^{-2}$	$-1.61^{+0.07}_{-0.08}$	298^{+120}_{-83}	810/1626/1638	$(0.05^{+0.01}_{-0.01}) \times 10^{52}$	$(2.6^{+0.1}_{-0.1}) \times 10^{-2}$	$-1.50^{+0.01}_{-0.01}$	97^{+11}_{-11}	$-5.00^{+0.37}_{-0.05}$	732/1472/1488	$(0.04^{+0.01}_{-0.01}) \times 10^{52}$	-154.0
131011741	3~4	11	$(1.3^{+0.3}_{-0.2}) \times 10^{-2}$	$-0.86^{+0.16}_{-0.16}$	403^{+252}_{-248}	817/1640/1652	$(2.5^{+2.0}_{-1.1}) \times 10^{52}$	$(1.3^{+0.2}_{-0.2}) \times 10^{-2}$	$-0.86^{+0.15}_{-0.15}$	462^{+149}_{-148}	$-4.99^{+1.91}_{-0.71}$	817/1642/1658	$(2.5^{+1.2}_{-1.1}) \times 10^{52}$	2.0
131105087	108~109	26	$(2.2^{+0.2}_{-0.2}) \times 10^{-2}$	$-1.22^{+0.06}_{-0.06}$	688^{+233}_{-183}	787/1580/1592	$(3.7^{+0.7}_{-0.7}) \times 10^{52}$	$(2.2^{+0.2}_{-0.2}) \times 10^{-2}$	$-1.21^{+0.07}_{-0.07}$	507^{+126}_{-126}	$-2.39^{+0.84}_{-0.84}$	787/1581/1598	$(4.1^{+1.1}_{-0.9}) \times 10^{52}$	1.6
131108862	0~1	46	$(6.8^{+0.3}_{-0.3}) \times 10^{-2}$	$-0.75^{+0.05}_{-0.05}$	389^{+44}_{-41}	1054/2114/2126	$(2.6^{+0.5}_{-0.5}) \times 10^{53}$	$(8.4^{+0.7}_{-0.7}) \times 10^{-2}$	$-0.59^{+0.07}_{-0.07}$	332^{+34}_{-34}	$-1.93^{+0.07}_{-0.07}$	1034/2075/2092	$(3.2^{+0.5}_{-0.5}) \times 10^{53}$	-38.4
131231198	22.5~23.5	159	$(2.8^{+0.1}_{-0.1}) \times 10^{-1}$	$-0.89^{+0.02}_{-0.02}$	325^{+13}_{-13}	1325/2657/2669	$(2.9^{+0.1}_{-0.1}) \times 10^{52}$	$(2.9^{+0.1}_{-0.1}) \times 10^{-1}$	$-0.85^{+0.02}_{-0.02}$	329^{+12}_{-12}	$-2.67^{+0.14}_{-0.14}$	1317/2642/2652	$(3.4^{+0.2}_{-0.2}) \times 10^{52}$	-14.3
140206275	14~15	85	$(1.5^{+0.04}_{-0.04}) \times 10^{-1}$	$-0.74^{+0.02}_{-0.03}$	319^{+18}_{-16}	1299/2605/2617	$(6.1^{+0.5}_{-0.5}) \times 10^{53}$	$(1.8^{+0.1}_{-0.1}) \times 10^{-1}$	$-0.63^{+0.04}_{-0.04}$	314^{+19}_{-19}	$-2.22^{+0.08}_{-0.08}$	1280/2569/2585	$(7.0^{+0.7}_{-0.6}) \times 10^{53}$	-36.1
140213807	6~7	87	$(2.1^{+0.2}_{-0.2}) \times 10^{-1}$	$-0.97^{+0.04}_{-0.04}$	87^{+6}_{-6}	959/1923/1936	$(2.6^{+0.5}_{-0.5}) \times 10^{52}$	$(2.7^{+0.3}_{-0.3}) \times 10^{-1}$	$-0.87^{+0.05}_{-0.05}$	82^{+3}_{-3}	$-2.92^{+0.16}_{-0.16}$	955/1917/1934	$(2.8^{+0.6}_{-0.6}) \times 10^{52}$	-5.9
140506880	0~1	23	$(9.4^{+2.2}_{-1.8}) \times 10^{-2}$	$-0.71^{+0.15}_{-0.15}$	122^{+27}_{-22}	673/1353/1365	$(0.7^{+0.2}_{-0.2}) \times 10^{52}$	$(1.8^{+0.6}_{-0.6}) \times 10^{-1}$	$-0.32^{+0.23}_{-0.23}$	118^{+12}_{-12}	$-2.33^{+0.16}_{-0.16}$	669/1345/1361	$(1.0^{+0.5}_{-0.4}) \times 10^{52}$	-7.6
140508128	5~6	103	$(1.9^{+0.1}_{-0.1}) \times 10^{-1}$	$-0.78^{+0.03}_{-0.03}$	341^{+22}_{-22}	505/1016/1026	$(7.5^{+0.7}_{-0.7}) \times 10^{52}$	$(2.1^{+0.1}_{-0.1}) \times 10^{-1}$	$-0.73^{+0.04}_{-0.04}$	376^{+20}_{-20}	$-2.57^{+0.12}_{-0.12}$	493/994/1008	$(8.7^{+0.8}_{-0.7}) \times 10^{52}$	-22.0
140606133	0.5~1.5	29	$(3.2^{+0.2}_{-0.2}) \times 10^{-2}$	$-1.24^{+0.05}_{-0.05}$	1029^{+416}_{-300}	1172/2350/2363	$(0.2^{+0.06}_{-0.06}) \times 10^{52}$	$(3.2^{+0.2}_{-0.3}) \times 10^{-2}$	$-1.24^{+0.05}_{-0.05}$	728^{+279}_{-239}	$-2.06^{+0.24}_{-0.24}$	1172/2351/2368	$(0.3^{+0.1}_{-0.1}) \times 10^{52}$	0.9
140620219	7~8	16	$(2.7^{+0.9}_{-0.7}) \times 10^{-2}$	$-1.10^{+0.17}_{-0.17}$	133^{+50}_{-37}	563/1132/1144	$(1.9^{+1.0}_{-0.9}) \times 10^{52}$	$(2.6^{+0.7}_{-0.7}) \times 10^{-2}$	$-1.11^{+0.16}_{-0.16}$	120^{+19}_{-18}	$-5.00^{+0.04}_{-0.04}$	563/1134/1150	$(1.9^{+0.8}_{-0.8}) \times 10^{52}$	2.1
140703026	10~11	13	$(1.4^{+0.3}_{-0.3}) \times 10^{-2}$	$-0.88^{+0.17}_{-0.16}$	313^{+110}_{-110}	847/1700/1712	$(7.0^{+2.3}_{-2.3}) \times 10^{52}$	$(1.8^{+0.4}_{-0.4}) \times 10^{-2}$	$-0.75^{+0.19}_{-0.19}$	265^{+65}_{-65}	$-2.30^{+0.47}_{-0.47}$	846/1701/1717	$(8.0^{+1.1}_{-1.1}) \times 10^{52}$	1.0
140808038	0.5~1.5	28	$(1.1^{+0.3}_{-0.2}) \times 10^{-1}$	$-0.35^{+0.13}_{-0.13}$	75^{+9}_{-9}	682/1370/1382	$(1.1^{+0.4}_{-0.4}) \times 10^{53}$	$(1.2^{+0.3}_{-0.3}) \times 10^{-1}$	$-0.32^{+0.15}_{-0.15}$	121^{+9}_{-9}	$-3.44^{+1.03}_{-0.91}$	682/1372/1387	$(1.2^{+0.5}_{-0.4}) \times 10^{53}$	1.5
140907672	9~10	10	$(4.3^{+2.4}_{-1.6}) \times 10^{-2}$	$-0.46^{+0.28}_{-0.28}$	70^{+23}_{-17}	878/1761/1774	$(0.3^{+0.3}_{-0.3}) \times 10^{52}$	$(4.9^{+2.3}_{-2.4}) \times 10^{-2}$	$-0.39^{+0.28}_{-0.29}$	103^{+14}_{-13}	$-3.19^{+0.39}_{-0.39}$	877/1763/1780	$(0.4^{+0.4}_{-0.2}) \times 10^{52}$	1.8
141028455	13~14	44	$(5.9^{+0.3}_{-0.3}) \times 10^{-2}$	$-0.79^{+0.04}_{-0.04}$	381^{+44}_{-38}	874/1754/1766	$(1.9^{+0.3}_{-0.3}) \times 10^{53}$	$(6.6^{+0.5}_{-0.5}) \times 10^{-2}$	$-0.71^{+0.06}_{-0.06}$	376^{+40}_{-40}	$-2.27^{+0.18}_{-0.18}$	870/1748/1764	$(2.2^{+0.3}_{-0.3}) \times 10^{53}$	-6.3
141220252	0~1	40	$(9.0^{+1.0}_{-0.9}) \times 10^{-2}$	$-0.51^{+0.08}_{-0.08}$	136^{+14}_{-14}	984/1975/1987	$(2.3^{+0.4}_{-0.4}) \times 10^{52}$	$(9.0^{+0.9}_{-0.9}) \times 10^{-2}$	$-0.50^{+0.08}_{-0.08}$	203^{+11}_{-11}	$-5.00^{+0.08}_{-0.08}$	984/1977/1993	$(2.2^{+0.6}_{-0.6}) \times 10^{52}$	2.1
141221338	0~1	14	$(1.6^{+0.3}_{-0.3}) \times 10^{-2}$	$-1.08^{+0.16}_{-0.16}$	304^{+178}_{-114}	618/1242/1253	$(1.1^{+0.4}_{-0.4}) \times 10^{52}$	$(1.6^{+0.3}_{-0.3}) \times 10^{-2}$	$-1.08^{+0.15}_{-0.15}$	279^{+81}_{-78}	$-3.58^{+1.39}_{-0.90}$	618/1244/1259	$(1.2^{+0.5}_{-0.5}) \times 10^{52}$	2.0
141225959	1~2	8	$(1.2^{+0.8}_{-0.5}) \times 10^{-2}$	$-0.39^{+0.48}_{-0.48}$	173^{+83}_{-83}	573/1152/1163	$(0.2^{+0.5}_{-0.1}) \times 10^{52}$	$(1.2^{+0.2}_{-0.2}) \times 10^{-2}$	$-0.37^{+0.24}_{-0.22}$	273^{+1}_{-1}	$-4.74^{+1.66}_{-0.04}$	573/1154/1169	$(0.2^{+0.0}_{-0.0}) \times 10^{52}$	2.0
150301818	2~3	11	$(1.6^{+0.5}_{-0.4}) \times 10^{-2}$	$-1.00^{+0.19}_{-0.18}$	210^{+119}_{-78}	902/1810/1822	$(0.9^{+0.5}_{-0.5}) \times 10^{52}$	$(1.6^{+0.4}_{-0.4}) \times 10^{-2}$	$-1.00^{+0.17}_{-0.17}$	209^{+52}_{-54}	$-5.00^{+2.67}_{-0.44}$	902/1812/1829	$(0.9^{+0.5}_{-0.5}) \times 10^{52}$	2.0
150314205	1~2	124	$(3.0^{+0.1}_{-0.1}) \times 10^{-1}$	$-0.37^{+0.02}_{-0.02}$	245^{+9}_{-9}	974/1954/1966	$(4.1^{+3.0}_{-2.8}) \times 10^{52}$	$(3.3^{+0.1}_{-0.1}) \times 10^{-1}$	$-0.30^{+0.03}_{-0.03}$	357^{+12}_{-12}	$-2.70^{+0.12}_{-0.12}$	963/1934/1949	$(4.7^{+0.4}_{-0.4}) \times 10^{53}$	-20.5
150403913	11~12	77	$(8.8^{+0.2}_{-0.2}) \times 10^{-2}$	$-0.87^{+0.03}_{-0.03}$	875^{+82}_{-82}	838/1681/1693	$(4.8^{+0.6}_{-0.6}) \times 10^{53}$	$(9.6^{+0.3}_{-0.3}) \times 10^{-2}$	$-0.80^{+0.12}_{-0.12}$	749^{+62}_{-62}	$-2.30^{+0.11}_{-0.11}$	820/1648/1663	$(4.6^{+0.4}_{-0.4}) \times 10^{53}$	-33.4
150514774	0~1	44	$(1.5^{+0.2}_{-0.2}) \times 10^{-1}$	$-0.65^{+0.09}_{-0.09}$	77^{+8}_{-8}	908/1822/1835	$(0.5^{+0.1}_{-0.1}) \times 10^{52}$	$(2.2^{+0.5}_{-0.5}) \times 10^{-1}$	$-0.46^{+0.12}_{-0.12}$	90^{+6}_{-6}	$-2.68^{+0.18}_{-0.18}$	903/1813/1830	$(0.6^{+0.2}_{-0.2}) \times 10^{52}$	-9.0
150821406	15~16	32	$(3.0^{+0.2}_{-0.2}) \times 10^{-2}$	$-1.05^{+0.06}_{-0.06}$	578^{+157}_{-122}	675/1355/1367	$(0.7^{+0.2}_{-0.2}) \times 10^{52}$	$(3.0^{+0.2}_{-0.2}) \times 10^{-2}$	$-1.05^{+0.06}_{-0.06}$	541^{+110}_{-98}	$-3.03^{+0.84}_{-1.29}$	674/1357/1372	$(0.8^{+0.2}_{-0.2}) \times 10^{52}$	1.8
151027166	0.1~1.1	29	$(3.8^{+0.5}_{-0.4}) \times 10^{-2}$	$-1.00^{+0.08}_{-0.08}$	266^{+63}_{-54}	962/1931/1943	$(0.5^{+0.2}_{-0.1}) \times 10^{52}$	$(5.2^{+0.9}_{-0.9}) \times 10^{-2}$	$-0.81^{+0.11}_{-0.11}$	182^{+26}_{-26}	$-2.06^{+0.12}_{-0.12}$	958/1924/1940	$(0.8^{+0.2}_{-0.2}) \times 10^{52}$	-6.6
160509374	16~17	137	$(2.2^{+0.05}_{-0.06}) \times 10^{-1}$	$-0.92^{+0.02}_{-0.02}$	416^{+40}_{-31}	1457/2919/2932	$(1.3^{+0.1}_{-0.1}) \times 10^{53}$	$(2.5^{+0.1}_{-0.1}) \times 10^{-1}$	$-0.84^{+0.03}_{-0.03}$	350^{+19}_{-19}	$-2.21^{+0.07}_{-0.07}$	1424/2856/2873	$(1.6^{+0.1}_{-0.1}) \times 10^{53}$	-63.0
160625945	189~190	285	$(1.8^{+0.06}_{-0.06}) \times 10^1$	$-0.79^{+0.01}_{-0.01}$	1103^{+30}_{-30}	1893/3792/3805	$(1.5^{+0.1}_{-0.1}) \times 10^{54}$	$(5.2^{+0.1}_{-0.1}) \times 10^{-1}$	$-0.67^{+0.01}_{-0.01}$	852^{+29}_{-29}	$-2.30^{+0.04}_{-0.04}$	1657/3322/3338	$(1.3^{+0.03}_{-0.03}) \times 10^{54}$	-470.9
160629930	14~15	18	$(2.9^{+0.5}_{-0.5}) \times 10^{-2}$	$-0.68^{+0.13}_{-0.12}$	173^{+41}_{-34}	846/1699/1711	$(8.9^{+2.0}_{-2.0}) \times 10^{52}$	$(2.9^{+0.4}_{-0.5}) \times 10^{-2}$	$-0.68^{+0.13}_{-0.13}$	228^{+34}_{-34}	$-4.80^{+2.52}_{-0.32}$	846/1701/1717	$(9.8^{+2.5}_{-2.5}) \times 10^{52}$	2.0
160804065	9~10	10	$(1.4^{+0.8}_{-0.5}) \times 10^{-2}$	$-1.13^{+0.26}_{-0.26}$	158^{+127}_{-72}	858/1721/1734	$(0.1^{+0.1}_{-0.1}) \times 10^{52}$	$(1.4^{+0.3}_{-0.3}) \times 10^{-2}$	$-1.13^{+0.17}_{-0.17}$	137^{+1}_{-1}	$-3.26^{+1.02}_{-1.02}$	858/1723/1740	$(0.1^{+0.03}_{-0.03}) \times 10^{52}$	2.0
161014522	7~8	17	$(3.5^{+0.7}_{-0.6}) \times 10^{-2}$	$-0.55^{+0.15}_{-0.15}$	150^{+36}_{-29}	904/1814/1827	$(6.5^{+3.1}_{-2.1}) \times 10^{52}$	$(3.5^{+0.7}_{-0.7}) \times 10^{-2}$	$-0.55^{+0.15}_{-0.15}$	218^{+25}_{-25}	$-5.00^{+0.35}_{-0.05}$	904/1816/1833	$(6.3^{+1.9}_{-1.9}) \times 10^{52}$	2.1
161017745	4~5	11	$(1.2^{+0.2}_{-0.2}) \times 10^{-2}$	$-1.23^{+0.14}_{-0.14}$	792^{+361}_{-361}	370/746/756	$(3.3^{+1.5}_{-1.5}) \times 10^{52}$	$(1.2^{+0.2}_{-0.2}) \times 10^{-2}$	$-1.23^{+0.14}_{-0.14}$	602^{+277}_{-282}	$-5.00^{+0.01}_{-0.01}$	370/748/761	$(3.4^{+1.5}_{-1.5}) \times 10^{52}$	2.1
161117066	116~117	28	$(1.1^{+0.5}_{-0.3}) \times 10^{-1}$	$-0.75^{+0.19}_{-0.19}$	53^{+10}_{-10}	556/1118/1130	$(1.2^{+0.7}_{-0.5}) \times 10^{52}$	$(1.1^{+0$						

Table 3 (continued)

ID	Time from T_0		COMP			Band			Difference					
	$t_{\text{start}} \sim t_{\text{stop}}$ (s)	(2)	(3)	(4)	(5)	(6)	(7)	(8)	(9)	(10)	(11)	(12)	(13)	(14)
	$t_{\text{start}} \sim t_{\text{stop}}$ (s)	S	K ($\text{ph.s}^{-1} \cdot \text{cm}^{-2} \text{keV}^{-1}$)	α	E_c (keV)	likeli/AIC/BIC	$L_{p,\text{iso}}$ (erg.s^{-1})	K ($\text{ph.s}^{-1} \cdot \text{cm}^{-2} \text{keV}^{-1}$)	α	E_p (keV)	β	likeli/AIC/BIC	$L_{p,\text{iso}}$ (erg.s^{-1})	ΔAIC
161129300	27~28	13	$(2.4^{+0.7}_{-0.5}) \times 10^{-2}$	$-0.63^{+0.19}_{-0.19}$	160^{+56}_{-42}	815/1636/1649	$(0.1^{+0.1}_{-0.0}) \times 10^{52}$	$(2.4^{+0.6}_{-0.6}) \times 10^{-2}$	$-0.63^{+0.19}_{-0.18}$	218^{+37}_{-37}	$-5.00^{+0.17}_{-0.02}$	815/1638/1655	$(0.12^{+0.04}_{-0.04}) \times 10^{52}$	2.1
170214649	62~63	43	$(4.9^{+0.2}_{-0.2}) \times 10^{-2}$	$-0.88^{+0.06}_{-0.05}$	760^{+138}_{-114}	1201/2408/2420	$(3.7^{+0.7}_{-0.6}) \times 10^{53}$	$(5.7^{+0.4}_{-0.4}) \times 10^{-2}$	$-0.75^{+0.06}_{-0.06}$	521^{+79}_{-78}	$-1.84^{+0.07}_{-0.07}$	1176/2360/2377	$(3.8^{+0.6}_{-0.6}) \times 10^{53}$	-47.4
170405777	30~31	35	$(5.5^{+0.3}_{-0.3}) \times 10^{-2}$	$-0.75^{+0.06}_{-0.06}$	323^{+38}_{-38}	1056/2118/2131	$(4.1^{+0.6}_{-0.6}) \times 10^{53}$	$(5.8^{+0.4}_{-0.4}) \times 10^{-2}$	$-0.73^{+0.06}_{-0.06}$	372^{+37}_{-37}	$-2.59^{+0.32}_{-0.32}$	1056/2119/2136	$(4.4^{+0.6}_{-0.6}) \times 10^{53}$	0.9
170607971	2~3	33	$(3.7^{+0.3}_{-0.4}) \times 10^{-2}$	$-1.40^{+0.08}_{-0.08}$	369^{+147}_{-106}	637/1280/1292	$(0.2^{+0.1}_{-0.1}) \times 10^{52}$	$(6.1^{+1.7}_{-1.7}) \times 10^{-2}$	$-1.13^{+0.15}_{-0.15}$	117^{+25}_{-24}	$-2.09^{+0.11}_{-0.11}$	635/1278/1293	$(0.3^{+0.1}_{-0.1}) \times 10^{52}$	-2.8
170705115	9~10	46	$(9.1^{+0.8}_{-0.7}) \times 10^{-2}$	$-0.87^{+0.06}_{-0.06}$	195^{+24}_{-21}	680/1366/1377	$(9.0^{+1.5}_{-1.2}) \times 10^{52}$	$(9.6^{+1.0}_{-1.0}) \times 10^{-2}$	$-0.84^{+0.07}_{-0.07}$	207^{+19}_{-18}	$-2.82^{+0.45}_{-0.46}$	679/1367/1382	$(1.0^{+0.2}_{-0.2}) \times 10^{53}$	1.0
171010792	68~69	175	$(4.0^{+0.1}_{-0.1}) \times 10^{-1}$	$-1.14^{+0.02}_{-0.02}$	222^{+10}_{-10}	922/1849/1861	$(0.5^{+0.0}_{-0.0}) \times 10^{52}$	$(4.1^{+0.1}_{-0.1}) \times 10^{-1}$	$-1.13^{+0.02}_{-0.02}$	186^{+6}_{-6}	$-3.38^{+0.48}_{-0.48}$	921/1850/1865	$(0.56^{+0.05}_{-0.05}) \times 10^{52}$	0.1
180703876	4~5	34	$(3.5^{+0.2}_{-0.2}) \times 10^{-2}$	$-0.83^{+0.05}_{-0.05}$	592^{+121}_{-163}	916/1838/1851	$(0.9^{+0.3}_{-0.2}) \times 10^{52}$	$(3.9^{+0.4}_{-0.4}) \times 10^{-2}$	$-0.73^{+0.08}_{-0.08}$	508^{+110}_{-100}	$-2.14^{+0.21}_{-0.21}$	914/1835/1852	$(1.0^{+0.3}_{-0.3}) \times 10^{52}$	-3.0
180720598	16~17	188	$(3.2^{+0.4}_{-0.4}) \times 10^{-1}$	$-0.95^{+0.01}_{-0.01}$	1098^{+60}_{-60}	2040/4085/4098	$(1.2^{+0.1}_{-0.1}) \times 10^{53}$	$(3.6^{+0.1}_{-0.1}) \times 10^{-1}$	$-0.84^{+0.01}_{-0.01}$	732^{+37}_{-37}	$-2.15^{+0.03}_{-0.03}$	1846/3701/3718	$(1.2^{+0.1}_{-0.1}) \times 10^{53}$	-384.3
180728728	11.4~12.4	249	$(4.0^{+0.1}_{-0.1}) \times 10^{-1}$	$-1.57^{+0.01}_{-0.01}$	335^{+17}_{-17}	918/1842/1853	$(0.8^{+0.1}_{-0.1}) \times 10^{51}$	$(4.1^{+0.1}_{-0.1}) \times 10^{-1}$	$-1.57^{+0.01}_{-0.01}$	143^{+4}_{-4}	$-3.52^{+0.61}_{-0.62}$	918/1844/1859	$(0.8^{+0.1}_{-0.1}) \times 10^{51}$	2.0
181010247	0~1	9	$(0.8^{+0.3}_{-0.3}) \times 10^{-2}$	$-1.16^{+0.21}_{-0.21}$	379^{+396}_{-195}	620/1246/1257	$(0.6^{+0.5}_{-0.3}) \times 10^{52}$	$(0.9^{+0.3}_{-0.3}) \times 10^{-2}$	$-1.15^{+0.23}_{-0.20}$	293^{+163}_{-139}	$-2.17^{+0.26}_{-1.10}$	620/1248/1263	$(0.7^{+0.5}_{-0.3}) \times 10^{52}$	2.0
181020792	7~8	44	$(5.9^{+0.3}_{-0.3}) \times 10^{-2}$	$-0.59^{+0.05}_{-0.06}$	361^{+42}_{-38}	738/1483/1494	$(4.0^{+0.7}_{-0.6}) \times 10^{53}$	$(6.0^{+0.3}_{-0.3}) \times 10^{-2}$	$-0.59^{+0.05}_{-0.05}$	504^{+43}_{-40}	$-3.19^{+1.02}_{-1.21}$	738/1484/1500	$(4.3^{+0.8}_{-0.8}) \times 10^{53}$	1.8
190114873	4~5	287	$(8.3^{+0.1}_{-0.1}) \times 10^{-1}$	$-0.51^{+0.01}_{-0.01}$	403^{+6}_{-10}	2624/5253/5266	$(6.5^{+0.2}_{-0.2}) \times 10^{52}$	$(8.3^{+0.1}_{-0.1}) \times 10^{-1}$	$-0.51^{+0.01}_{-0.01}$	600^{+7}_{-7}	$-4.12^{+0.38}_{-0.38}$	2622/5251/5269	$(6.7^{+0.2}_{-0.2}) \times 10^{52}$	-2.0
190530430	18~19	199	$(4.1^{+0.4}_{-0.4}) \times 10^{-1}$	$-0.78^{+0.01}_{-0.01}$	659^{+18}_{-18}	1314/2634/2646	$(2.3^{+0.1}_{-0.1}) \times 10^{54}$	$(4.1^{+0.4}_{-0.4}) \times 10^{-1}$	$-0.78^{+0.01}_{-0.01}$	803^{+16}_{-16}	$-5.00^{+0.14}_{-0.02}$	1314/2636/2651	$(2.3^{+0.1}_{-0.1}) \times 10^{54}$	1.4
200524211	6~7	33	$(3.5^{+0.4}_{-0.3}) \times 10^{-2}$	$-1.01^{+0.08}_{-0.07}$	418^{+115}_{-93}	982/1970/1981	$(2.2^{+0.5}_{-0.5}) \times 10^{52}$	$(6.2^{+1.4}_{-1.5}) \times 10^{-2}$	$-0.68^{+0.15}_{-0.15}$	184^{+36}_{-34}	$-1.83^{+0.08}_{-0.08}$	977/1963/1978	$(3.2^{+1.1}_{-1.0}) \times 10^{52}$	-7.1
200613229	12~13	76	$(1.7^{+0.1}_{-0.1}) \times 10^{-1}$	$-0.69^{+0.04}_{-0.04}$	138^{+9}_{-9}	618/1241/1253	$(3.4^{+0.3}_{-0.3}) \times 10^{52}$	$(1.7^{+0.1}_{-0.1}) \times 10^{-1}$	$-0.69^{+0.04}_{-0.04}$	180^{+7}_{-7}	$-5.00^{+0.01}_{-0.01}$	618/1244/1259	$(3.4^{+0.3}_{-0.3}) \times 10^{52}$	2.4
200826187	0~1	73	$(3.0^{+0.2}_{-0.2}) \times 10^{-1}$	$-0.68^{+0.04}_{-0.04}$	96^{+5}_{-10}	1848/3702/3715	$(1.1^{+0.1}_{-0.1}) \times 10^{52}$	$(5.9^{+0.8}_{-0.8}) \times 10^{-1}$	$-0.33^{+0.07}_{-0.07}$	96^{+4}_{-4}	$-2.42^{+0.06}_{-0.06}$	1805/3617/3635	$(1.5^{+0.3}_{-0.3}) \times 10^{52}$	-84.7
200829582	20~21	177	$(7.2^{+0.1}_{-0.1}) \times 10^{-1}$	$-0.61^{+0.02}_{-0.02}$	352^{+10}_{-9}	1337/2680/2691	$(5.7^{+0.3}_{-0.3}) \times 10^{53}$	$(8.3^{+0.2}_{-0.2}) \times 10^{-1}$	$-0.48^{+0.02}_{-0.02}$	401^{+10}_{-10}	$-2.48^{+0.19}_{-0.19}$	1204/2416/2431	$(6.5^{+0.3}_{-0.3}) \times 10^{53}$	-264.1
201020732	9~10	79	$(2.3^{+0.1}_{-0.1}) \times 10^{-1}$	$-0.60^{+0.03}_{-0.03}$	182^{+9}_{-9}	1460/2927/2939	$(2.4^{+0.2}_{-0.2}) \times 10^{52}$	$(2.5^{+0.1}_{-0.1}) \times 10^{-1}$	$-0.54^{+0.04}_{-0.04}$	233^{+11}_{-11}	$-2.72^{+0.21}_{-0.21}$	1456/2920/2936	$(2.8^{+0.3}_{-0.3}) \times 10^{52}$	-7.1
201216963	25~26	116	$(1.6^{+0.1}_{-0.1}) \times 10^{-1}$	$-1.06^{+0.02}_{-0.02}$	500^{+42}_{-37}	790/1587/1598	$(8.4^{+0.8}_{-0.7}) \times 10^{52}$	$(1.7^{+0.1}_{-0.1}) \times 10^{-1}$	$-1.01^{+0.03}_{-0.03}$	400^{+32}_{-30}	$-2.42^{+0.14}_{-0.14}$	783/1574/1589	$(9.6^{+0.9}_{-0.8}) \times 10^{52}$	-12.8
210204270	202~203	58	$(7.2^{+0.5}_{-0.5}) \times 10^{-2}$	$-1.34^{+0.04}_{-0.04}$	342^{+57}_{-49}	767/1540/1551	$(1.4^{+0.2}_{-0.2}) \times 10^{52}$	$(7.3^{+0.5}_{-0.5}) \times 10^{-2}$	$-1.33^{+0.04}_{-0.04}$	220^{+26}_{-24}	$-2.74^{+0.53}_{-0.61}$	766/1541/1556	$(1.6^{+0.4}_{-0.2}) \times 10^{52}$	0.9
210610628	1~2	9	$(1.3^{+0.1}_{-0.1}) \times 10^{-2}$	$-1.03^{+0.26}_{-0.05}$	184^{+148}_{-26}	758/1522/1534	$(5.0^{+4.5}_{-1.0}) \times 10^{52}$	$(1.3^{+0.5}_{-0.5}) \times 10^{-2}$	$-1.03^{+0.26}_{-0.05}$	179^{+58}_{-32}	$-4.71^{+2.51}_{-2.39}$	758/1524/1540	$(4.8^{+1.5}_{-1.5}) \times 10^{52}$	2.0
210610827	30~31	58	$(1.1^{+0.1}_{-0.1}) \times 10^{-1}$	$-0.44^{+0.05}_{-0.05}$	313^{+25}_{-25}	748/1503/1514	$(7.2^{+1.0}_{-1.0}) \times 10^{52}$	$(1.2^{+0.1}_{-0.1}) \times 10^{-1}$	$-0.38^{+0.06}_{-0.06}$	446^{+32}_{-32}	$-2.77^{+0.28}_{-0.28}$	747/1502/1517	$(8.3^{+1.2}_{-1.2}) \times 10^{52}$	-1.1
210619999	1~2	282	$(7.8^{+0.8}_{-0.8}) \times 10^{-2}$	$-0.70^{+0.01}_{-0.01}$	425^{+9}_{-10}	2402/4810/4823	$(2.1^{+0.1}_{-0.1}) \times 10^{54}$	$(9.4^{+0.2}_{-0.2}) \times 10^{-1}$	$-0.55^{+0.02}_{-0.02}$	400^{+11}_{-11}	$-2.25^{+0.03}_{-0.03}$	2195/4397/4415	$(2.3^{+0.1}_{-0.1}) \times 10^{54}$	-412.9
210722871	2~3	8	$(1.8^{+1.3}_{-0.8}) \times 10^{-2}$	$-1.03^{+0.30}_{-0.32}$	111^{+83}_{-47}	627/1261/1272	$(0.3^{+0.3}_{-0.1}) \times 10^{52}$	$(0.6^{+0.1}_{-0.1}) \times 10^{-2}$	$-0.86^{+0.12}_{-0.12}$	125^{+11}_{-11}	$-5.00^{+0.01}_{-0.01}$	2684/5375/5391	$(0.8^{+0.2}_{-0.1}) \times 10^{51}$	8.3
211023546	85~86	74	$(4.8^{+0.5}_{-0.5}) \times 10^{-2}$	$-1.95^{+0.06}_{-0.06}$	283^{+88}_{-66}	591/1189/1200	$(2.1^{+0.4}_{-0.3}) \times 10^{51}$	$(5.8^{+4.6}_{-4.6}) \times 10^{-1}$	$-1.00^{+0.29}_{-0.29}$	21^{+2}_{-2}	$-2.26^{+0.04}_{-0.04}$	595/1197/1213	$(0.2^{+0.4}_{-0.4}) \times 10^{52}$	2.1
220101215	88~89	27	$(9.2^{+1.3}_{-1.3}) \times 10^{-2}$	$-0.28^{+0.11}_{-0.11}$	102^{+12}_{-12}	703/1413/1424	$(3.2^{+0.7}_{-0.7}) \times 10^{53}$	$(9.2^{+1.4}_{-1.4}) \times 10^{-2}$	$-0.28^{+0.11}_{-0.11}$	176^{+11}_{-11}	$-5.00^{+0.03}_{-0.03}$	703/1415/1430	$(3.2^{+0.7}_{-0.7}) \times 10^{53}$	1.6
220107615	10~11	40	$(5.4^{+0.3}_{-0.3}) \times 10^{-2}$	$-0.66^{+0.06}_{-0.06}$	315^{+36}_{-36}	693/1391/1403	$(3.5^{+0.5}_{-0.5}) \times 10^{52}$	$(5.5^{+0.4}_{-0.5}) \times 10^{-2}$	$-0.65^{+0.06}_{-0.07}$	411^{+39}_{-39}	$-2.88^{+0.71}_{-0.71}$	692/1393/1408	$(4.0^{+0.7}_{-0.7}) \times 10^{52}$	1.6
220527387	7~8	139	$(6.0^{+0.3}_{-0.3}) \times 10^{-1}$	$-0.46^{+0.03}_{-0.03}$	109^{+4}_{-4}	879/1765/1776	$(3.7^{+0.2}_{-0.2}) \times 10^{52}$	$(7.2^{+0.5}_{-0.5}) \times 10^{-1}$	$-0.36^{+0.04}_{-0.04}$	153^{+4}_{-4}	$-2.96^{+0.13}_{-0.12}$	862/1732/1747	$(4.2^{+0.4}_{-0.4}) \times 10^{52}$	-33.0

NOTE—Same as Table 2 but for the 1-s peak spectrum.

Table 4. Time-integrated Spectral Fit Results for those GRBs required an Additional Model

ID	$T_{\text{start}} \sim T_{\text{stop}}$	T_0	Model	Standard Model				Additional Model				Total Flux	Information criteria Difference
				Band or COMP	α	E_p or E_c	β	Blackbody	kT	F_{BB}	F_{tot}		
(1)	(2)	(3)	(4)	(5)	(6)	(7)	(8)	(9)	(10)	(11)	(12)	(13)	(14)
Time-integrated spectral analysis													
090618353	-1~110	196	CPL+BB	$(3.1 \pm 0.1) \times 10^{-2}$	-1.45 ± 0.02	729 ⁺⁷⁷ ₋₇₂	...	$(1.5 \pm 0.1) \times 10^{-4}$	21 ± 1	$(2.9 \pm 0.4) \times 10^{-7}$	$(2.6 \pm 0.2) \times 10^{-6}$	2501/5013/5030	-348.6
090902462	-1~20	271	CPL+BB	$(8.1 \pm 0.1) \times 10^{-2}$	-1.15 ± 0.01	1228 ⁺⁵⁴ ₋₅₄	...	$(0.7 \pm 0.1) \times 10^{-6}$	158 ± 3	$(4.8 \pm 0.5) \times 10^{-6}$	$(1.6 \pm 0.1) \times 10^{-5}$	5068/10147/10168	-925.0
110721200	-1~20	92	Band+BB	$(1.8 \pm 0.1) \times 10^{-2}$	-1.20 ± 0.03	3392 ⁺³¹³ ₋₃₀₂	-2.10 ± 0.11	$(9.6 \pm 2.4) \times 10^{-6}$	33 ± 3	$(1.2 \pm 0.4) \times 10^{-7}$	$(3.9 \pm 0.6) \times 10^{-6}$	3117/6245/6270	-7.9
131231198	0.06~40	355	CPL+BB	$(5.7 \pm 0.1) \times 10^{-2}$	-1.40 ± 0.01	566 ⁺³² ₋₃₂	...	$(1.2 \pm 0.1) \times 10^{-4}$	23 ± 0	$(3.1 \pm 0.4) \times 10^{-7}$	$(4.1 \pm 0.2) \times 10^{-6}$	4558/9125/9146	-331.2
150314205	-1~15	210	Band+BB	$(9.2 \pm 0.3) \times 10^{-2}$	-0.72 ± 0.02	414 ⁺¹⁶ ₋₁₆	-3.20 ± 0.35	$(2.8 \pm 0.8) \times 10^{-5}$	29 ± 3	$(2.0 \pm 0.8) \times 10^{-7}$	$(6.7 \pm 0.5) \times 10^{-6}$	2344/4701/4724	-14.5
150403913	-1~30	118	Band+BB	$(2.1 \pm 0.1) \times 10^{-2}$	-1.04 ± 0.02	851 ⁺⁶² ₋₆₁	-2.74 ± 0.22	$(2.8 \pm 0.5) \times 10^{-5}$	26 ± 1	$(1.3 \pm 0.3) \times 10^{-7}$	$(2.5 \pm 0.2) \times 10^{-6}$	2592/5196/5219	-115.6
160509374	-1~40	226	Band+BB	$(4.3 \pm 0.1) \times 10^{-2}$	-1.07 ± 0.01	670 ⁺³³ ₋₃₃	-2.40 ± 0.08	$(4.8 \pm 0.4) \times 10^{-5}$	26 ± 1	$(2.3 \pm 0.3) \times 10^{-7}$	$(5.3 \pm 0.2) \times 10^{-6}$	4522/9055/9080	-208.7
160625945	-1~225	720	Band+BB	$(2.2 \pm 0.1) \times 10^{-2}$	-0.91 ± 0.03	843 ⁺⁷⁷ ₋₇₉	-2.32 ± 0.09	$(5.8 \pm 0.8) \times 10^{-6}$	40 ± 2	$(1.6 \pm 0.3) \times 10^{-7}$	$(3.8 \pm 0.4) \times 10^{-6}$	4726/9465/9489	-30.2
181020792	-1~20	29	CPL+BB	$(1.7 \pm 0.1) \times 10^{-2}$	-0.89 ± 0.05	593 ⁺¹¹¹ ₋₉₄	...	$(5.1 \pm 1.8) \times 10^{-6}$	38 ± 4	$(1.0 \pm 0.5) \times 10^{-7}$	$(1.9 \pm 0.4) \times 10^{-6}$	2264/4537/4556	-3.9
190114873	-1~116	239	CPL+BB	$(2.9 \pm 0.1) \times 10^{-2}$	-1.34 ± 0.01	1733 ⁺¹⁹⁰ ₋₁₉₀	...	$(0.4 \pm 0.1) \times 10^{-6}$	126 ± 5	$(1.2 \pm 0.2) \times 10^{-6}$	$(5.3 \pm 0.4) \times 10^{-6}$	6049/12109/12131	-587.5
210619999	-1~70	358	Band+BB	$(6.3 \pm 0.2) \times 10^{-2}$	-1.17 ± 0.01	471 ⁺²⁵ ₋₂₇	-2.39 ± 0.08	$(1.1 \pm 0.1) \times 10^{-4}$	23 ± 1	$(3.0 \pm 0.5) \times 10^{-7}$	$(5.8 \pm 0.3) \times 10^{-6}$	5932/11876/11902	-28.6
L-s peak spectral analysis													
090424592	4~5	133	CPL+BB	$(4.7 \pm 0.3) \times 10^{-1}$	-0.55 ± 0.07	145 ⁺⁸ ₋₉	...	$(2.4 \pm 1.5) \times 10^{-3}$	12 ± 2	$(0.5 \pm 0.5) \times 10^{-6}$	$(1.2 \pm 0.1) \times 10^{-5}$	1665/3339/3360	-10.0
090618353	63~64	103	CPL+BB	$(1.5 \pm 0.1) \times 10^{-1}$	-0.98 ± 0.04	652 ⁺⁶⁵ ₋₆₂	...	$(4.2 \pm 1.5) \times 10^{-4}$	22 ± 2	$(0.9 \pm 0.3) \times 10^{-6}$	$(1.7 \pm 0.2) \times 10^{-5}$	633/1275/1292	-29.0
090902462	9~10	135	CPL+BB	$(9.3 \pm 0.3) \times 10^{-2}$	-1.69 ± 0.02	7201 ⁺²⁷⁵⁶ ₋₁₉₀₁	...	$(1.5 \pm 0.1) \times 10^{-6}$	188 ± 4	$(1.9 \pm 0.3) \times 10^{-5}$	$(3.2 \pm 0.3) \times 10^{-5}$	1628/3266/3286	-965.3
131108862	0~1	46	CPL+BB	$(3.1 \pm 0.3) \times 10^{-2}$	-1.17 ± 0.05	2917 ⁺¹²⁷³ ₋₅₉₄	...	$(1.9 \pm 0.4) \times 10^{-5}$	48 ± 4	$(1.0 \pm 0.5) \times 10^{-6}$	$(7.5 \pm 1.2) \times 10^{-6}$	1042/2094/2115	-11.2
150314205	1~2	124	Band+BB	$(2.5 \pm 0.2) \times 10^{-1}$	-0.30 ± 0.06	429 ⁺²⁰ ₋₂₀	-3.12 ± 0.26	$(1.8 \pm 0.7) \times 10^{-4}$	27 ± 3	$(1.0 \pm 0.5) \times 10^{-6}$	$(2.1 \pm 0.2) \times 10^{-5}$	948/1909/1932	-17.5
150403913	11~12	77	Band+BB	$(7.9 \pm 0.4) \times 10^{-2}$	-0.80 ± 0.04	963 ⁺¹⁰⁴ ₋₁₀₁	-2.45 ± 0.14	$(7.8 \pm 3.1) \times 10^{-5}$	27 ± 3	$(0.4 \pm 0.3) \times 10^{-6}$	$(1.5 \pm 0.2) \times 10^{-5}$	808/1629/1652	-11.7
160625945	189~190	285	Band+BB	$(3.6 \pm 0.1) \times 10^{-1}$	-0.83 ± 0.02	1465 ⁺¹⁸² ₋₁₈₂	-2.65 ± 0.08	$(9.2 \pm 1.1) \times 10^{-5}$	50 ± 2	$(5.8 \pm 1.3) \times 10^{-6}$	$(1.1 \pm 0.1) \times 10^{-4}$	1594/3201/3225	-112.4
170214649	62~63	43	CPL+BB	$(2.9 \pm 0.2) \times 10^{-2}$	-1.17 ± 0.05	4802 ⁺¹⁶⁴³ ₋₁₂₁₅	...	$(9.0 \pm 3.2) \times 10^{-6}$	55 ± 7	$(0.8 \pm 0.4) \times 10^{-6}$	$(7.8 \pm 1.1) \times 10^{-6}$	1181/2372/2393	-27.1
180720598	16~17	188	Band+BB	$(3.2 \pm 0.1) \times 10^{-1}$	-0.89 ± 0.02	914 ⁺⁶⁶ ₋₆₆	-2.22 ± 0.04	$(6.1 \pm 2.6) \times 10^{-5}$	36 ± 5	$(1.0 \pm 1.0) \times 10^{-6}$	$(6.3 \pm 0.5) \times 10^{-5}$	1837/3686/3711	-6.5
190114873	4~5	287	CPL+BB	$(6.3 \pm 0.2) \times 10^{-1}$	-0.72 ± 0.02	485 ⁺²³ ₋₂₃	...	$(1.3 \pm 0.2) \times 10^{-5}$	115 ± 4	$(2.3 \pm 0.4) \times 10^{-5}$	$(9.2 \pm 0.7) \times 10^{-5}$	2525/5059/5081	-185.4
190530430	18~19	199	CPL+BB	$(3.6 \pm 0.1) \times 10^{-1}$	-0.69 ± 0.02	640 ⁺²⁰ ₋₂₁	...	$(6.9 \pm 1.6) \times 10^{-4}$	21 ± 1	$(1.5 \pm 0.5) \times 10^{-6}$	$(6.0 \pm 0.3) \times 10^{-5}$	1272/2555/2574	-72.1
201020732	9~10	79	CPL+BB	$(1.6 \pm 0.2) \times 10^{-1}$	-0.76 ± 0.07	249 ⁺³² ₋₃₂	...	$(6.0 \pm 1.1) \times 10^{-5}$	33 ± 3	$(0.7 \pm 0.3) \times 10^{-6}$	$(7.9 \pm 1.5) \times 10^{-6}$	1456/2921/2942	2.8
210619999	1~2	282	Band+BB	$(6.4 \pm 0.2) \times 10^{-1}$	-0.63 ± 0.02	584 ⁺²¹ ₋₂₁	-2.51 ± 0.05	$(7.6 \pm 1.0) \times 10^{-4}$	27 ± 1	$(4.3 \pm 0.9) \times 10^{-6}$	$(8.2 \pm 0.4) \times 10^{-5}$	2087/4186/4212	-202.9
220527387	7~8	139	CPL+BB	$(3.3 \pm 0.5) \times 10^{-1}$	-0.69 ± 0.09	157 ⁺²¹ ₋₁₈	...	$(3.6 \pm 0.9) \times 10^{-4}$	25 ± 2	$(1.5 \pm 0.8) \times 10^{-6}$	$(1.0 \pm 0.2) \times 10^{-5}$	868/1747/1766	-10.5

NOTE—(1) GRB name. (2) The selected source interval $T_{\text{start}} \sim T_{\text{stop}}$ (in units of s). (3) The corresponding significance S . (4) The used hybrid model. (5)-(8) The best-fit parameters for the Band or COMP model: normalization K (in units of $\text{ph.s}^{-1} \text{cm}^{-2} \text{keV}^{-1}$), low-energy power-law index α , peak energy E_p (or cut-off energy E_c) of the νF_ν spectrum (in units of keV), and high-energy power-law index β . (9)-(10) The best-fit parameters for the additional model: normalization K (in units of $\text{ph.s}^{-1} \text{cm}^{-2} \text{keV}^{-1}$), and blackbody temperature kT (in units of keV), the thermal (νF_ν) energy flux F_{BB} (in units of $\text{erg cm}^{-2} \text{s}^{-1}$), and the total (νF_ν) energy flux F_{tot} (in units of $\text{erg cm}^{-2} \text{s}^{-1}$); the likelihood and the statistical information criteria (AIC and BIC); and the difference of BIC between Band+BB (or CPL+BB) and Band-alone (or CPL-alone): Δ BIC = BIC(Band+BB) - BIC(Band) or BIC(CPL+BB) - BIC(CPL).

Table 5 Results of the Average and Deviation Values of the Parameter Distribution

	Sample size	Gaussian fit result	Source
Global properties			
Observed-frame duration [T_{90}]	153	$\log_{10}(41.20) \pm 0.49$ s	this paper
Rest-frame duration [$T_{90,z}$]	153	$\log_{10}(15.16) \pm 0.57$ s	this paper
k_c	103	0.95 ± 0.11	this paper
Bolometric ($1-10^4$ keV) fluence [$S_7^{\text{Bolometric}}$]	103	$\log_{10}(2.99 \times 10^5) \pm 0.67$ erg cm $^{-2}$	this paper
GBM (8 keV-40 MeV) fluence [S_7^{GBM}]	103	$\log_{10}(3.01 \times 10^5) \pm 0.67$ erg cm $^{-2}$	this paper
Time-integrated spectra, peak energy [$E_{p,z}$]	117	$\log_{10}(533) \pm 0.40$ keV	this paper
1-s peak spectra, peak energy [$E_{p,z}$]	102	$\log_{10}(619) \pm 0.38$ keV	this paper
Time-integrated spectra, isotropic total energy [$E_{\gamma,\text{iso}}$]	117	$\log_{10}(5.33 \times 10^{52}) \pm 0.85$ erg	this paper
1-s peak spectra, isotropic peak luminosity [$L_{p,\text{iso}}$]	102	$\log_{10}(3.54 \times 10^{52}) \pm 0.88$ erg s $^{-1}$	this paper
Model-wise properties			
Time-integrated Band-like spectra, peak energy [$E_{p,z}$]	85	$\log_{10}(485) \pm 0.38$ keV	this paper
Time-integrated CPL-like spectra, peak energy [$E_{p,z}$]	24	...	this paper
1-s peak Band-like spectra, peak energy [$E_{p,z}$]	39	$\log_{10}(674) \pm 0.40$ keV	this paper
1-s peak CPL-like spectra, peak energy [$E_{p,z}$]	47	$\log_{10}(512) \pm 0.32$ keV	this paper
Time-integrated Band-like spectra, isotropic total energy [$E_{\gamma,\text{iso}}$]	85	$\log_{10}(6.96 \times 10^{52}) \pm 0.69$ erg	this paper
Time-integrated CPL-like spectra, isotropic total energy [$E_{\gamma,\text{iso}}$]	24	$\log_{10}(6.58 \times 10^{51}) \pm 0.68$ erg	this paper
1-s peak Band-like spectra, isotropic peak luminosity [$L_{p,\text{iso}}$]	39	$\log_{10}(7.28 \times 10^{52}) \pm 1.45$ erg s $^{-1}$	this paper
1-s peak CPL-like spectra, isotropic peak luminosity [$L_{p,\text{iso}}$]	47	$\log_{10}(2.11 \times 10^{52}) \pm 0.74$ erg s $^{-1}$	this paper
Comparison with other samples			
Peak energy [$E_{p,z}$]	58	$\log_{10}(896) \pm 0.49$ keV	Amati et al. (2008)
Isotropic total energy [$E_{\gamma,\text{iso}}$]	58	$\log_{10}(1.16 \times 10^{53}) \pm 0.88$ erg	Amati et al. (2008)
Peak energy [$E_{p,z}$]	101	$\log_{10}(139) \pm 0.42$ keV	Yonetoku et al. (2010)
Isotropic peak luminosity [$L_{p,\text{iso}}$]	101	$\log_{10}(3.86 \times 10^{52}) \pm 0.76$ erg s $^{-1}$	Yonetoku et al. (2010)

Table 6. Results of Linear Regression Analysis for the Spectral-energy Relations

Sample	Preferred Spectral model Number	Expression	$E_{\gamma,iso}^{Div}$ or $L_{p,iso}^{Div}$	R	p
$E_{p,z}-E_{\gamma,iso}$ (Amati) Correlation					
Band-like IGRBs	Band	$E_{p,z}/(\text{keV}) = (229 \pm 29) \left(\frac{E_{\gamma,iso}/(\text{erg})}{E_{\gamma,iso}^{Div}} \right)$	(0.42 ± 0.05)	$2 \times 10^{52} \text{erg}$	$0.71 < 10^{-4}$
CPL-like IGRBs	CPL	$E_{p,z}/(\text{keV}) = (341 \pm 65) \left(\frac{E_{\gamma,iso}/(\text{erg})}{E_{\gamma,iso}^{Div}} \right)$	(0.25 ± 0.12)	$2 \times 10^{52} \text{erg}$	$0.11 \quad 0.67$
All Band-like bursts (sGRBs+IGRBs)	Band	$E_{p,z}/(\text{keV}) = (235 \pm 36) \left(\frac{E_{\gamma,iso}/(\text{erg})}{E_{\gamma,iso}^{Div}} \right)$	(0.41 ± 0.06)	$2 \times 10^{52} \text{erg}$	$-0.07 \quad 0.74$
All CPL-like bursts (sGRBs+IGRBs)	CPL	$E_{p,z}/(\text{keV}) = (336 \pm 83) \left(\frac{E_{\gamma,iso}/(\text{erg})}{E_{\gamma,iso}^{Div}} \right)$	(0.00 ± 0.13)	$2 \times 10^{52} \text{erg}$	$0.86 < 10^{-4}$
$E_{p,z}-L_{p,iso}$ (Yonetoku) Correlation					
Band-like IGRBs	Band	$E_{p,z}/(\text{keV}) = (307 \pm 34) \left(\frac{L_{p,iso}/(\text{erg.s}^{-1})}{L_{p,iso}^{Div}} \right)$	(0.34 ± 0.04)	$2 \times 10^{52} \text{erg s}^{-1}$	$0.83 < 10^{-4}$
CPL-like IGRBs	CPL	$E_{p,z}/(\text{keV}) = (454 \pm 55) \left(\frac{L_{p,iso}/(\text{erg.s}^{-1})}{L_{p,iso}^{Div}} \right)$	(0.40 ± 0.08)	$2 \times 10^{52} \text{erg s}^{-1}$	$0.69 < 10^{-4}$
All Band-like bursts (sGRBs+IGRBs)	Band	$E_{p,z}/(\text{keV}) = (300 \pm 34) \left(\frac{L_{p,iso}/(\text{erg.s}^{-1})}{L_{p,iso}^{Div}} \right)$	(0.36 ± 0.04)	$2 \times 10^{52} \text{erg s}^{-1}$	$0.84 < 10^{-4}$
All CPL-like bursts (sGRBs+IGRBs)	CPL	$E_{p,z}/(\text{keV}) = (475 \pm 83) \left(\frac{L_{p,iso}/(\text{erg.s}^{-1})}{L_{p,iso}^{Div}} \right)$	(0.40 ± 0.12)	$2 \times 10^{52} \text{erg s}^{-1}$	$0.63 < 10^{-4}$

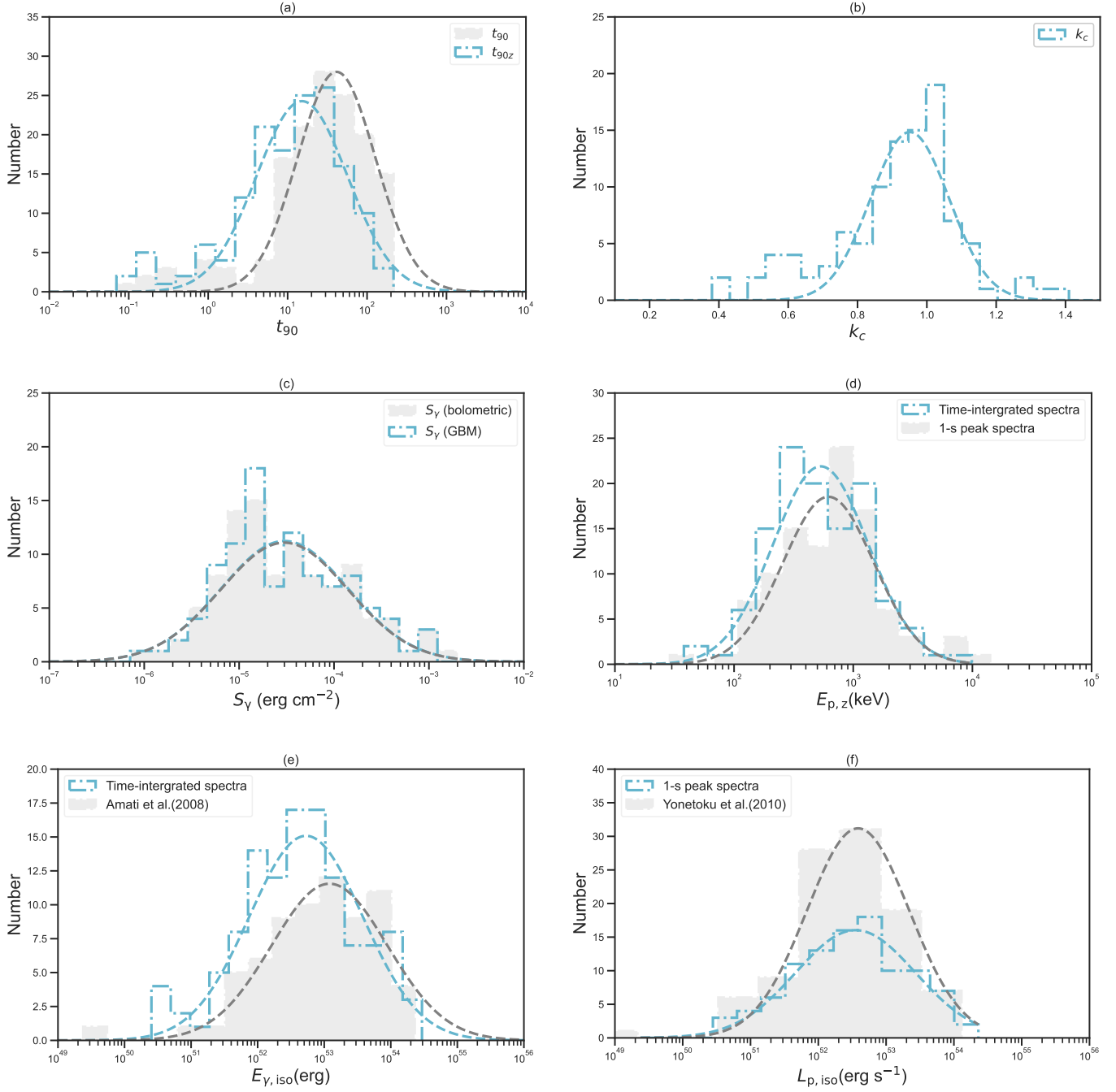


Figure 1. Global parameter distributions of (a) T_{90} (cyan dotted dashed line) and $T_{90,z}$ (grey shaded area), (b) k_c , (c) $S_\gamma^{\text{bolometric}}$ (cyan dotted dashed line) and S_γ^{GBM} (grey shaded area), (d) $E_{p,z}$ between time-intergrated spectra (cyan dotted dashed line) and 1-s peak spectra (grey shaded area), (e) $E_{\gamma,iso}$ between time-intergrated spectra (cyan dotted dashed line) and the same defined in Amati et al. (2008) (grey shaded area), and (f) $L_{\gamma,iso}$ between 1-s peak spectra (dotted dashed line) and Yonetoku et al. (2010) (grey shaded area). The (cyan and grey) dashed lines represent their best Gaussian fits.

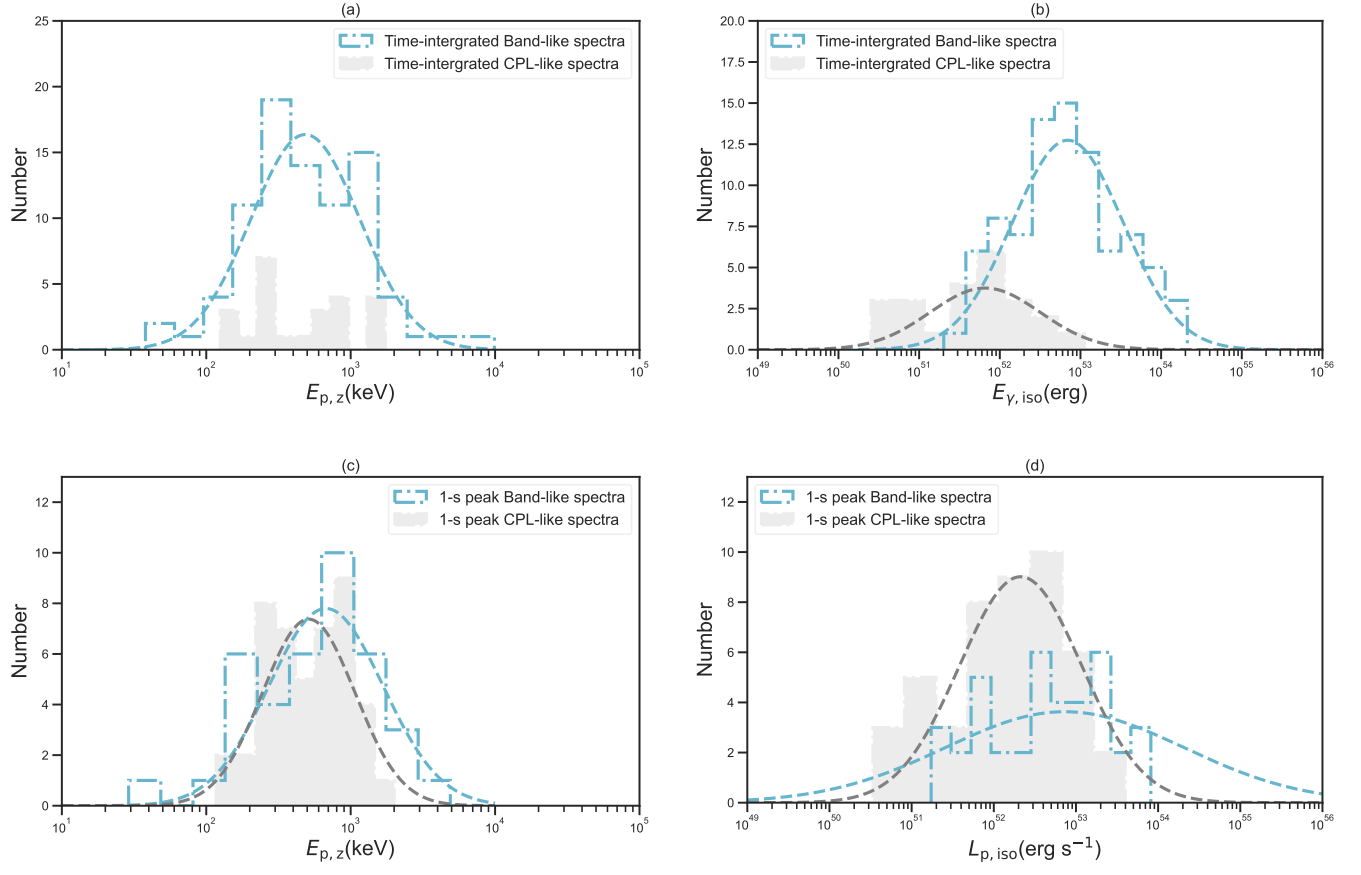


Figure 2. Same as Figure 1 but for the model-wise parameter distributions (Band versus CPL).

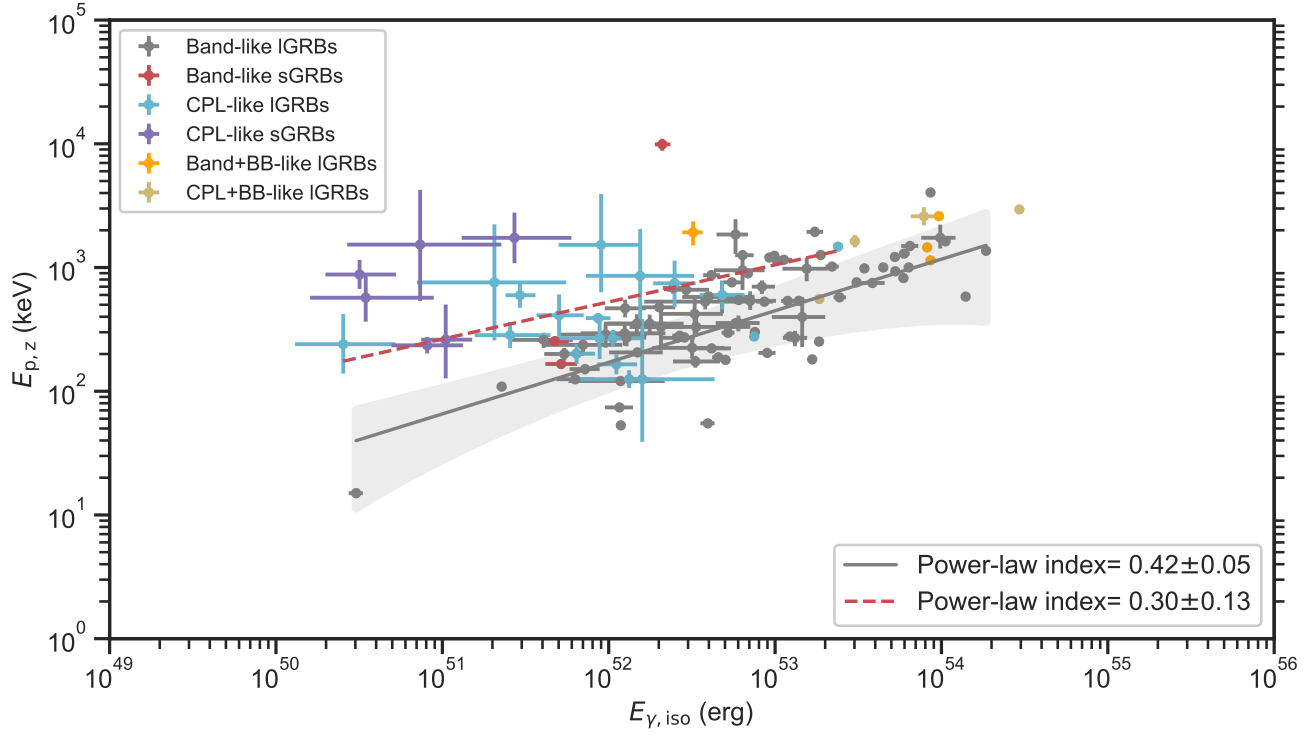


Figure 3. 109 GRBs with firm estimates of redshift and well-measured E_p , plotted in the $E_{p,z}-E_{\gamma, iso}$ plane. Data points with magenta, cyan, and orange indicate the Band-like bursts, CPL-like bursts, Band+BB-like bursts, and CPL+BB-like bursts, respectively. The solid line (grey) is the best fit using the power-law model with 2σ (95% confidence interval) error region (shadow area) for the Band-like IGRBs while the red dashed line represents the best fit for the CPL-like IGRBs.

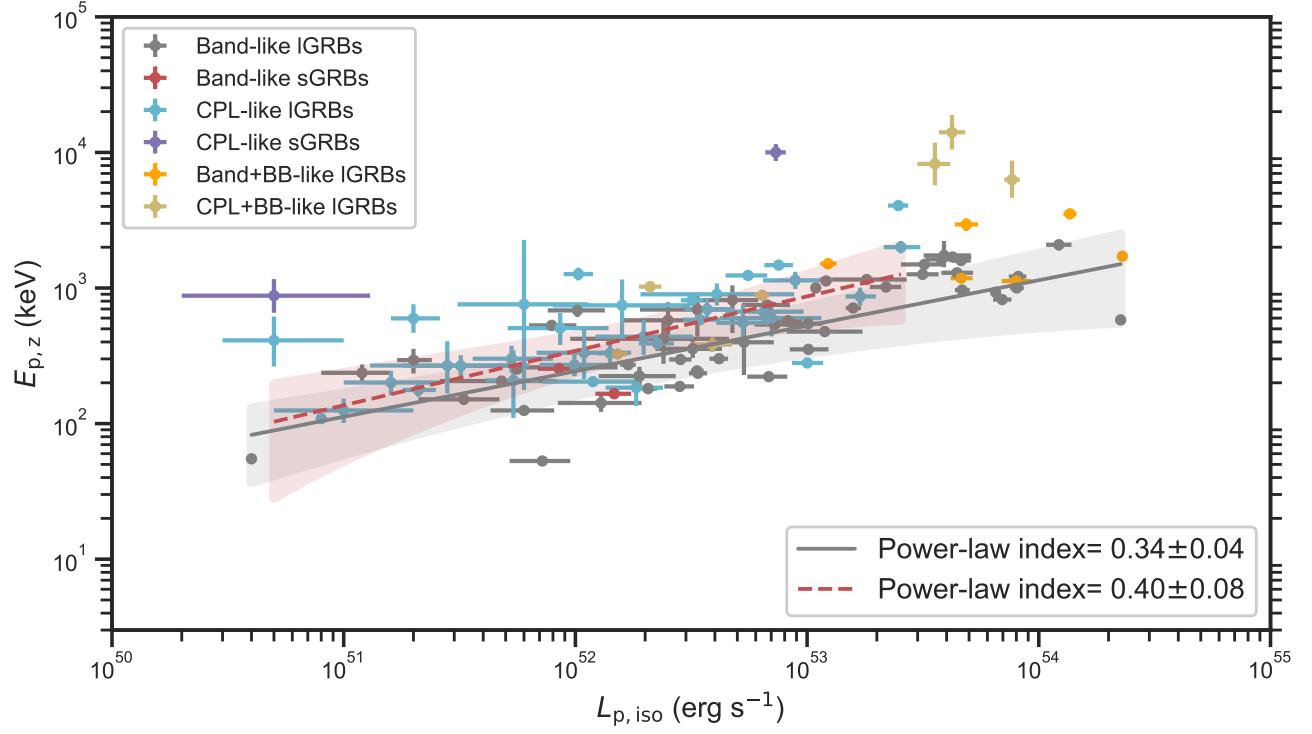


Figure 4. Same as Figure 3 but for the Yonetoku ($E_{p,z}$ - $L_{p,iso}$) correlation analysis using 92 GRBs with firm estimates of redshift and well-measured E_p from the time-integrated spectral analysis and the peak luminosity $L_{p,iso}$ from the 1-s peak spectral analysis. The symbols and colors are the same as Figure 3.

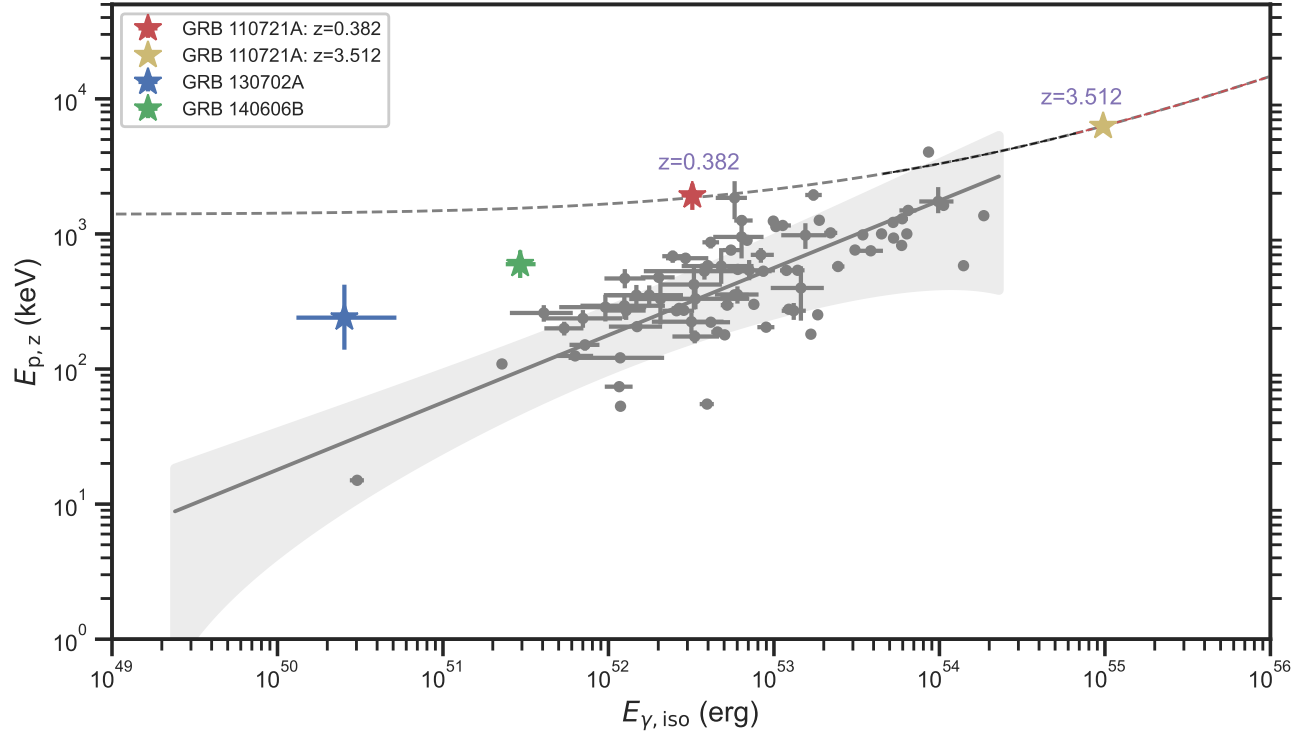


Figure 5. Three outliers (star data points) and 64 IGRBs (circular data points) in the $E_{p,z}$ - $E_{\gamma, iso}$ plane. The dash lines represent the redshift evolution in the $E_{p,z}$ - $E_{\gamma, iso}$ plane for the three outliers. Colors with grey black and red denote the low (from 0.01 to 1), intermediate (from 1 to 3), and high redshift (from 3 to 10) regions.

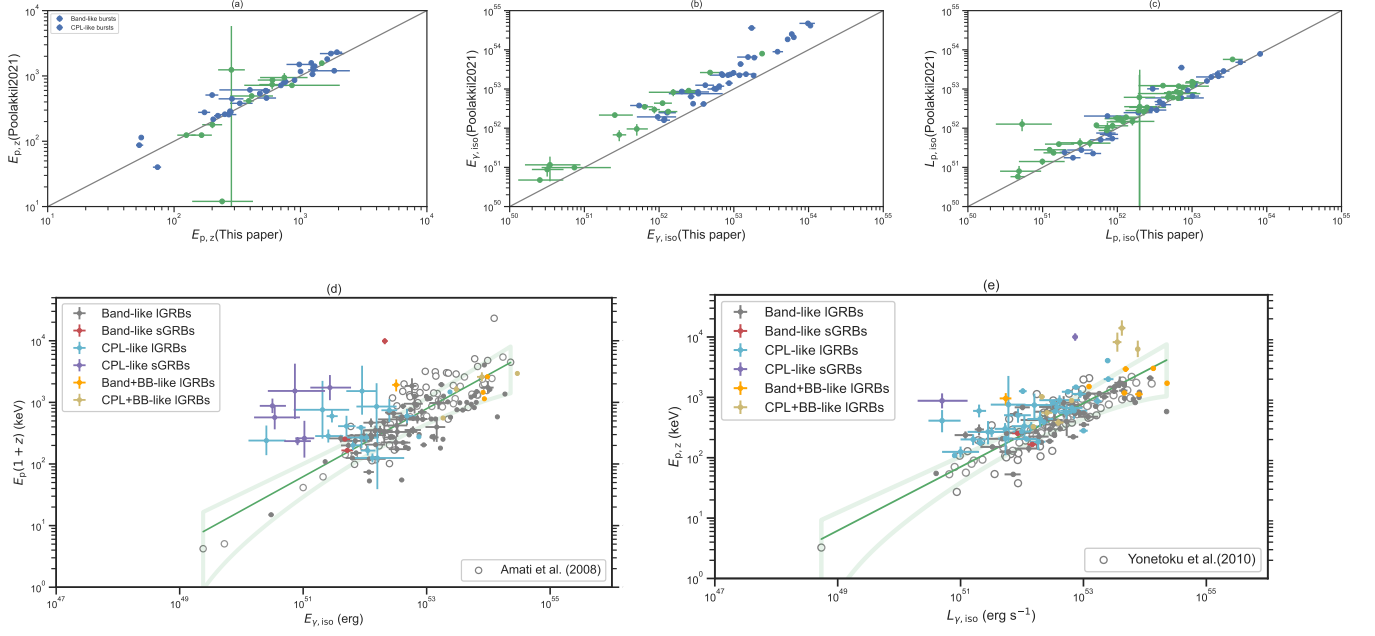


Figure 6. Upper panel: Parameter comparison ($E_{p,z}$, $E_{\gamma,iso}$, and $L_{p,iso}$) between our study and Poolakkil et al. (2021) by using 2-dimensional plots. Different color represents different groups: blue color (Band-like bursts) and green color (CPL-like bursts). **Lower panel:** Different burst samples from the $E_{p,z}$ - $E_{\gamma,iso}$ and $E_{p,z}$ - $L_{p,iso}$ planes are compared. The data points indicated by hollow points represent the sample defined in Amati et al. (2008) and Yonetoku et al. (2010). The solid green lines are the best fit using the power-law model with 2σ (95% confidence interval) error region (shadow area) to the sample defined in Amati et al. (2008) and Yonetoku et al. (2010), respectively. The data points indicated by the other colors (the same as Figure 3) represent the burst samples defined in this paper based on their model-wise properties.

APPENDIX

In this appendix, we provide additional figures and tables.

A1. CORRELATION COEFFICIENT BY MARKOV CHAIN MONTE CARLO ALGORITHM

The correlation coefficient is used to assess the reliability of the correlation between the cosmological rest-frame peak energy (E_p) and either the isotropic-bolometric-equivalent emission energy ($E_{\gamma,iso}$) or the isotropic-bolometric-equivalent peak luminosity ($L_{p,iso}$) for our samples. By implementing the Python package PyMC3 (Salvatier et al. 2016), we use a normal-LKJ correlation prior distribution and the Markov chain Monte Carlo (MCMC) algorithm to obtain the covariance matrix of the multivariate normal distribution, and the correlation coefficient between the parameters is obtained as a result (Chib & Winkelmann 2001) by iterating 10^5 times and burning the first 10^4 times of the MCMC samples. Our results are summarized in Table A1, including the expected values (μ_1) and standard deviation (σ_1) of the normal distribution of the analyzed parameters, and their correlation coefficients, as well as the related Highest Density Interval (HDI) of the posterior distributions, ranging from 3% to 97%. In Figure A1, using the Band-like IGRB sample as an example, we show an MCMC iteration for the mean values and standard deviation of the E_p and $E_{\gamma,iso}$, and their correlation coefficient, including the value of 10^5 iterations (right) and their distribution (left).

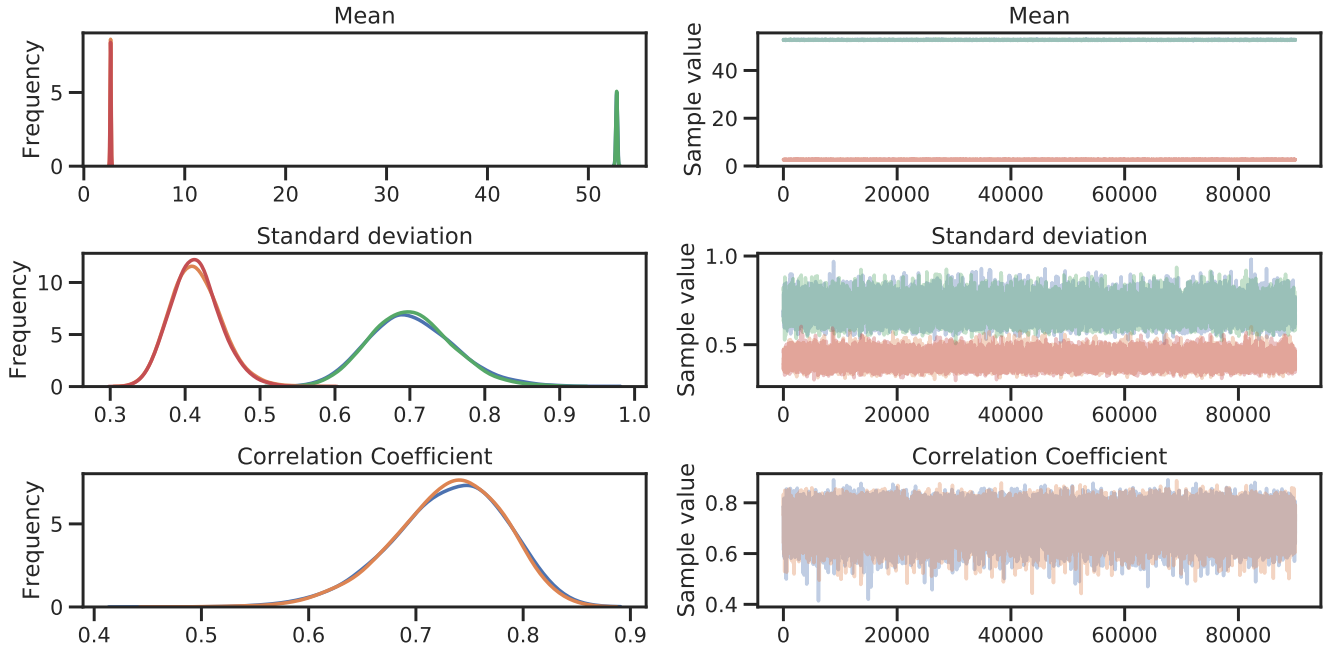


Figure A1. MCMC iteration for the mean values and standard deviation of the E_p and $E_{\gamma,iso}$, and their correlation coefficient for our Band-like IGRB sample, including the value of 10^5 iterations (right) and their distribution (left).

Table A1. Results of correlation coefficient of Markov chain Monte Carlo algorithm.

Sample	μ_1	σ_1	μ_2	σ_2	Correlation Coefficient	hdi interval
	$\log_{10}(E_{\gamma, \text{iso}} \text{ or } L_{\text{p, iso}})$		$\log_{10}(E_{\text{p, z}})$		$(E_{\gamma, \text{iso}} - E_{\text{p, z}})$ or $(L_{\text{p, iso}} - E_{\text{p, z}})$	[3% to 97%]
$E_{\text{p, z}} - E_{\gamma, \text{iso}}$ (Amati) Correlation						
Band-like IGRBs	52.80±0.08	0.70±0.06	2.65±0.05	0.41±0.03	0.73±0.05	[0.62 to 0.83]
CPL-like IGRBs	51.99±0.16	0.70±0.11	2.59±0.08	0.37±0.07	0.22±0.22	[-0.22 to 0.63]
All Band-like bursts (sGRBs+IGRBs)	52.78±0.08	0.73±0.06	2.67±0.05	0.44±0.03	0.68±0.06	[0.55 to 0.78]
All CPL-like bursts (sGRBs+IGRBs)	51.72±0.16	0.79±0.10	2.65±0.08	0.38±0.06	-0.01±0.20	[-0.40 to 0.37]
$E_{\text{p, z}} - L_{\text{p, iso}}$ (Yonetoku) Correlation						
Band-like IGRBs	52.66±0.13	0.79±0.09	2.77±0.07	0.45±0.05	0.64±0.10	[0.43 to 0.82]
CPL-like IGRBs	52.15±0.12	0.83±0.08	2.70±0.05	0.31±0.03	0.70±0.08	[0.54 to 0.83]
All Band-like bursts (sGRBs+IGRBs)	52.64±0.12	0.77±0.09	2.78±0.08	0.48±0.06	0.61±0.10	[0.41 to 0.80]
All CPL-like bursts (sGRBs+IGRBs)	52.09±0.12	0.85±0.07	2.70±0.04	0.30±0.03	0.65±0.08	[0.49 to 0.81]